COPY NO. _____

TECHNICAL REPORT 4965

COMPONENT PARTS ASSEMBLY WITH JOINTS, ADHESIVE-MECHANICAL

PART 4. ANALYSIS AND TEST OF BONDED AND WELDBONDED LAP JOINTS

RICHARD A. MITCHELL, RUTH M. WOOLLEY
SAUL M. BAKER
NATIONAL BUREAU OF STANDARDS
WASHINGTON, DC 20234

MARCH 1976

WILLIAM C. TANNER, PICATINNY ARSENAL
PROJECT OFFICER

PICATINNY ARSENAL
DOVER, NEW JERSEY

The findings in this report are not to be construed as an official Department of the Army position.

DISPOSITION

Destroy this report when no longer needed. Do not return to the originator.

REPORT DOCUMENTATION PAGE

READ INSTRUCTIONS BEFORE COMPLETING FORM

1. REPORT NUMBER: Technical Report 4965	2. GOVT ACCESSION NO.
3. RECIPIENT'S CATALOG NUMBER	
4. TITLE (and Subtitle): COMPONENT PARTS ASSEMBLY WITH JOINTS, ADHESIVE-MECHANICAL PART 4 ANALYSIS AND TEST OF BONDED AND WELDBONDED LAP JOINTS	5. TYPE OF REPORT & PERIOD COVERED: Final Report-March 1976
	6. PERFORMING ORG. REPORT NUMBER: NBSIR 76-1053
7. AUTHOR(s): Richard A. Mitchell, Ruth M. Woolley, Saul M. Baker	8. CONTRACT OR GRANT NUMBER(s)
9. PERFORMING ORGANIZATION NAME AND ADDRESS: Engineering Mechanics Section, Mechanics Division Institute for Basic Standards National Bureau of Standards, Washington, D.C.	10. PROGRAM ELEMENT, PROJECT, TASK AREA & WORK UNIT NUMBERS
11. CONTROLLING OFFICE NAME AND ADDRESS: Picatinny Arsenal Dover, New Jersey 07801	12. REPORT DATE: March 1976 13. NUMBER OF PAGES: 70
14. MONITORING AGENCY NAME & ADDRESS (If different from Controlling Office)	15. SECURITY CLASS. (of this report) 15a. DECLASSIFICATION/DOWNGRADING SCHEDULE

16. DISTRIBUTION STATEMENT (of this Report)

Approved for public release, distribution unlimited.

17. DISTRIBUTION STATEMENT (of the abstract entered in Block 20, if different from Report)

18. SUPPLEMENTARY NOTES

19. KEY WORDS (Continue on reverse side if necessary and identify by block number)

Adhesive-bonded joints; bonded joints; cyclic loading; debond analysis; double-lap-joint analysis; fatigue tests; finite element analysis; joints; nonlinear analysis; single-lap-joint analysis; single-lap-joint bending; spotwelded joints; weldbonded joints.

20. ABSTRACT (Continue on reverse side if necessary and identify by block number)

Finite element computer techniques were used to study the linear and nonlinear structural response of bonded and weldbonded lap joints. Although the techniques used are applicable to either single-lap or double-lap joints, the emphasis was on the single-lap joint problem with the attendant complication of joint bending. Nonlinear algorithms were developed to account for nonlinear stress-strain characteristics of the adhesive, and the joined metal sheet, weld-heat softening of the metal sheet, progressive debonding of the

20. Abstract (continued)

adhesive, and nonlinear cyclic loading. The nonlinear modes of response were simulated by sequences of linear solutions.

Eight different single-lap joint configurations, designed so as to constitute an experimental parameter study, were studied in a laboratory testing program. Representative specimens were subjected to quasi-static tensile strength and cyclic-load tests and to tensile fatigue tests. The quasi-static and fatigue data generally plot into clear S-N patterns that are in a reasonable relationship to the lap joint design parameters. For the most part, strains measured on the surfaces of the test specimens were in reasonably good agreement with those computed by finite element analysis, provided out-of-plane bending effects were accounted for. The dominant failure modes were consistent with the computer analyses.

TABLE OF CONTENTS

		Page
1.	INTRODUCTION	2
2.	LINEAR ANALYSIS	2
	2.1 Planform Analysis	5
	2.2 Longitudinal Cross-Section Analysis	5
	2.3 Bending Effects	8
3.	NONLINEAR ANALYSIS	13
	3.1 Nonlinear Adhesive Shear	13
	a. Planform Algorithms	16
	b. Longitudinal Cross-Section Algorithm	20
	3.2 Nonlinear Metal Algorithm	20
	3.3 Numerical Examples	23
	a. Monotonically Increasing Load	23
	b. Cyclic Load	27
	c. Adherend Yield	31
4.	LAP JOINT TENSILE TESTS	31
	4.1 Lap Joint Specimens	31
	4.2 Quasi-Static Tests	40
	4.3 Fatigue Tests	40
	4.4 Failure Modes	49
5.	ANALYTICAL-EXPERIMENTAL STRAIN COMPARISONS	49
6.	CONCLUSION	61
7.	REFERENCES	65

ANALYSIS AND TEST OF BONDED AND WELDBONDED LAP JOINTS

Richard A. Mitchell, Ruth M. Woolley, and Saul M. Baker

ABSTRACT

Finite element computer techniques were used to study the linear and nonlinear structural response of bonded and weldbonded lap joints. Although the techniques used are applicable to either single-lap or double-lap joints, the emphasis was on the single-lap joint problem with the attendant complication of joint bending. Nonlinear algorithms were developed to account for nonlinear stress-strain characteristics of the adhesive and the joined metal sheet, weld-heat softening of the metal sheet, progressive debonding of the adhesive, and nonlinear cyclic loading. The nonlinear modes of response were simulated by sequences of linear solutions.

Eight different single-lap joint configurations, designed so as to constitute an experimental parameter study, were studied in a laboratory testing program. Representative specimens were subjected to quasi-static tensile strength and cyclic-load tests and to tensile fatigue tests. The quasi-static and fatigue data generally plot into clear S-N patterns that are in a reasonable relationship to the lap joint design parameters. For the most part, strains measured on the surfaces of the test specimens were in reasonably good agreement with those computed by finite element analysis, provided out-of-plane bending effects were accounted for. The dominant failure modes were consistent with the computer analyses.

Key Words: Adhesive-bonded joints; bonded joints; cyclic loading; debond analysis; double-lap-joint analysis; fatigue tests; finite element analysis; joints; nonlinear analysis; single-lap-joint analysis; single-lap-joint bending; spotwelded joints; weldbonded joints.

1. INTRODUCTION

The structural response of a bonded or weldbonded lap joint is an extremely complex mechanics problem. These joints are characterized by material discontinuities, nonlinear material properties, and out-of-plane bending, each of which can have a first order effect on a critical stress state. In order to properly interpret laboratory tests of these joints, and in order to more nearly optimize their designs, it is necessary to have some understanding of the highly nonuniform stress and strain fields throughout the joints. The finite element techniques described in this report are intended for use in developing such an understanding.

Techniques for the linear analysis of these joints were described in an earlier report [1]. In the present report, algorithms are described for approximating the nonlinear response of these joints by a sequence of linear solutions. Because of the complex and nonlinear nature of this problem, there is a high potential for obtaining finite element solutions that deviate far from the physical joint responses they are intended to simulate. Laboratory testing of lap joints representative of those simulated on the computer is one of the most effective methods for detecting excessive errors in the finite element model. The laboratory testing program reported here was intended to serve this purpose within the limited range represented by the specimens and tests.

2. LINEAR ANALYSIS

Because they form the basis for the nonlinear analysis to follow, the linear planform and longitudinal cross-section analyses reported earlier [1] will first be briefly described. Figure 1 shows a single-lap weldbonded joint, similar to one studied in the laboratory testing program, and a comparable double-lap joint. Figure 2 is a schematic (not to scale) detail of a spotweld region in such a single-lap joint. In Figure 2 the solid circle represents the visible mark at the edge of the surface of contact between the spotwelding electrode and the metal sheet. The inner dashed circle outlines the weld nugget. The area between the two dashed circles, sometimes referred to as a "halo", is effectively unbonded due to the displacement and heating of the adhesive during the spotwelding process. Beyond the halo is a region of transition to full adhesive thickness. The precise shape and dimensions of these spotweld features are functions of several variables, including the thickness and stiffness of both the metal sheet and the uncured adhesive and such welding parameters as pressure, current, resistance, time, and electrode shape. For purposes of describing their general configurations, bonded joints and spotwelded joints can be thought of as special cases of the weldbonded joint.

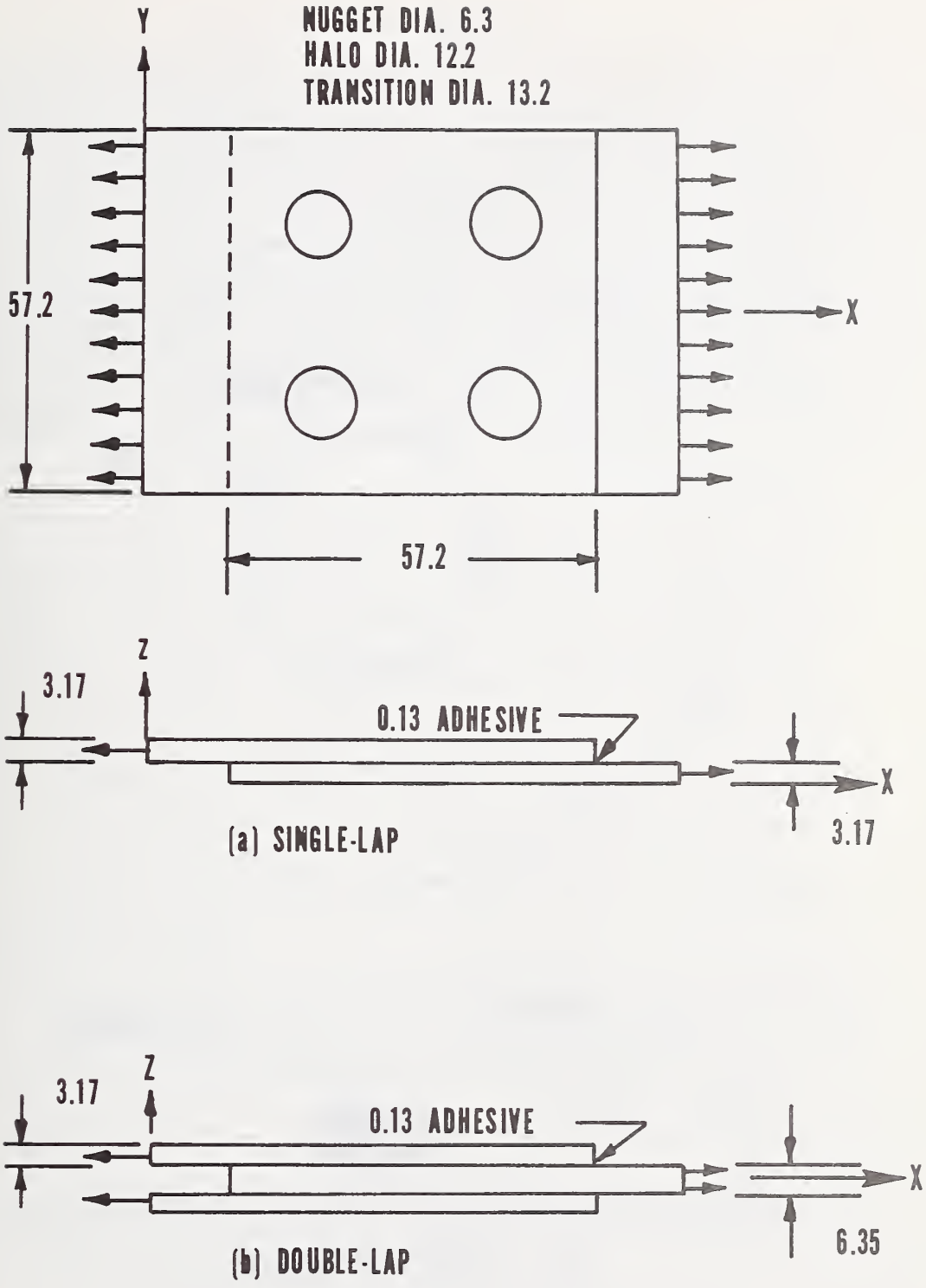

Figure 1. COMPARABLE SINGLE-LAP AND DOUBLE-LAP WELDBONDED JOINTS. DEMINSIONS ARE IN MILLIMETERS (1 in = 25.4 mm).

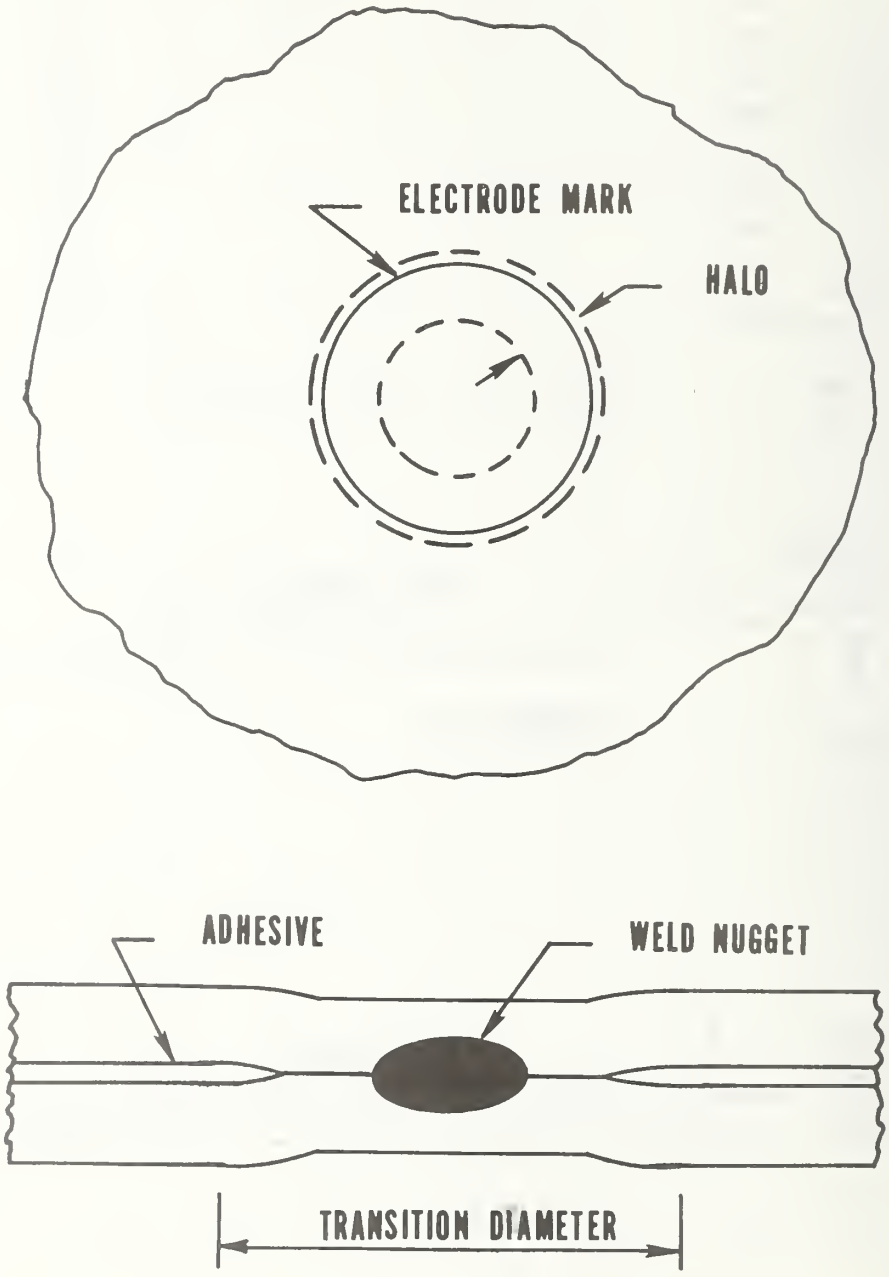

Figure 2. SCHEMATIC DESCRIPTION OF A SPOTWELD IN A SINGLE-LAP WELD-BONDED JOINT.

2.1 Planform Analysis

The general approach used here parallels one used earlier for the planform analysis of composite-reinforced cutouts and cracks [2, 3]. Figure 3(a) shows the network of triangular finite elements used for the analysis of the weldbonded joint shown in Figure 1 and a similar spotwelded joint. Figure 3(b) shows the network used for the analysis of a similar bonded joint. Because of symmetry about the x axis, only the upper half of a joint is analyzed. The joined sheets are each divided into separate networks of triangular, constant strain (linearly varying displacement), plane stress elements that are congruent within the overlap region. Within a bonded and/or welded region the two congruent networks are coupled together by an array of special shear-stiffness elements linking conjugate pairs of nodal points. External normal and shear loads are assumed to act only at the edge of a sheet, in the midplane, and out-of-plane deflections are ignored.

The direct stiffness matrices of the triangular elements are computed in the usual way (see, for example, Zienkiewicz [4]), but a different formulation based on the following assumptions is used to compute the shear stiffness coupling elements. Within the area of a spotweld nugget (Figure 2) there is no adhesive and the two metal sheets are assumed to be perfectly joined (continuous). There is also no adhesive in the halo region surrounding a nugget but here the two metal sheets are assumed to be unbonded. Within the shear-stiffness element the shear stress is assumed to vary linearly through the metal sheet thickness. That is, the shear stress is assumed to have a maximum value at the adhesive layer, or at the midplane of a weld nugget, and to decrease uniformly to zero at a free surface or at the midplane of a double-lap joint. The effective area of a shear-stiffness element in the x-y plane is assumed to be equal to one-third the sum of the triangular areas meeting at an overlap nodal point. The effective material thicknesses within an element are assumed to be the thicknesses at the location of the conjugate nodal points.

The stiffness matrices of the traingular and the shear-stiffness elements are superposed to form the stiffness matrix of the entire structure. This latter matrix [K] relates the external forces applied to the joint {F} to the resulting nodal point displacements {w} according to the equation

$$\{F\} = [K]\ \{w\} \qquad (1)$$

This equation can be solved for nodal point displacements {w} throughout the joint. Then, strains and stresses within the separate elements can be computed directly by matrix multiplication [1, 4].

2.2 Longitudinal Cross-Section Analysis

Figure 4 shows finite element networks used for the cross-section analysis of the comparable single-lap and double-lap weldbonded joints described in Figure 1. Thickness dimensions and computed vertical deflections are exaggerated. In the double-lap case, symmetry is imposed

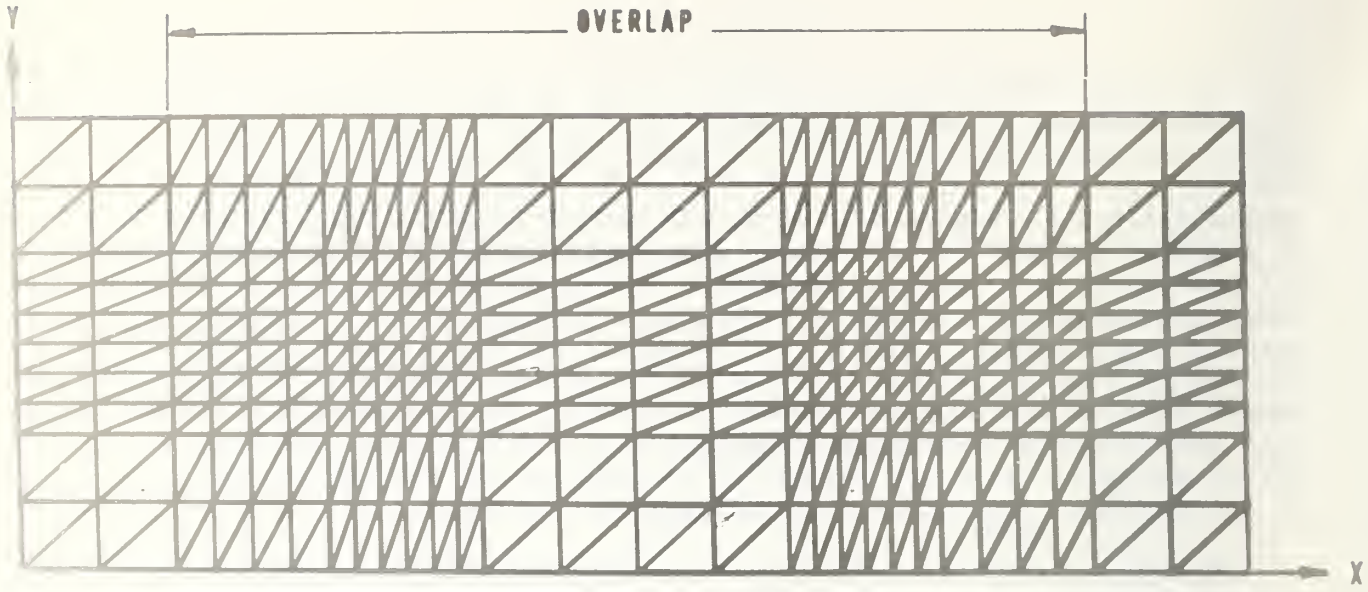

(a) WELDBONDED AND SPOTWELDED

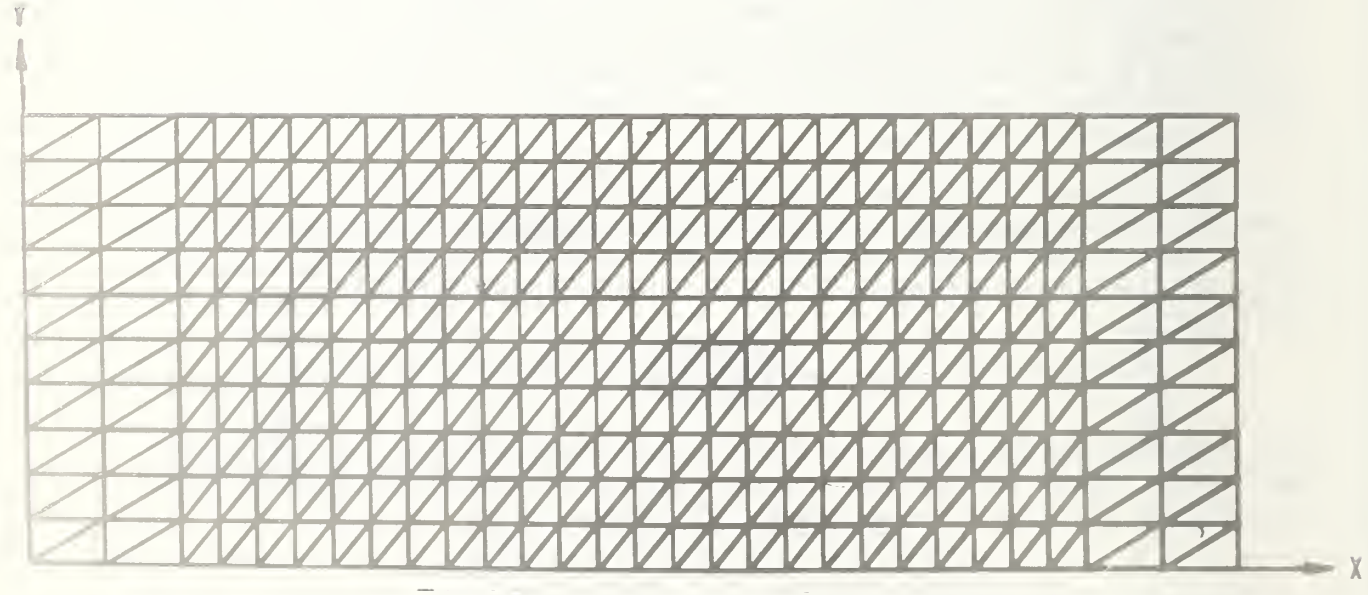

(b) BONDED

Figure 3. FINITE ELEMENT MESHES USED FOR PLANFORM ANALYSIS OF A WELDBONDED JOINT, A SPOTWELDED JOINT, AND A BONDED JOINT.

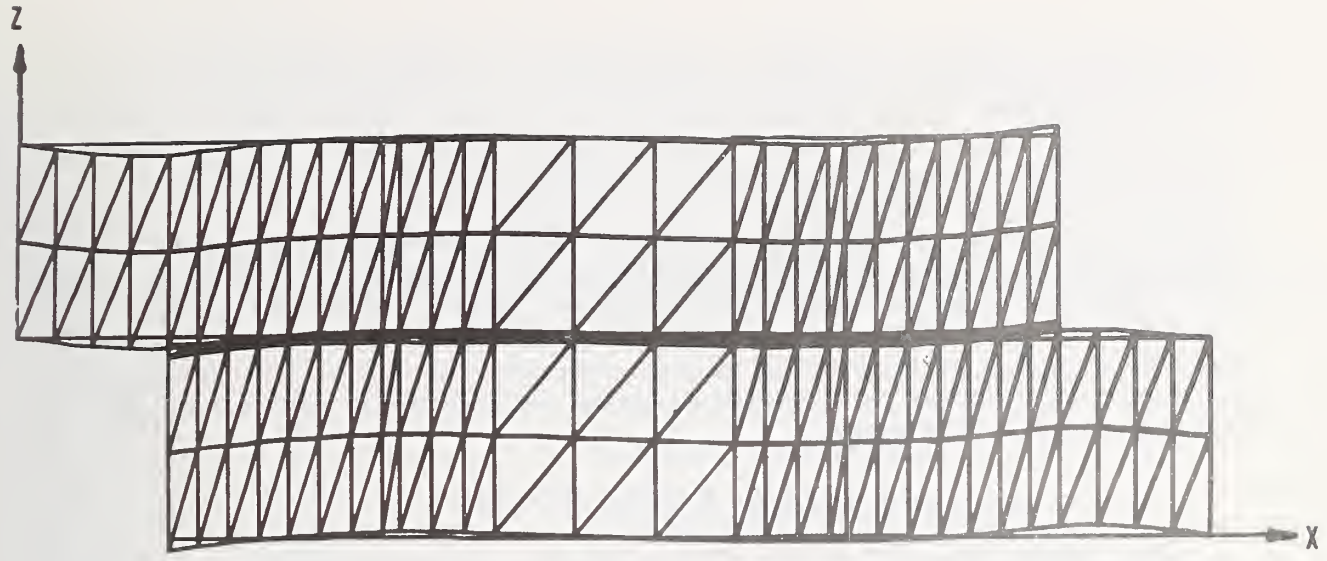

(a) SINGLE-LAP

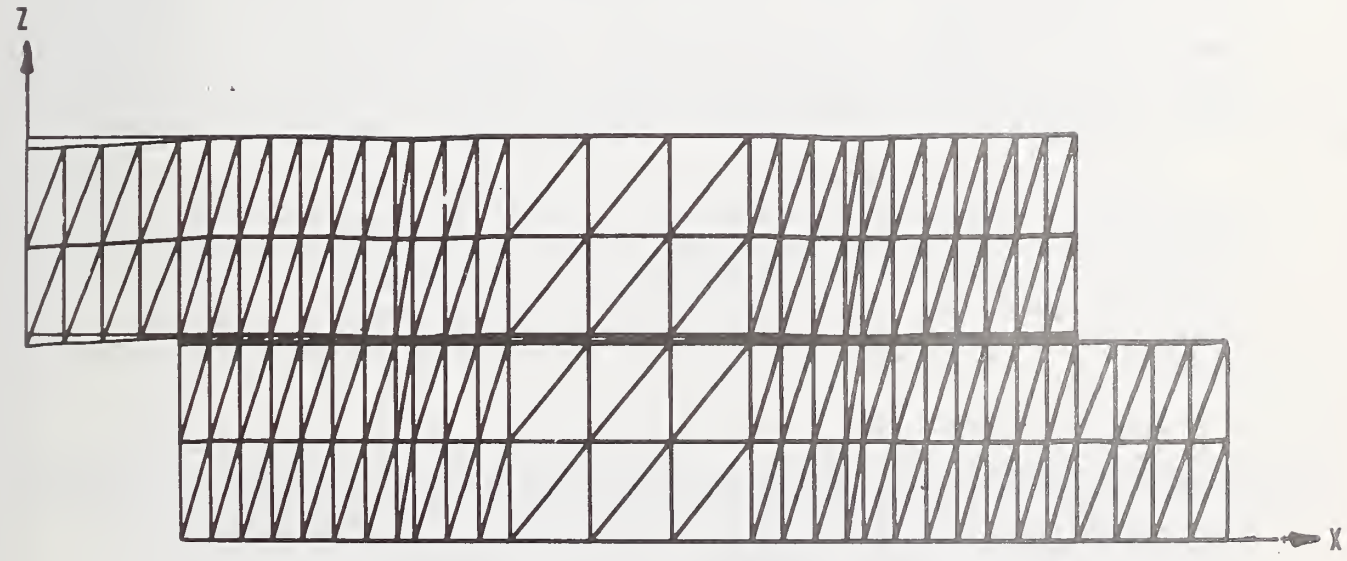

(b) DOUBLE-LAP

Figure 4. FINITE ELEMENT MESHES USED FOR LOGITUDINAL CROSS-SECTION ANALYSIS OF COMPARABLE SINGLE-LAP AND DOUBLE-LAP WELDBONDED JOINTS. THICKNESS DIMENSIONS EXAGGERATED 4 TIMES. VERTICAL DEFLECTIONS EXAGGERATED 20 TIMES.

about the horizontal (x) axis. In each case the sheet midthickness point at the left end was constrained with respect to x displacement and the load was applied to the midthickness point (of the finite element network) at the right end. In the cross-section analysis, linearly varying strain (quadratically varying displacement) elements are used to better approximate out-of-plane bending. The direct stiffness matrices of the triangular elements are computed using the area coordinate formulation described by Zienkiewicz [4]. The spotweld nuggets are approximated by triangular bondline elements of metal, rather than adhesive, equal in area (in plan) to the circular area of the spotwelds. A nugget region is bounded on each side by a region of transition to full adhesive thickness. The bondline thickness in a nugget or transition region is reduced to approximate the average adhesive thickness.

2.3 Bending Effects

The importance of bending effects will be demonstrated by a comparison of numerical results from both the planform and the longitudinal-cross-section computer programs. These results are for the joints shown in Figure 1 subjected to an applied tensile stress of 69 MPa (10,000 lbf/in^2). The joint materials were assumed to be linear elastic and isotropic with the following elastic constants:

Metal sheet: $E = 68.4$ GPa $(9.92 \times 10^6\ lbf/in^2)$, $\nu = 0.318$
Adhesive: $E = 4.67$ GPa $(0.677 \times 10^6\ lbf/in^2)$, $\nu = 0.35$

Figure 5 compares the adhesive shear stresses, τ, for the single-lap weldbonded joint as computed by the planform analysis with those computed by the cross-section analysis. The difference in shear stress distribution is largely due to joint bending which is included in the cross-section analysis but not in the planform analysis. This explanation is supported by a similar plot for a comparable double-lap joint (Figure 6) which shows much better agreement between the planform and the cross-section analyses.

Figure 7 compares the adhesive normal stresses (peel component, σ_z) computed by the cross-section analysis for both the single-lap and comparable double-lap weldbonded joints. The peak tensile stress values at the right end differ by less than 6 percent. The symmetry constraint imposed in the double-lap case causes the normal stress peak to be compressive at the left end. Peel stresses are not computed in the planform analysis.

Figure 8 compares the strains on the upper surface of the single-lap weldbonded joint as computed by the planform analysis with those computed by the cross-section analysis. The plotted points were obtained by applying a bending correction to the planform results. The bending curvatures (evident in Figure 4) were determined from the cross-section results by fitting a second degree curve through groups of five adjacent nodal points

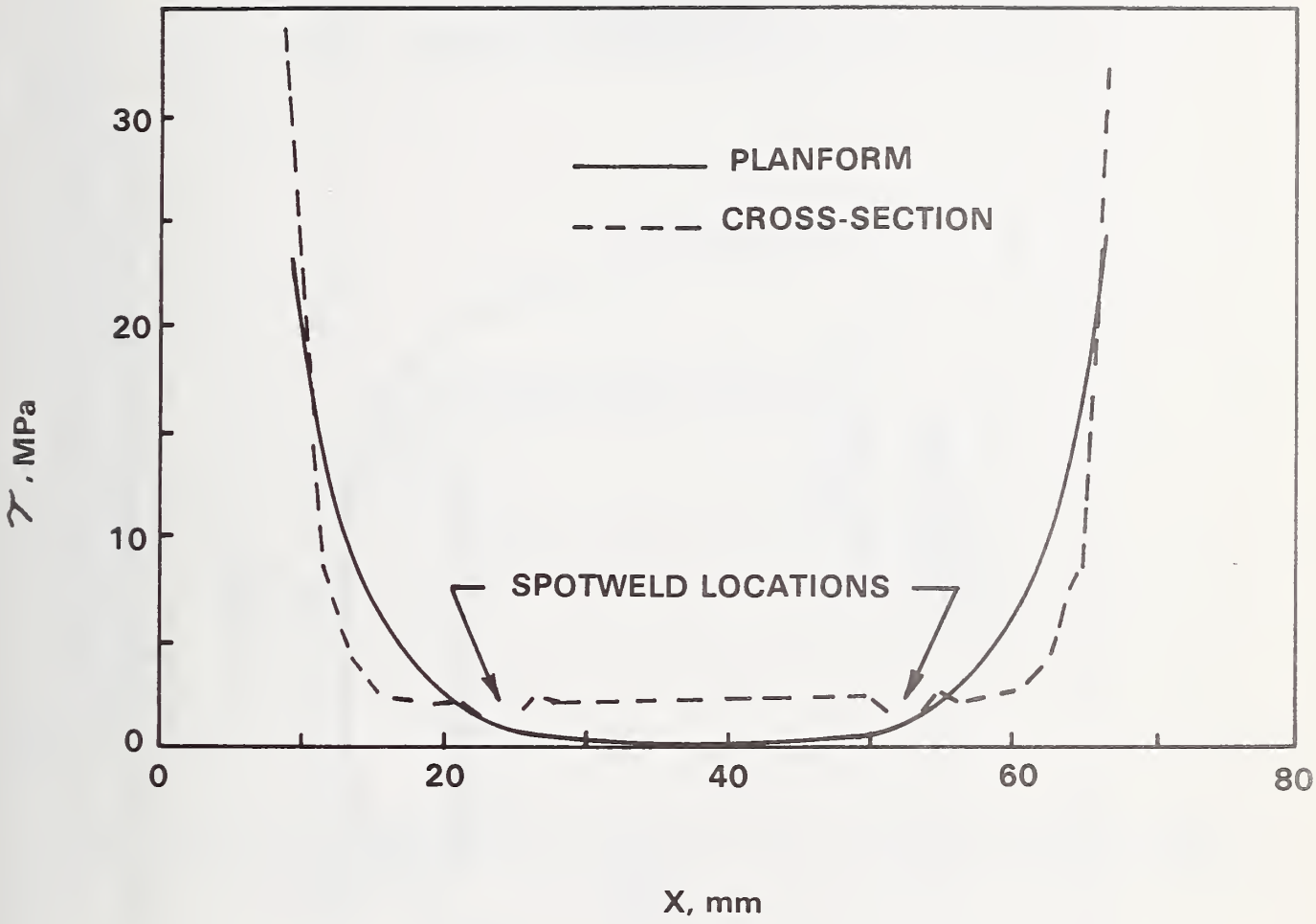

Figure 5. ADHESIVE LAP SHEAR STRESS IN SINGLE-LAP WELDBONDED JOINT, FROM PLANFORM ANALYSIS AND CROSS-SECTION ANALYSIS.

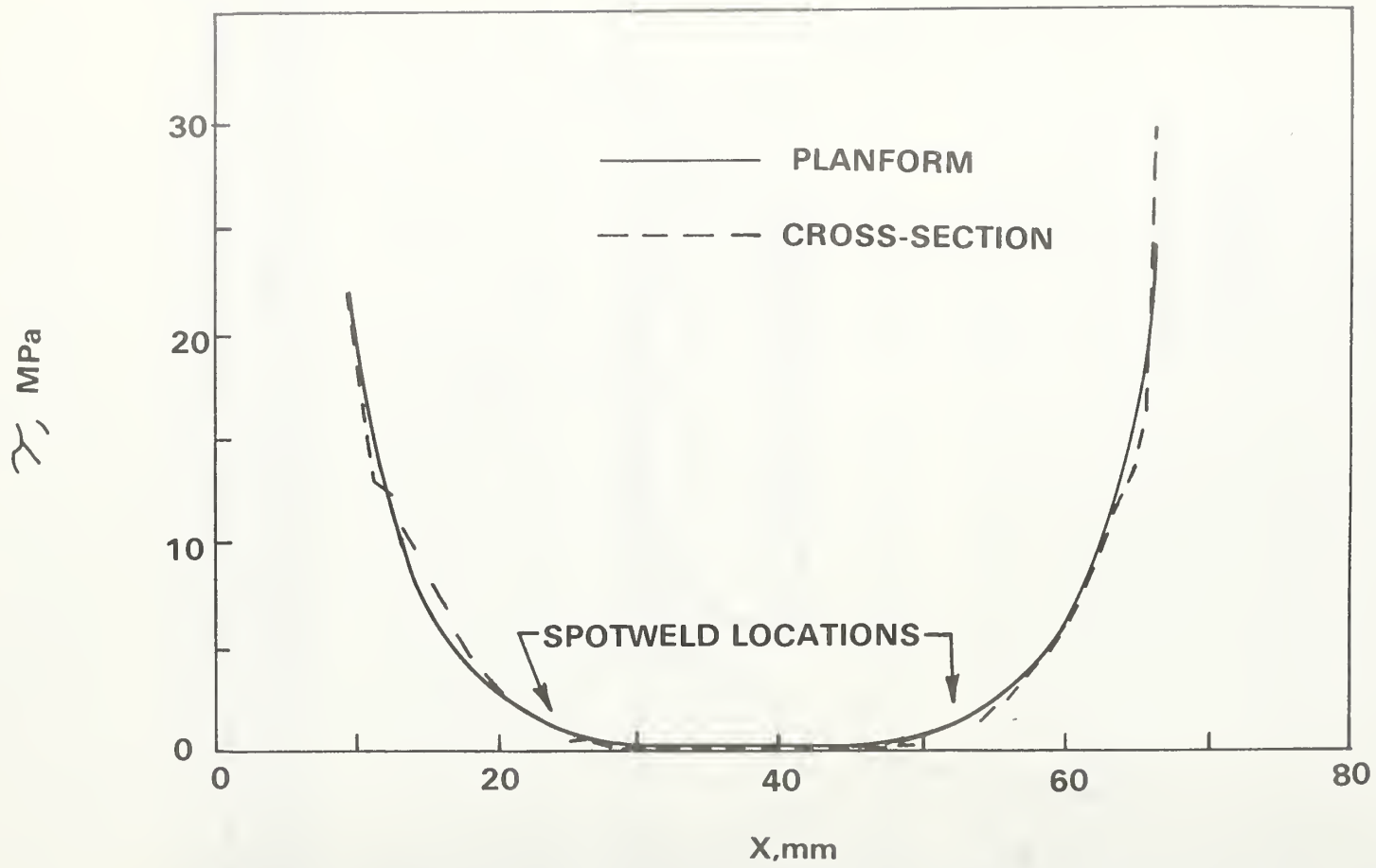

Figure 6. ADHESIVE LAP SHEAR STRESS IN DOUBLE-LAP WELDBONDED JOINT, FROM PLANFORM ANALYSIS AND CROSS-SECTION ANALYSIS.

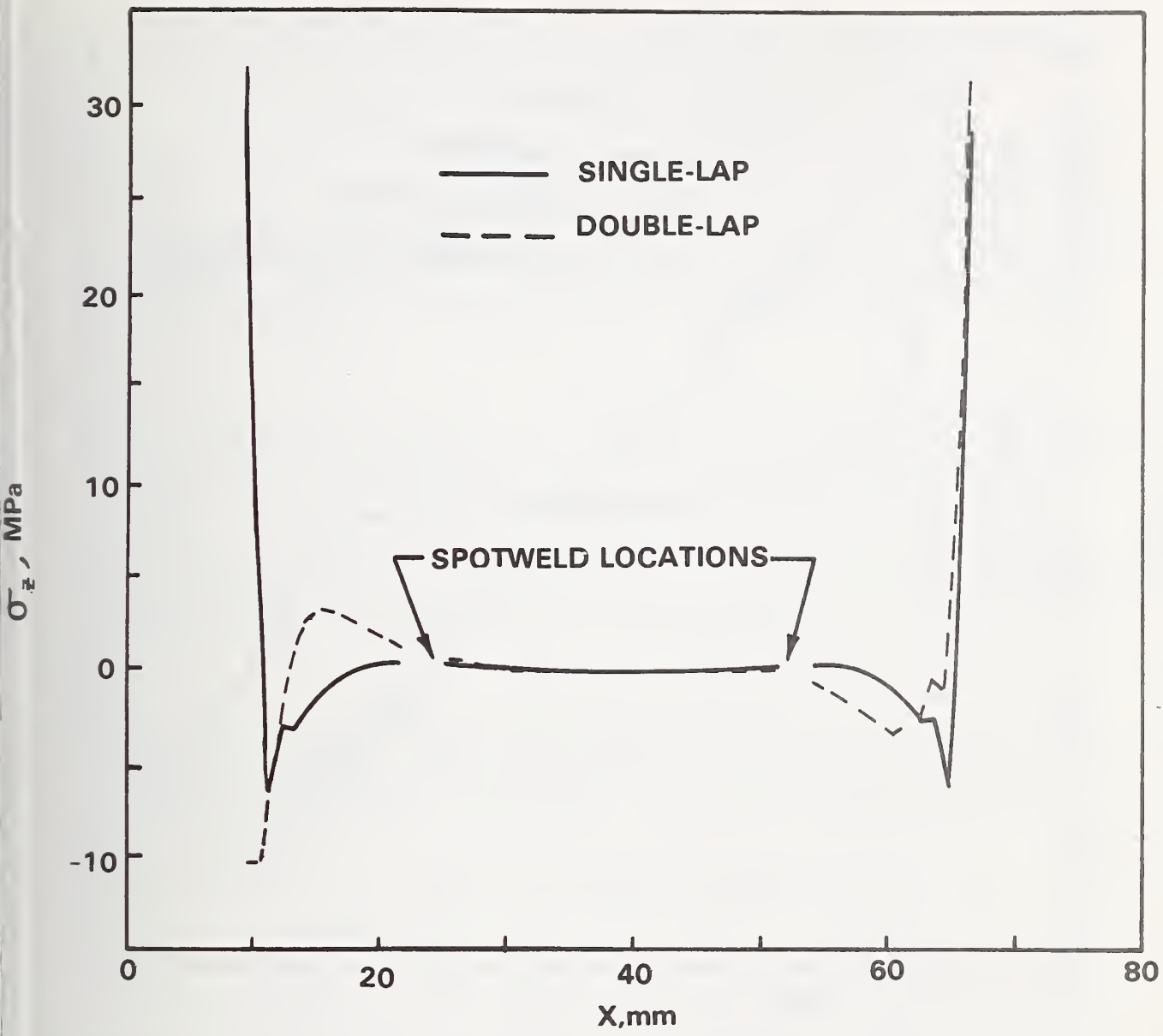

Figure 7. ADHESIVE NORMAL (PEEL) STRESS IN COMPARABLE SINGLE-LAP AND DOUBLE-LAP WELDBONDED JOINTS, FROM CROSS-SECTION ANALYSIS.

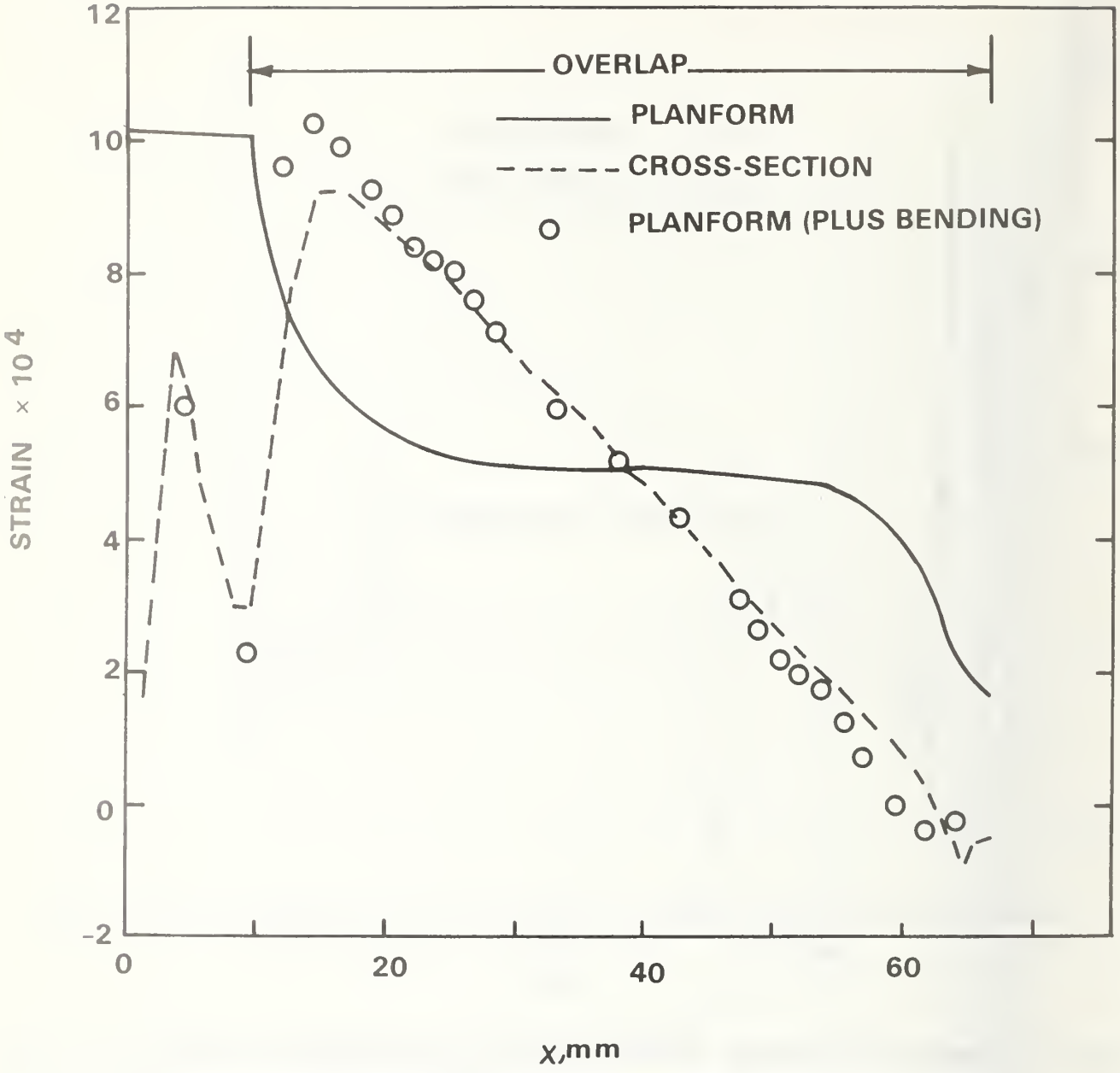

Figure 8. LONGITUDINAL STRAIN ON SURFACE OF SINGLE-LAP WELDBONDED JOINT.

along the length of the joint. The components of surface strain due to bending were then computed directly from these curvatures by assuming a linear variation in bending strain through the joint thickness.

Figure 9 compares the surface strains for the double-lap weldbonded joint as computed by the planform analysis with those computed by the cross-section analysis. Although bending is prevented by symmetry along the x axis in the cross-section analysis, there is some bending of the outer sheet at each end of the overlap, and there is considerable bending beyond the overlap (Figure 4). The plotted points were obtained by applying a bending correction (from the cross-section analysis) to the planform results.

3. NONLINEAR ANALYSIS

Nonlinear algorithms were developed to account for nonlinear stress-strain characteristics of the adhesive and the metal sheet, nonlinear cyclic loading, adhesive debonding, and weld-heat softening of the metal sheet. The nonlinear modes of response are simulated by a sequence of linear solutions. Between successive linear solutions, the linear material constants and/or bond couplings of the different finite elements are individually adjusted according to their stress state and, in the case of cyclic loading, according to their stress history.

3.1 Nonlinear Adhesive Shear

The nonlinear adhesive algorithms assume the shear stress-strain characteristics described schematically in Figure 10. The single valued function represented by the smooth curve passing through the origin is, in the first quadrant, defined by

$$\gamma = f(\tau) = \begin{cases} \dfrac{\tau}{G_o - A \exp\left[-B(\tau - \tau_p)^{-C}\right]}, & \tau > \tau_p \\ \dfrac{\tau}{G_o}, & 0 \leq \tau \leq \tau_p \end{cases} \qquad (2)$$

in which G_o, A, B, C, and τ_p are empirical material constants. For a material with an initial linear elastic range, G_o is the linear elastic shear modulus and τ_p is the proportional limit stress. The relationship plotted in Figure 10 was determined by fitting a curve to data from three similar "napkin ring" torsion tests on samples of the adhesive used to fabricate the lap joint test specimens.* The empirical material constants,

*These adhesive shear stress-strain data were furnished by Feltman Research Laboratory, Picatinny Arsenal, Dover, NJ. The torsion tests were conducted by the Singer Co., Little Falls, NJ, using the measurement techniques described in Reference 5.

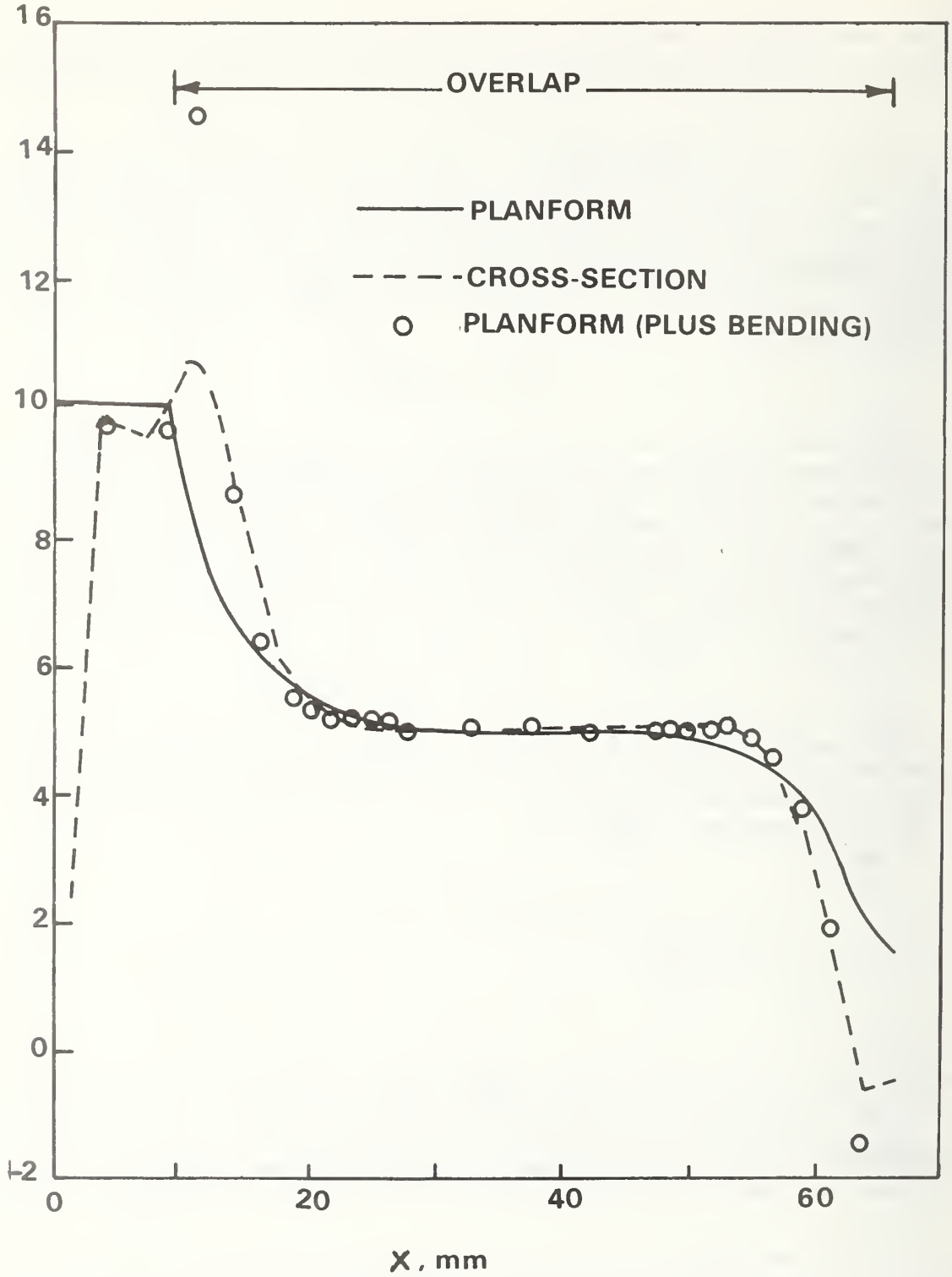

Figure 9. LONGITUDINAL STRAIN ON SURFACE OF DOUBLE-LAP WELDBONDED JOINT.

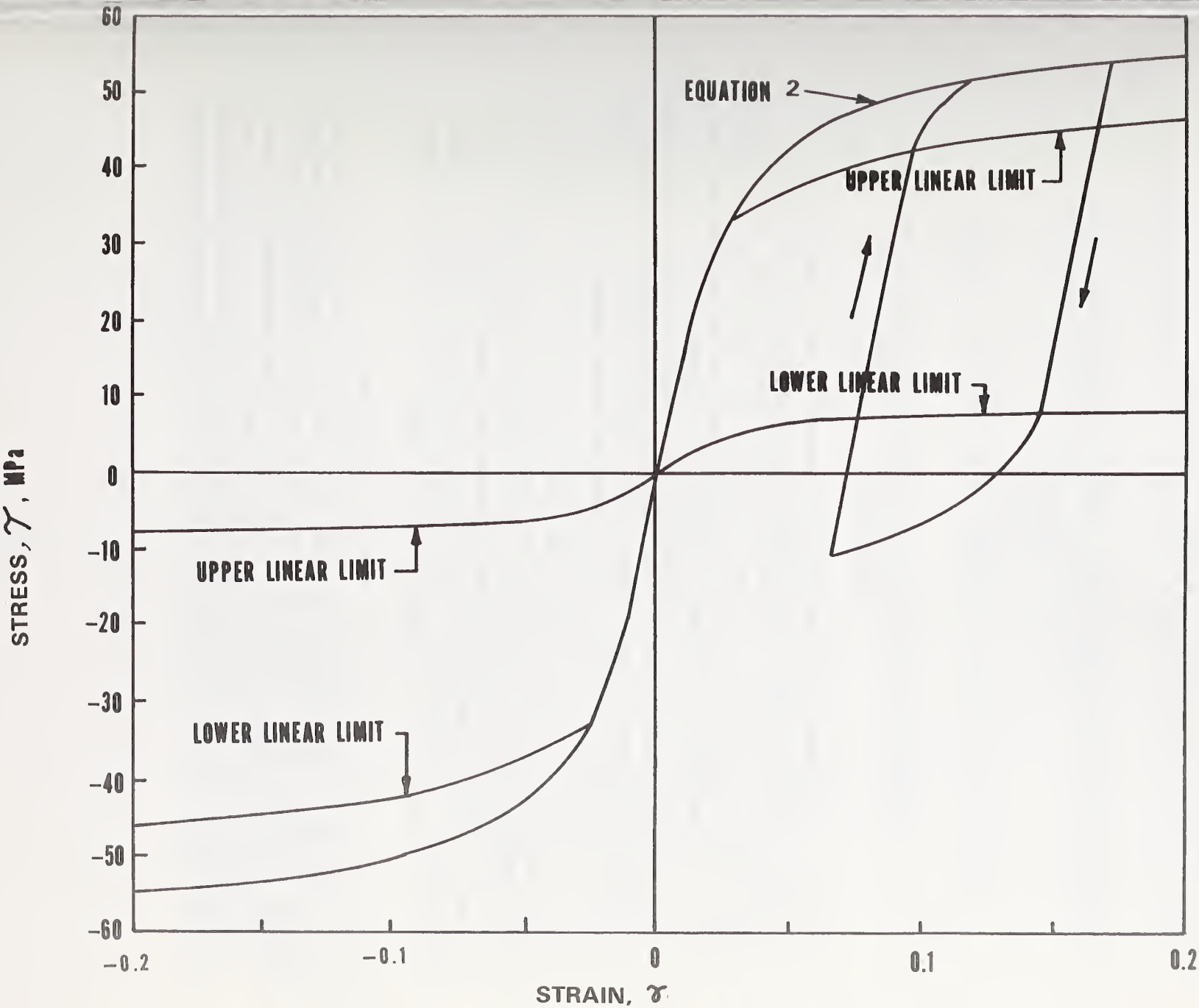

Figure 10. SCHEMATIC DESCRIPTION OF ASSUMED NONLINEAR SHEAR STRESS-STRAIN CHARACTERISTICS OF ADHESIVE.

where modulus and stress are expressed in MPa, are

$$G_o = 1.729 \times 10^9$$
$$A = 468.46 \times 10^9$$
$$B = 2949.3$$
$$C = .35$$
$$\tau_p = 0$$

If modulus and stress are expressed in lbf/in^2, the constants are

$$G_o = .2508 \times 10^6$$
$$A = 67.942 \times 10^6$$
$$B = 133.73$$
$$C = .35$$
$$\tau_p = 0$$

The elastic modulus of the nonlinear adhesive is assumed to be given by

$$E = 2G(1 + \nu) \qquad (3)$$

in which ν is Poisson's ration, which is assumed to be constant, and G is a variable secant modulus. The effective shear modulus of any finite element depends on both the stress and the stress history of that element. Specifically, an algebraic increase in stress to a point below an "upper linear limit" results in a linear algebraic increase in strain; an algebraic increase above an "upper linear limit" results in a nonlinear algebraic increase in strain. An algebraic decrease in stress to a point above a "lower linear limit" results in a linear algebraic decrease in strain; an algebraic decrease below a "lower linear limit" results in a nonlinear algebraic decrease in strain. If a change in stress results in an intersection with the single-valued stress-strain curve passing through the origin (defined by equation (2) in the first quadrant) further change in stress results in a change in strain along that curve. All linear stress-strain segments have a slope defined by the constant shear modulus G_o. The nonlinear stress-strain segments, other than equation (2), are programmed as explicit analytical functions with several coefficients read in as data. The coordinates of the discrete points that define the segmented "linear limits" are also read in as data.

a. Planform Algorithms

Nonlinear algorithms in the planform analysis account for three different nonlinear modes of response in the adhesive. One nonlinear mode occurs when the adhesive shear stresses are increased monotonically to a level above the proportional limit stress; a second mode occurs when these stresses are increased and decreased cyclically; a third mode occurs when these stresses exceed a prescribed limiting value and the adhesive debonds.

The monotonic loading algorithm searches for a finite element solution at each of a sequence of levels of increasing applied load. For each solution the adhesive shear stresses and strains throughout the joint are defined by a single-valued function such as equation (2). The algorithm for finding a solution for a particular level of applied load is:

1. Obtain a finite element solution for nodal point displacements throughout the joint. (This may be either the next previous solution at the current load level or a linearly scaled solution for a lower load level.)

2. Adjust the adhesive shear modulus of each shear coupling element. Perform steps a through d for each shear coupling element.

   a) Find the shear stress and strain for the element from the nodal displacements by matrix multiplication (point 1 in Figure 11).

   b) Find the point on the nonlinear stress-strain curve with the same strain value as the point found in step a (point 2 in Figure 11).

   c) Compute a secant modulus G* which is the slope of the line from the origin to the point found in step b (line 0-2 in Figure 11).

   d) Given G as the previous shear modulus for the element, compute a new shear modulus

$$\hat{G} = G + \beta(G^* - G)$$

   where β is the same for all elements and acts as a multiplier for the change in shear modulus. This is used to speed convergence.

3. Repeat steps 1 and 2 until converged.

The cyclic loading algorithm searches for finite element solutions, at each of a sequence of levels of cyclically changing applied load. For each solution the adhesive shear stresses and strains throughout the joint are defined by nonlinear cyclic loading and unloading relationships of the type described schematically in Figure 10. The initial finite element solution of a sequence of cyclic loading solutions is obtained by the monotonic loading algorithm. Subsequent finite element solutions for nodal point displacements at particular levels of applied cyclic load are obtained by the following algorithm.

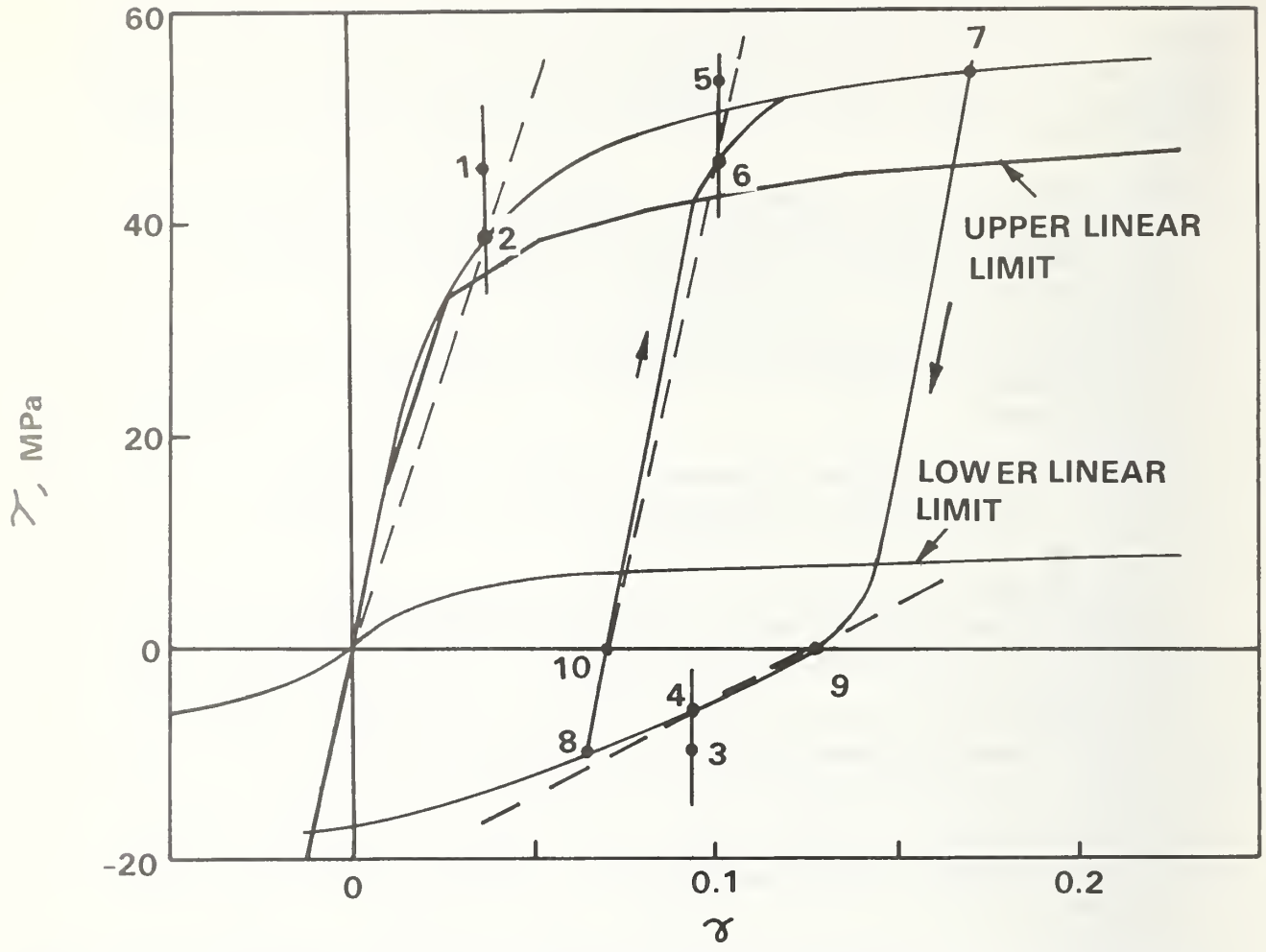

Figure 11. SCHEMATIC STRESS-STRAIN PLOT FOR NONLINEAR ANALYSIS ALGORITHMS.

1. Solve the linear problem using the element material properties of the final solution at the previous load.

2. Adjust the adhesive shear modulus. Perform steps a through g for each shear coupling element.

   a) Find the shear stress and strain for the element from the nodal displacements by matrix multiplication (points 3 and 5 for the two examples in Figure 11).

   b) Find the nonlinear stress-strain curve for this element. This is based on the solution at the last maximum or minimum load and whether this is an increasing or decreasing portion of the cycle. (The solution for the previous maximum or minimum is point 7 or 8 respectively in Figure 11.)

   c) Find the point on the curve with the same strain value as the point found in step a (points 4 and 6 in Figure 11).

   d) Find the point where the curve found in step b crosses the strain axis (points 9 and 10 in Figure 11).

   e) Compute a secant modulus G* which is the slope of the line from the point found in step c to the point found in step d (lines 9-4 and 10-6 in Figure 11). This is equivalent to translating the coordinate system and forces G* to be positive, better approximating the nonlinear curve.

   f) Given G as the previous shear modulus for the element, compute a new shear modulus

$$\hat{G} = G + \beta(G^* - G)$$

   where β is the same for all elements.

   g) Compute an "initial strain" for the element to correct for the fact that the lines found in step e do not pass through the origin. The amount of this "initial strain" is equal to the strain value of the point found in step d.

3. Repeat steps 1 and 2 until converged.

The adhesive debond algorithm effectively uncouples the shear-stiffness elements for which the next previous finite element solution indicated adhesive shear stresses above a prescribed limiting value. This algorithm can be used in conjunction with either the monotonic loading algorithm or the cyclic loading algorithm.

b. Longitudinal Cross-Section Algorithm

The only algorithm included in the longitudinal cross-section analysis to account for nonlinear adhesive deformation is a monotonic loading algorithm. This algorithm is the same as the monotonic loading algorithm in the planform analysis except for the following modification to step 2:

b) Find the point on the nonlinear stress-strain curve with the same stress value as the point found in step 2a.

3.2 Nonlinear Metal Algorithm

The nonlinear metal algorithm assumes a single-valued normal stress-strain relationship of the type represented by the solid curve in Figure 12. This curve is of the form

$$\varepsilon = f(\sigma) = \begin{cases} \dfrac{\sigma}{E_o - A \exp\left[-B(\sigma - \sigma_p)^{-C}\right]}, & \sigma > \sigma_p \\ \dfrac{\sigma}{E_o}, & 0 \leq \sigma \leq \sigma_p \end{cases} \qquad (4)$$

in which E_o, A, B, C, and σ_p are empirical material constants. For a material with an initial linear elastic range, E_o is the elastic modulus and σ_p is the proportional limit stress. The relationship plotted in Figure 12 was determined by fitting a curve (equation (4)) to a portion of a stress-strain curve for 7075-T6 aluminum alloy given in Reference 6. For that curve fit, the empirical material constants, where modulus and stress are expressed in MPa, are

$$E_o = 68.74 \times 10^9$$
$$A = 3.7914 \times 10^{27}$$
$$B = 271.82$$
$$C = .1$$
$$\sigma_p = 275.8 \times 10^6$$

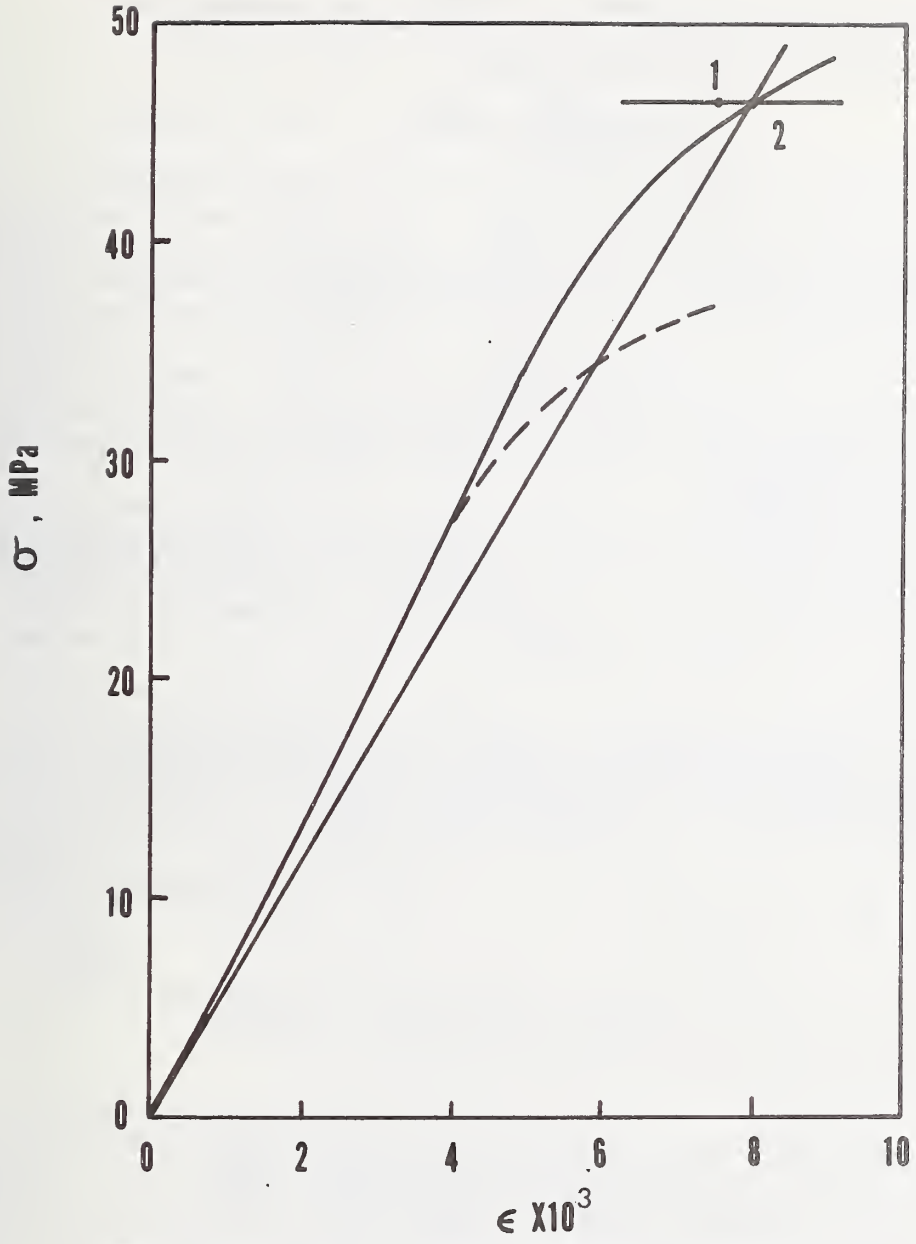

Figure 12. STRESS-STRAIN PLOT FOR METAL SHOWING OFFSET DUE TO WELD-HEAT SOFTENING.

If modulus and stress are expressed in lbf/in^2, the constants are

$$E_o = 9.97 \times 10^6$$
$$A = 5.4988 \times 10^{23}$$
$$B = 112.31$$
$$C = .1$$
$$\sigma_p = 40.0 \times 10^3$$

The shear modulus of the metal is assumed to be given by

$$G = \frac{E}{2(1 + \nu)} \tag{5}$$

in which ν is Poisson's ratio, which is assumed to be constant, and E is a variable secant modulus.

A single algorithm is used for either monotonic or cyclic loading in both the planform analysis and the longitudinal cross-section analysis. The algorithm below searches for a finite element solution for which the normal stresses in the metal are defined by a single-valued function such as equation (4).

1. Obtain a finite element solution for nodal point displacement throughout the joint. (This may be either the next previous solution at the current load level or a linearly scaled solution for a different load level.)

2. Adjust the metal elastic modulus. Repeat steps a through d for each metal element.

   a) Find the longitudinal (x axis) normal stress and strain for the element from the nodal displacements and matrix multiplication (point 1 in Figure 12).

   b) Find the point on the nonlinear stress-strain curve with the same stress value as the point found in step a (point 2 in Figure 12).

   c) Compute a secant modulus E* which is the slope of the line from the origin to the point found in step b (line 0-2 in Figure 12).

   d) Given E as the previous elastic modulus for the element, compute a new elastic modulus

$$\hat{E} = E + \beta(E^* - E)$$

where β is the same for all elements and acts as a multiplier for the change in elastic modulus.

3. Repeat steps 1 and 2 until converged.

A variation of the above algorithm is used to account for weld-heat softening of the metal sheet. Figure 13 illustrates the variation in metal hardness as a function of distance from the weld nugget for a weld-bonded specimen of 7075-T6 aluminum alloy.* The plotted curve is a cubic polynomial fitted to the data points. The weld-heat-softening algorithm is based on two assumptions: (1) that there is a percentage reduction in the proportional limit stress equal to the percentage reduction in microhardness number; (2) that the shape of the nonlinear portion of the stress-strain curve is not changed. These assumptions are illustrated by the dashed curve in Figure 12, corresponding to a 40 percent reduction in the microhardness number. For finite elements affected by weld-heat softening, the nonlinear algorithm uses the appropriately translated single-valued stress-strain curve.

3.3 Numerical Examples

The following numerical examples illustrate some types of results that can be obtained using the nonlinear algorithms. The nonlinear stress-strain relationships used are those shown in Figure 10 and 12. To conserve on computer costs for these numerical examples, the single-valued stress-strain curve for the adhesive was assumed to be linear, with a slope of G_o, up to a shear stress level of 13.8 MPa (2000 lbf/in^2). The linear elastic material constants used are:

Metal: $E = 68.74$ GPa (9.97×10^6 lbf/in^2), $\nu = 0.318$
Adhesive: $G_o^o = 1.729$ GPa (0.2508×10^6 lbf/in^2), $\nu = 0.35$

a. Monotonically Increasing Load

A sequence of solutions involving adhesive yielding, progressive debonding, and weld-heat softening were obtained for the single-lap weld-bonded joint shown in Figure 1, using the planform computer program and the finite element mesh shown in Figure 14. Two solutions were first obtained for an applied longitudinal tensile stress of 138 MPa (20 000 lbf/in^2) and then two solutions were obtained for twice that applied stress. At each load level, one solution assumed linear elastic material properties throughout and the other solution assumed the nonlinear stress-strain relationships. Figure 15 gives the adhesive shear stress variation along the longitudinal centerline of the joint for the four solutions. These

*These Knoop microhardness data were furnished by Feltman Research Laboratory, Picatinny Arsenal, Dover, NJ.

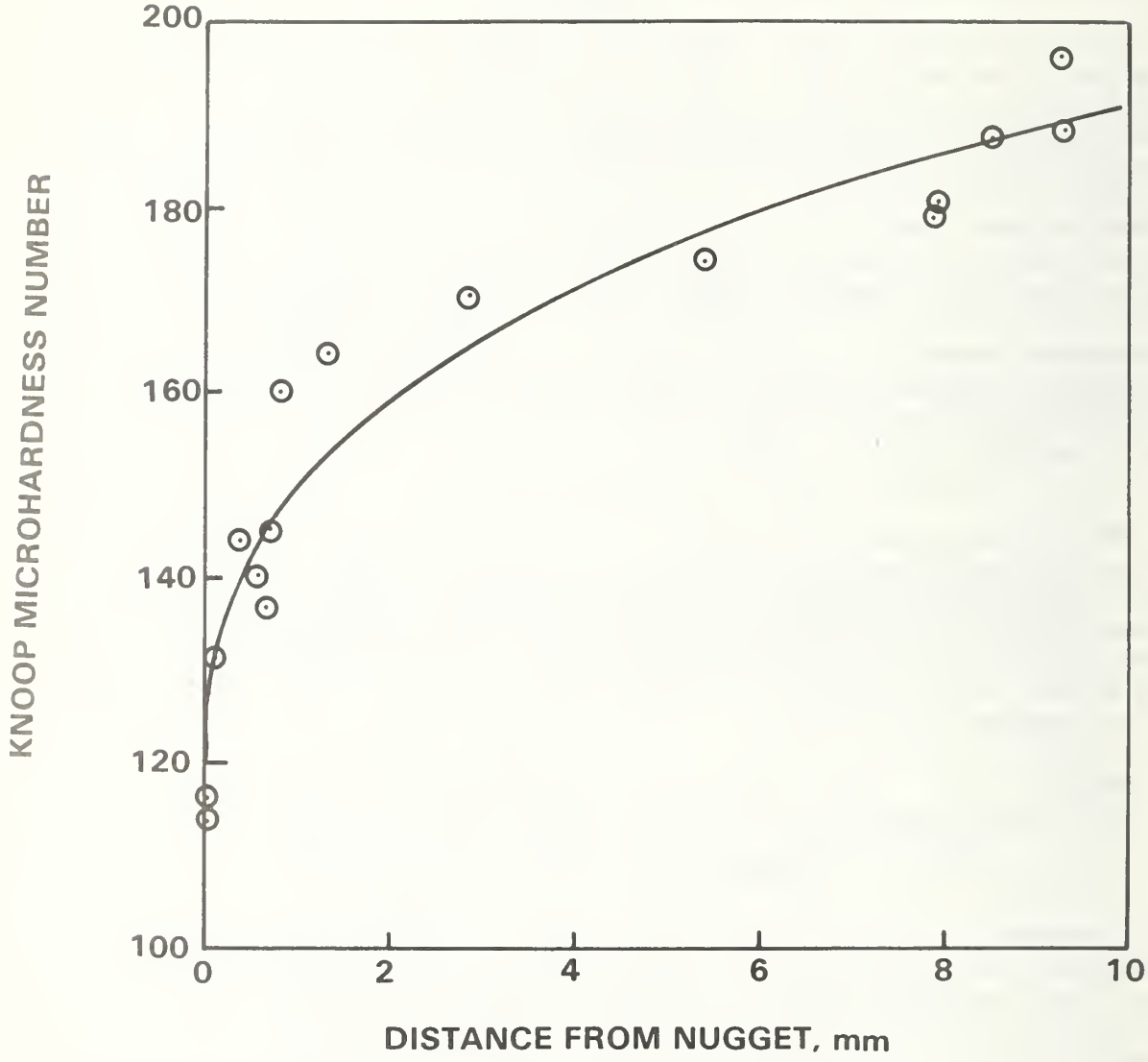

Figure 13. VARIATION IN HARDNESS ADJACENT TO SPOTWELD NUGGET.

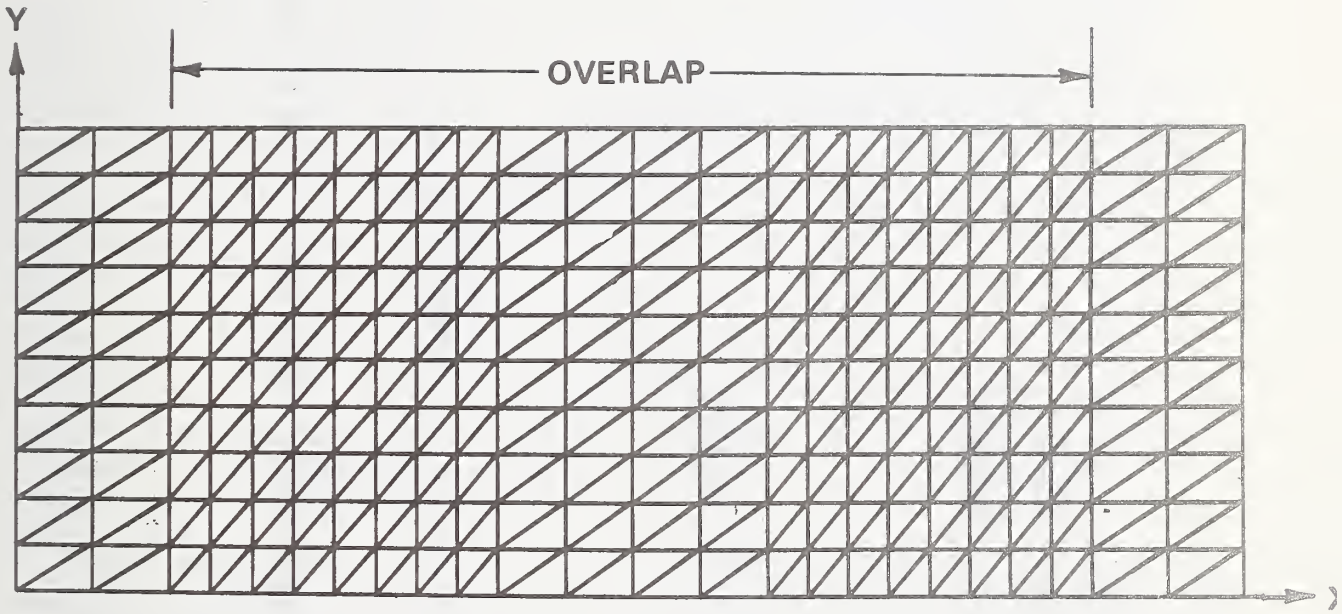

Figure 14. FINITE ELEMENT MESH USED FOR NONLINEAR PLANFORM ANALYSIS OF WELDBONDED JOINT.

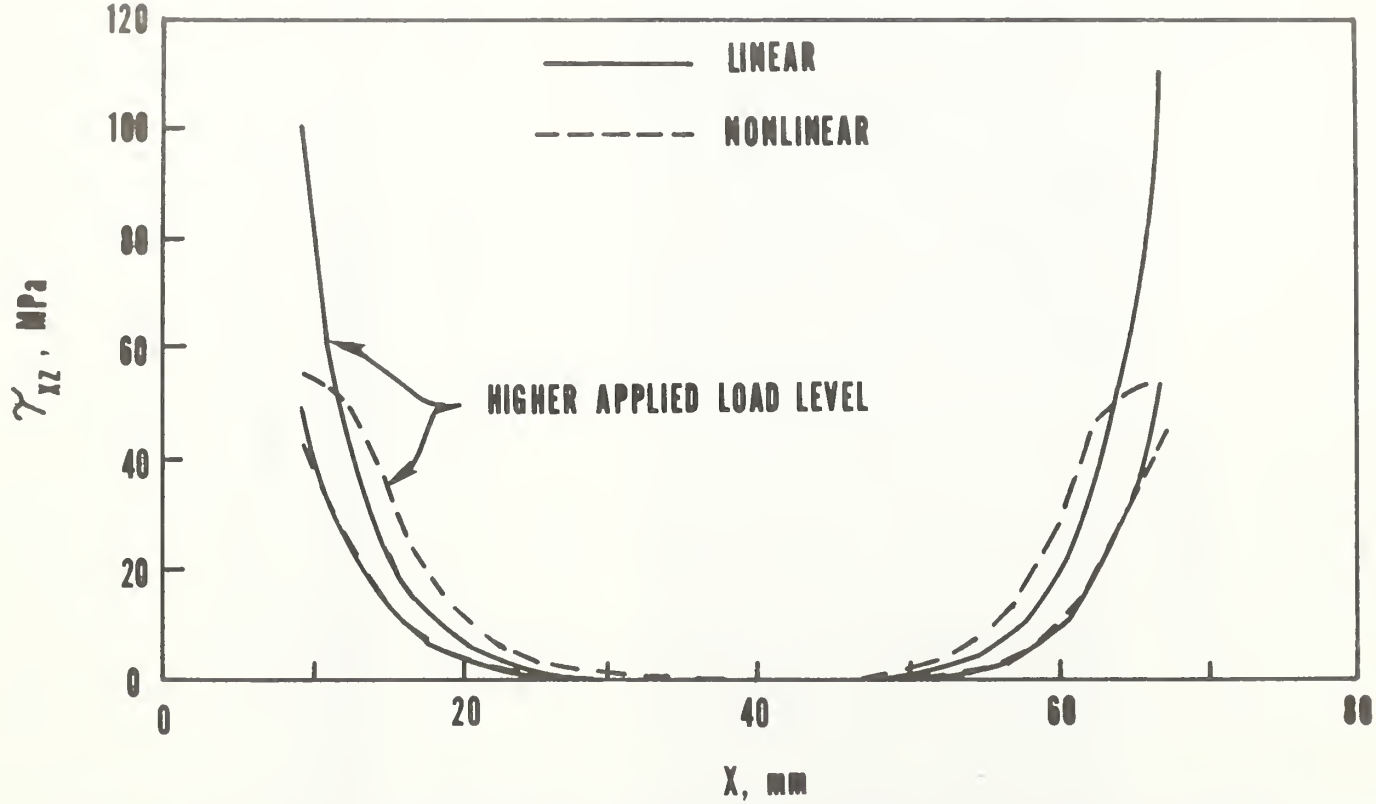

Figure 15. ADHESIVE SHEAR STRESS FROM LINEAR ANALYSIS AND NONLINEAR ANALYSIS.

results indicate a 19 percent reduction in peak stress due to adhesive nonlinearity at the lower load level and a 51 percent reduction at the higher load level. Figure 16 shows contour plots of lap shear stress for the two solutions at the higher load level. The adhesive nonlinearity accounts for the great reduction in the lap shear stress magnitude and stress gradient near the end of the overlap as well as the increase in stress gradient near the spotwelds.

Two additional nonlinear solutions were then obtained for an applied tensile stress of 276 MPa (40 000 lbf/in^2) with the assumption that any pair of conjugate nodal points in the metal adherends were uncoupled (debonded) where the adhesive shear stress exceeded 55 MPa (8000 lbf/in^2). Thus, there was a sequence of three nonlinear solutions at this load level. In the first of these solutions, the stresses at the nodal points at each corner of the overlap region were slightly over the debond stress. Therefore these corner points were uncoupled for the second nonlinear solution at this load level. In the second nonlinear solution, three additional nodal points near each corner were slightly over the debond stress, and therefore they were uncoupled for the third solution. In the third solution, a total of seventeen nodal points in the upper half of the joint were either already debonded or over the debond stress limit. These three solutions illustrate progressive debonding without any increase in applied tensile stress. Figure 17 shows contour plots of lap shear stress for two of these partial-debond solutions. The dark regions are dense contours linearly interpolated by the computer program between uncoupled points of zero stress and points of peak stress.

The applied tensile stress was then increased to 345 MPa (50 000 lbf/in^2) for a solution well within the nonlinear range of the metal sheet. The previous solutions in this sequence had involved no nonlinear deformation of the metal. For this solution it was assumed that the proportional limit of the metal in the vicinity of the spotwelds was reduced as described by the curves in Figures 12 and 13 due to weld-heat softening. It was also assumed that the seventeen nodal points that were debonded according to the previous solution at the 276 MPa (40 000 lbf/in^2) applied stress level remained uncoupled. Contour plots of the resulting lap shear stress and longitudinal tensile stress in the metal are given in Figure 18. No significant perturbation of the longitudinal tensile stress in the metal sheet due to weld-heat softening is evident in Figure 18(b). This is understandable, because the tensile stress levels indicated in the vicinity of the rightmost spotweld represent relatively small deviations from linearity, although they are above the proportional limit of the weld-softened metal.

b. Cyclic Load

A sequence of four solutions representing two cycles of loading into the nonlinear-adhesive range were obtained for the single-lap weldbonded joint shown in Figure 1 (but with an adhesive thickness of 0.066 mm (0.0026 in)) and the analysis mesh shown in Figure 14. An initial linear

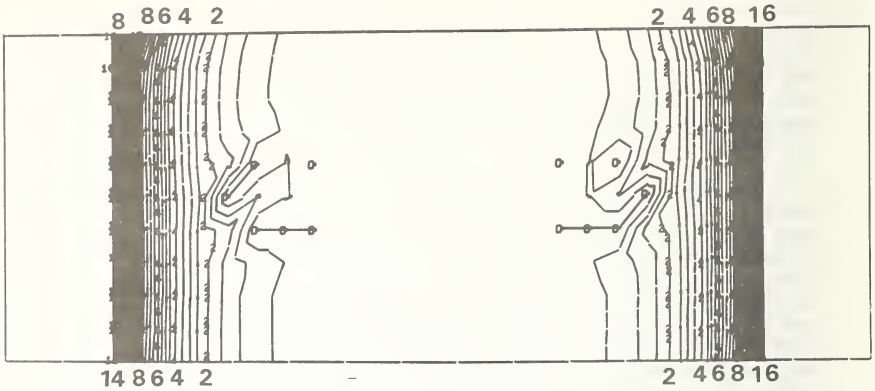

(a) LINEAR ANALYSIS

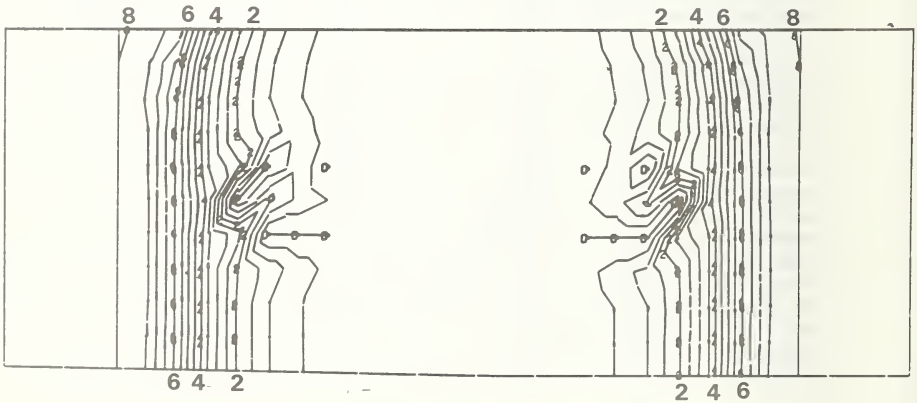

(b) NONLINEAR ANALYSIS

Figure 16. CONTOUR PLOTS OF LAP SHEAR STRESS AT HIGHER APPLIED LOAD LEVEL. CONTOUR INTERVAL IS 500 lbf/in^2 (3.45 MPa).

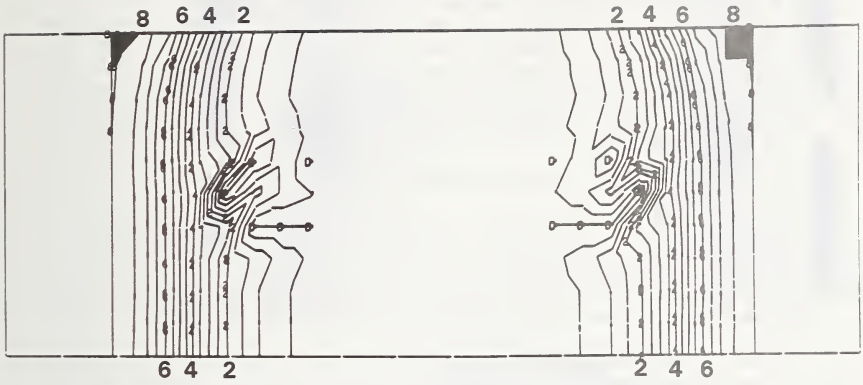

(a) TWO POINTS DEBONDED

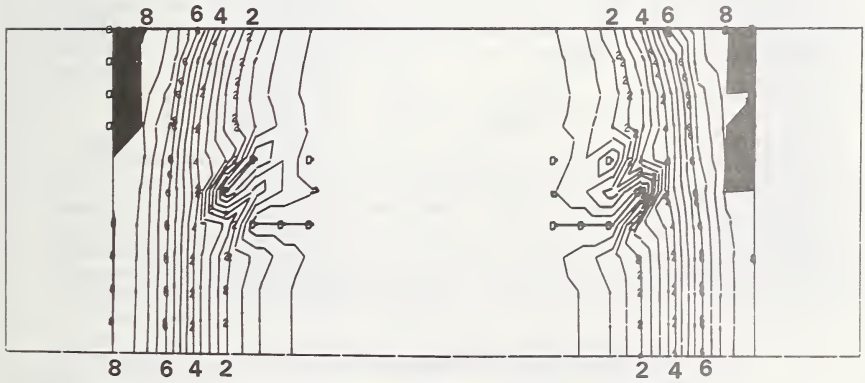

(b) EIGHT POINTS DEBONDED

Figure 17. CONTOUR PLOTS OF LAP SHEAR STRESS SHOWING PARTIAL DEBOND. CONTOUR INTERVAL IS 500 lbf/in^2 (3.45 MPa).

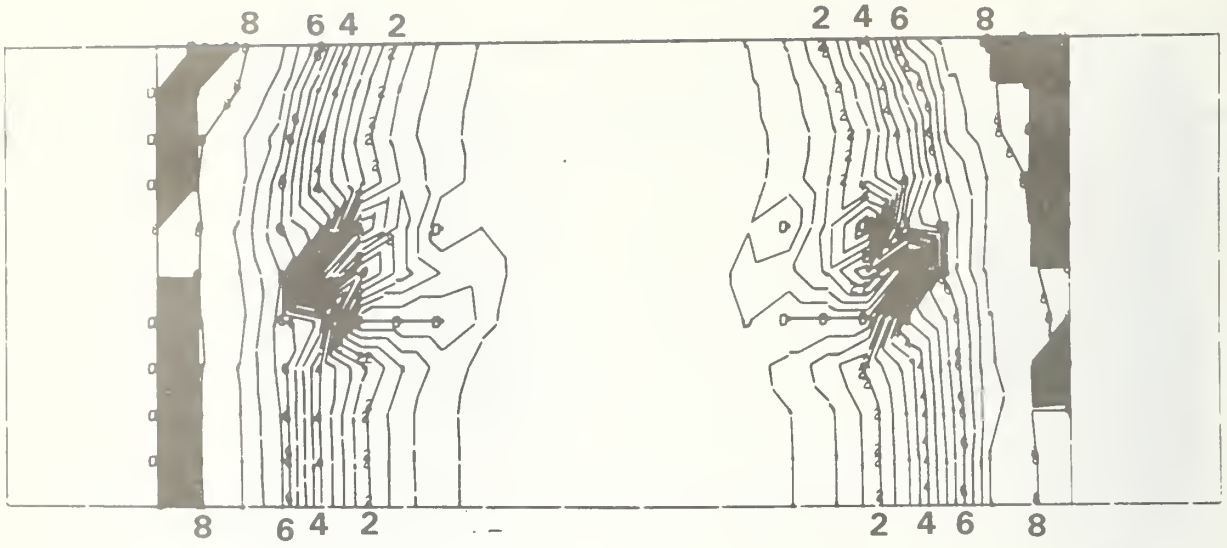

(a) LAP SHEAR STRESS
CONTOUR INTERVAL IS 500 lbf/in^2 (3.45 MPa).

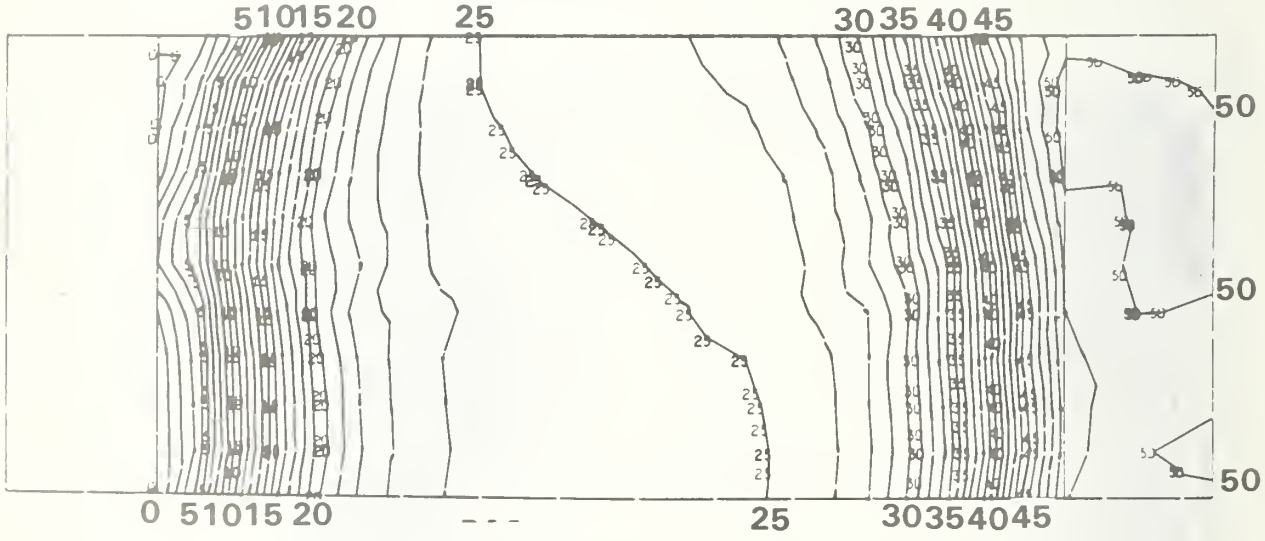

(b) LONGINTUDINAL NORMAL STRESS IN RIGHTMOST SHEET
CONTOUR INTERVAL IS 1000 lbf/in^2 (6.9 MPa).

Figure 18. CONTOUR PLOTS OF STRESS IN JOINT LOADED WITHIN THE NONLINEAR RANGE OF BOTH ADHESIVE AND METAL.

elastic solution was obtained for an applied longitudinal tensile stress of 20.7 MPa (3000 lbf/in^2). The applied tensile stress was then increased to 207 MPa (30 000 lbf/in^2) for a second solution, decreased back to 20.7 MPa (3000 lbf/in^2) for a third solution, and increased again to 207 MPa (30 000 lbf/in^2) for a fourth solution. The latter three solutions in this sequence involved extensive nonlinear deformation of the adhesive. Figure 19 gives the adhesive shear stress variation along the longitudinal centerline of the joint for the four solutions. These results indicate the residual stresses due to the nonlinear adhesive deformation.

c. Adherend Yield

Two solutions were obtained for a single-lap bonded joint similar to the weldbonded joint shown in Figure 1 (but with an adhesive thickness of 0.371 mm (0.0146 in)), using the longitudinal-cross-section computer program and the finite element mesh shown in Figure 20. The sheet midthickness point at the left end was restrained and a mean tensile stress of 345 MPa (50 000 lbf/in^2) was applied through the midthickness point at the right end. For one solution all material properties were assumed to be linear elastic. For the other solution the nonlinear-metal stress-strain relationship shown in Figure 12 was used, but the adhesive was assumed to be linear elastic. Figure 21 shows contour plots of the longitudinal component of normal stress for these two solutions. The linear-elastic solution gave a peak tensile stress at the end of the overlap 8 percent greater than that given by the nonlinear-metal solution. Figures 22 and 23 give, respectively, the variations in the adhesive shear stress and the normal (peel) stress along the length of the joint for both solutions. Although the yielding of the metal reduces the peak metal stress, the greater strain in the metal forces a significant increase in both components of adhesive stress.

4. LAP JOINT TENSILE TESTS

Eight different single-lap joint configurations, designed so as to constitute an experimental parameter study, were subjected to quasi-static tensile strength and cyclic load tests and to tensile fatigue tests. The quasi-static loads were applied in a 50 000 lbf capacity screw-powered universal testing machine and the fatigue loads were applied in a 50 000 lbf capacity servo-controlled electrohydraulic testing machine. These machines are described in Reference 7. The end fixtures shown attached to a broken specimen in Figure 24 were used in all tests. The single-pin fixtures and the flexibility of the long thin specimens assured relatively low eccentricity of the load applied at the specimen end tabs.

4.1 Lap Joint Specimens

Figure 25 is a drawing of the weldbonded joint that was the central reference design, a broken specimen of which is shown in Figure 24. The other seven test specimen designs were nominally the same as the central reference design except for one dimension. The eight designs were:

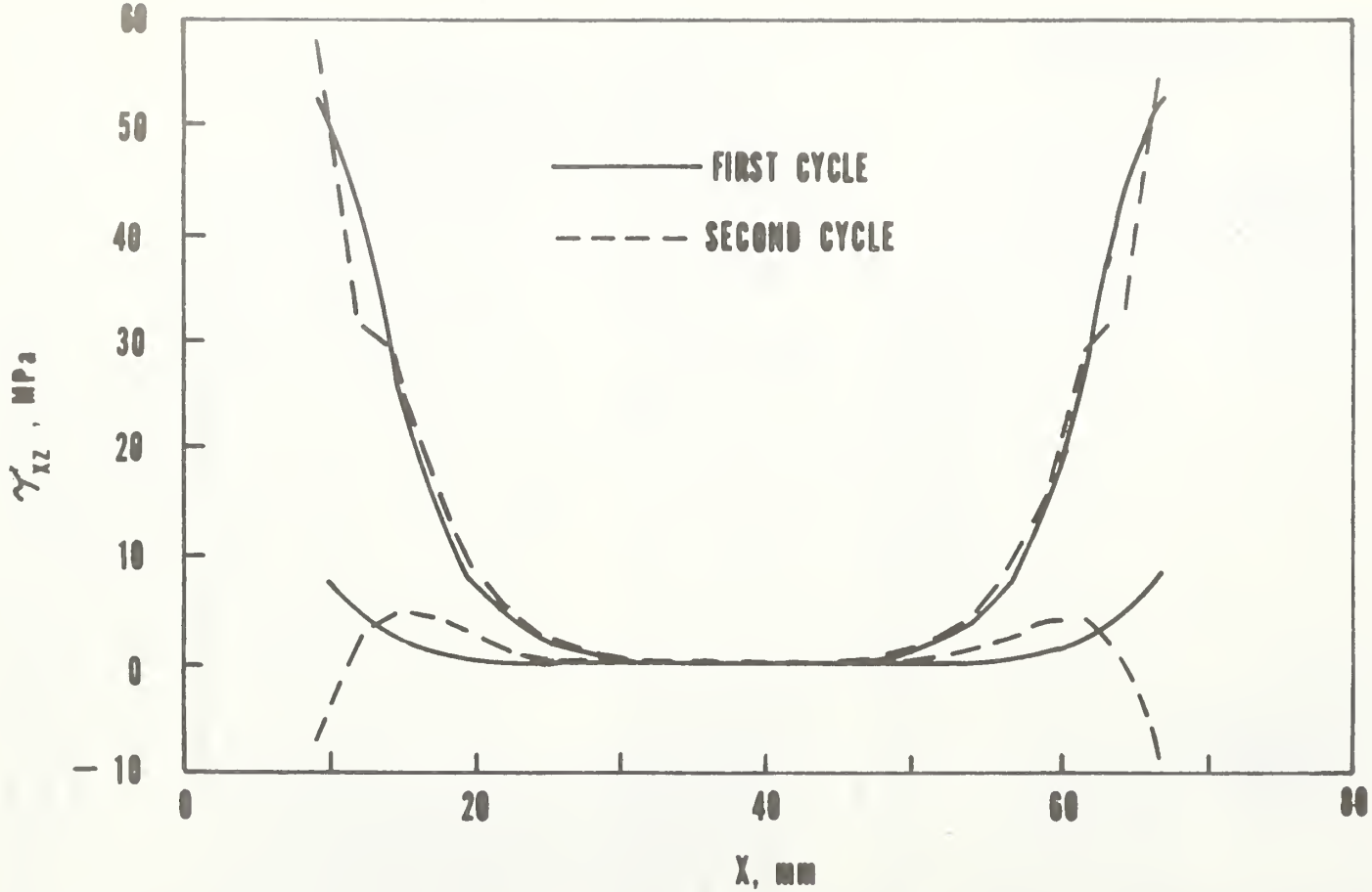

Figure 19. ADHESIVE SHEAR STRESS FROM NONLINEAR CYCLIC LOAD ANALYSIS.

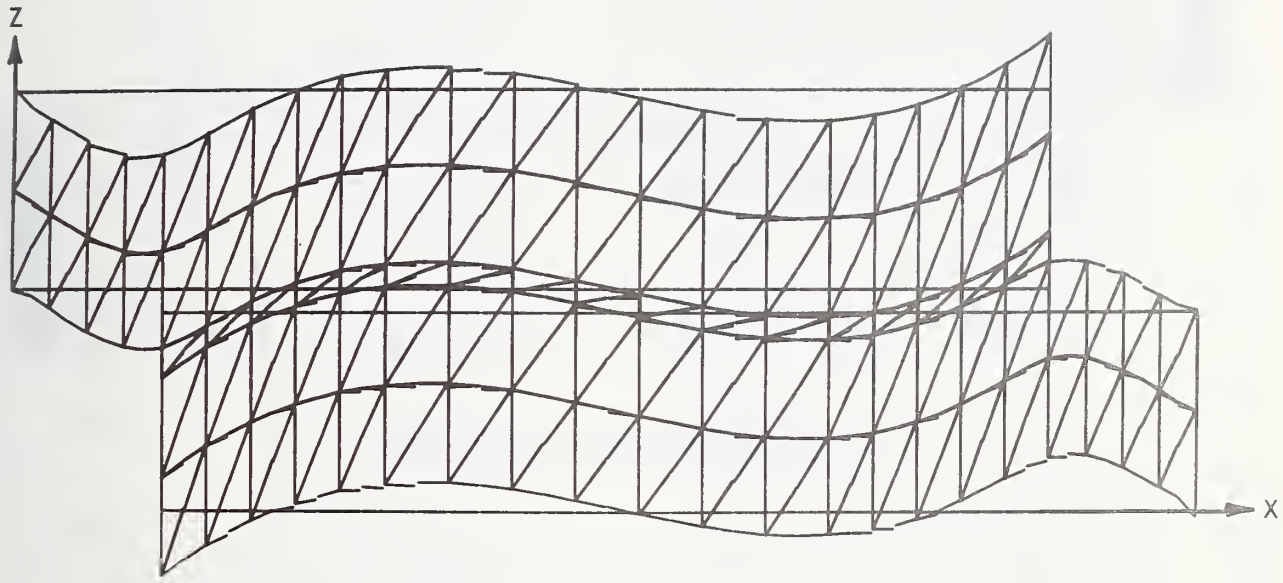

Figure 20. FINITE ELEMENT MESH USED FOR NONLINEAR CROSS-SECTION ANALYSIS OF A BONDED JOINT. THICKNESS DIMENSIONS EXAGGERATED 4 TIMES, VERTICAL DEFLECTIONS EXAGGERATED 20 TIMES.

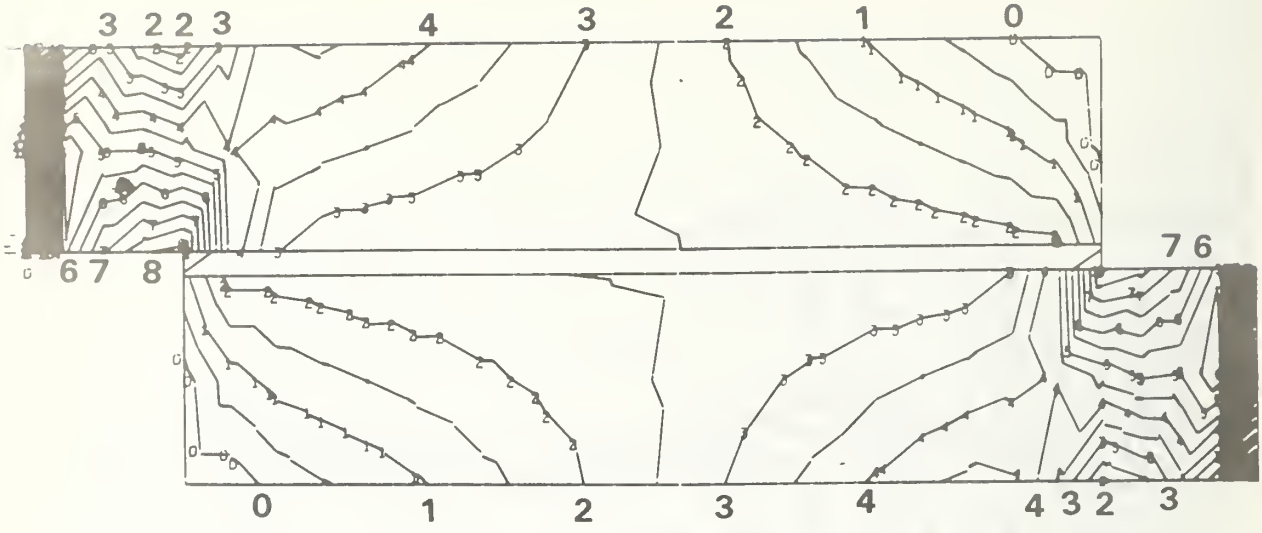

(a) LINEAR-ELASTIC ANALYSIS

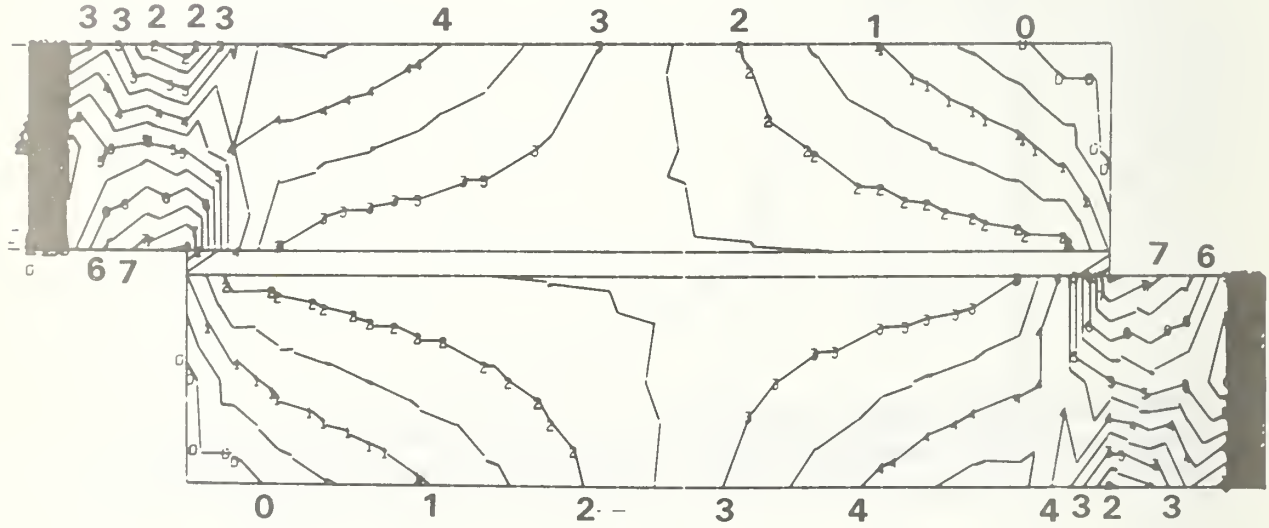

(b) NONLINEAR-METAL ANALYSIS

Figure 21. CONTOUR PLOTS OF LONGITUDINAL NORMAL STRESS IN A BONDED JOINT. CONTOUR INTERVAL IS 5000 lbf/in^2 (34,5 MPa).

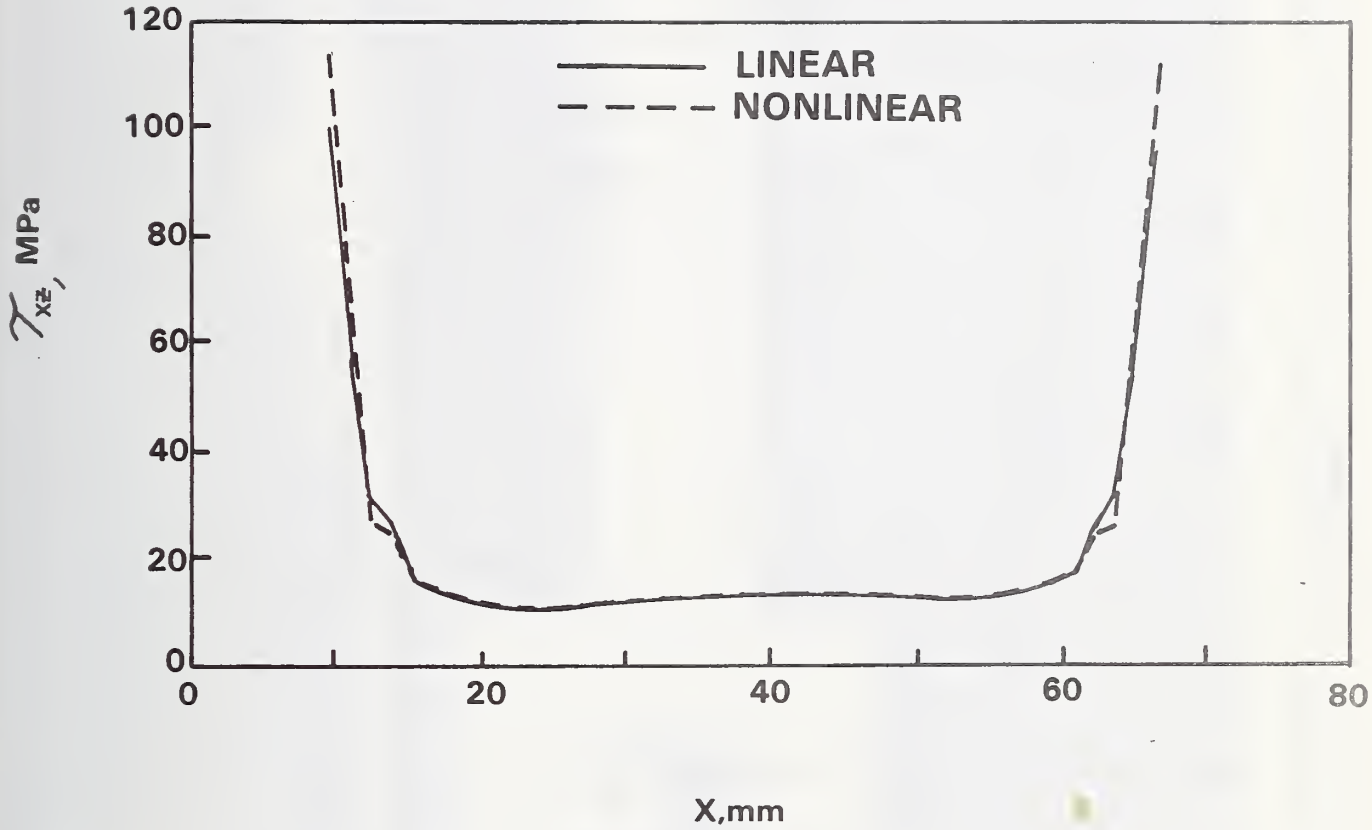

Figure 22. ADHESIVE SHEAR STRESS IN BONDED JOINT FROM LINEAR ANALYSIS AND NONLINEAR-METAL ANALYSIS.

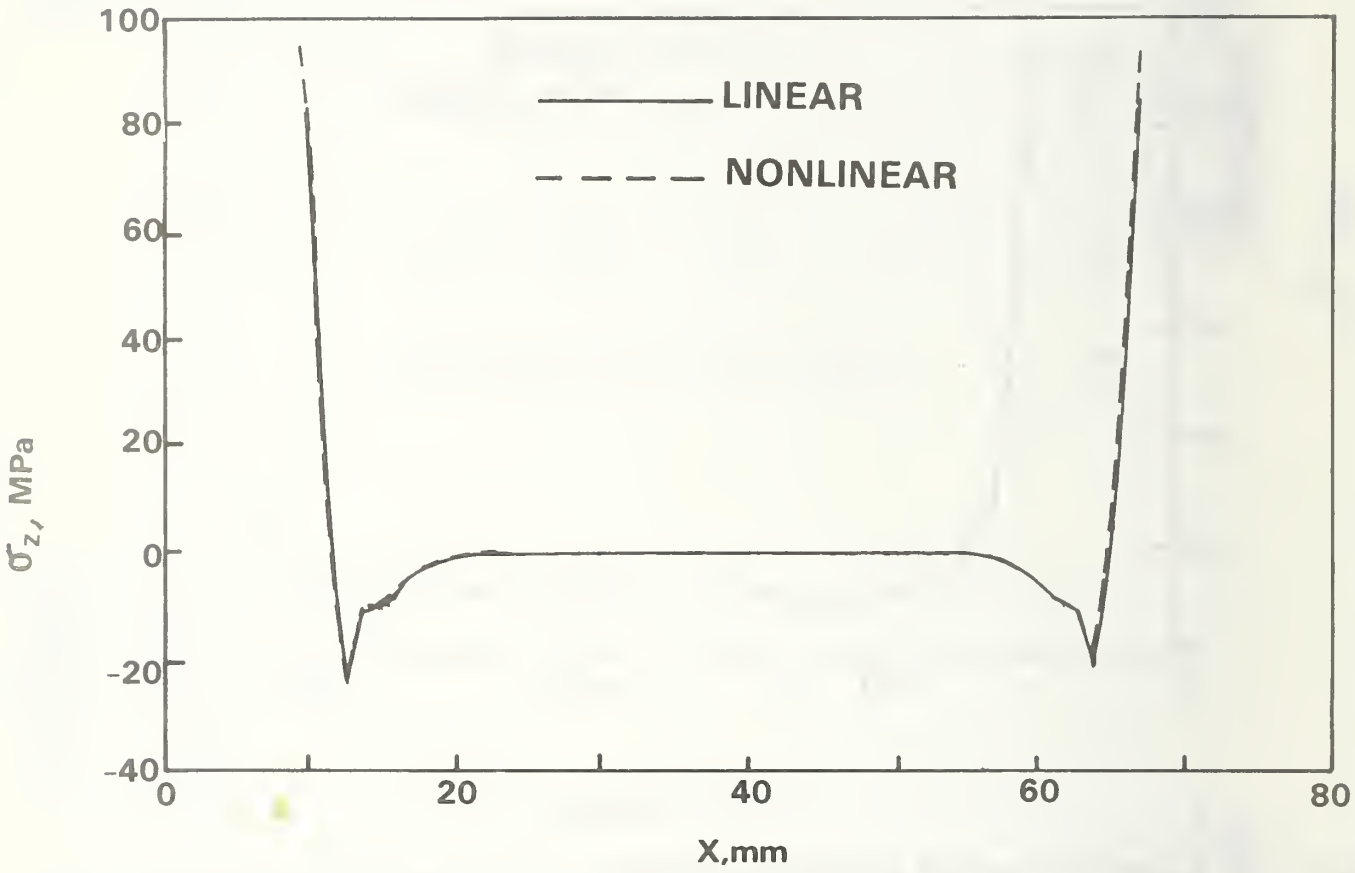

Figure 23. ADHESIVE NORMAL (PEEL) STRESS IN BONDED JOINT FROM LINEAR ANALYSIS AND NONLINEAR-METAL ANALYSIS.

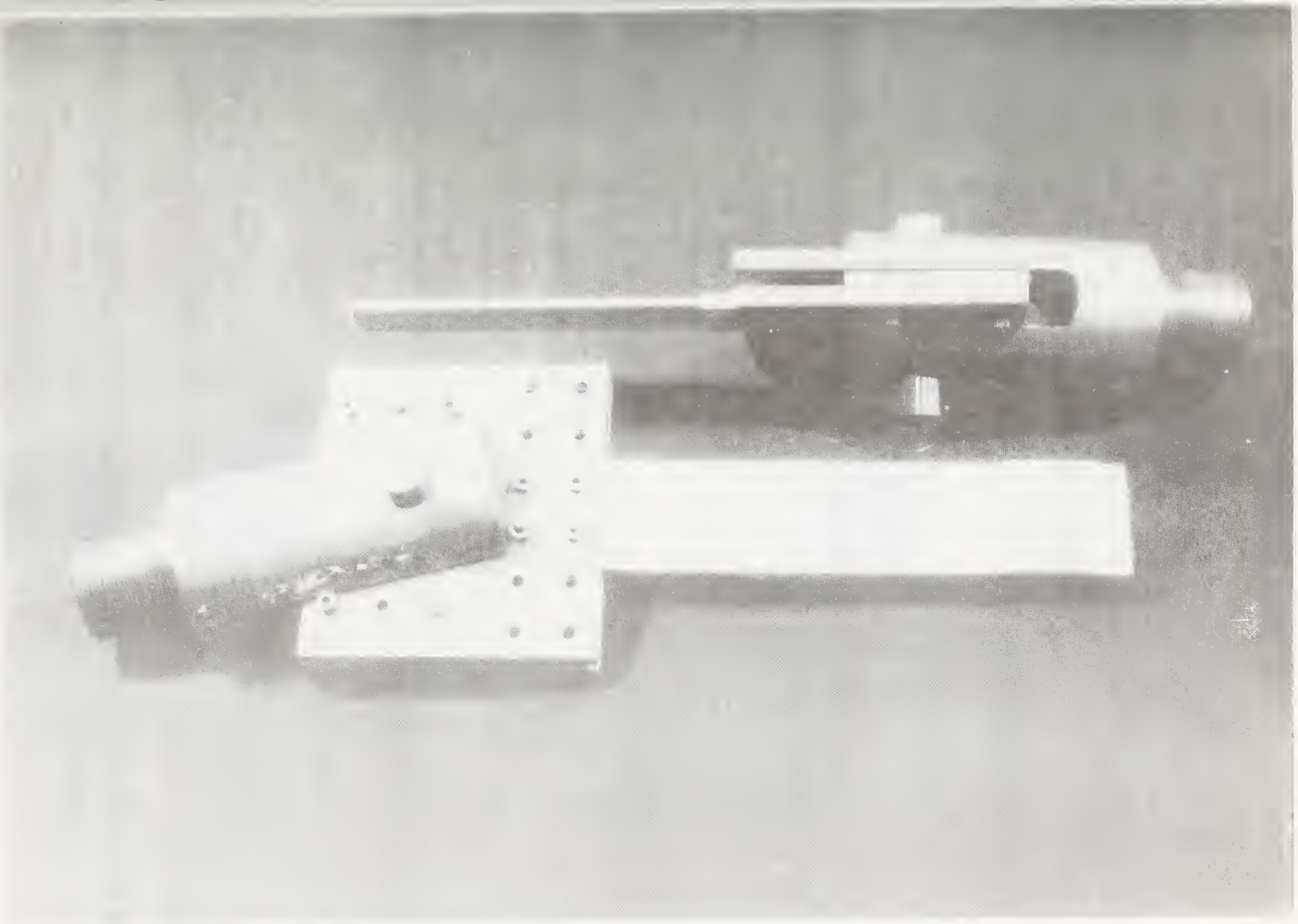

Figure 24. END FIXTURES ATTACHED TO A BROKEN WELDBONDED JOINT.

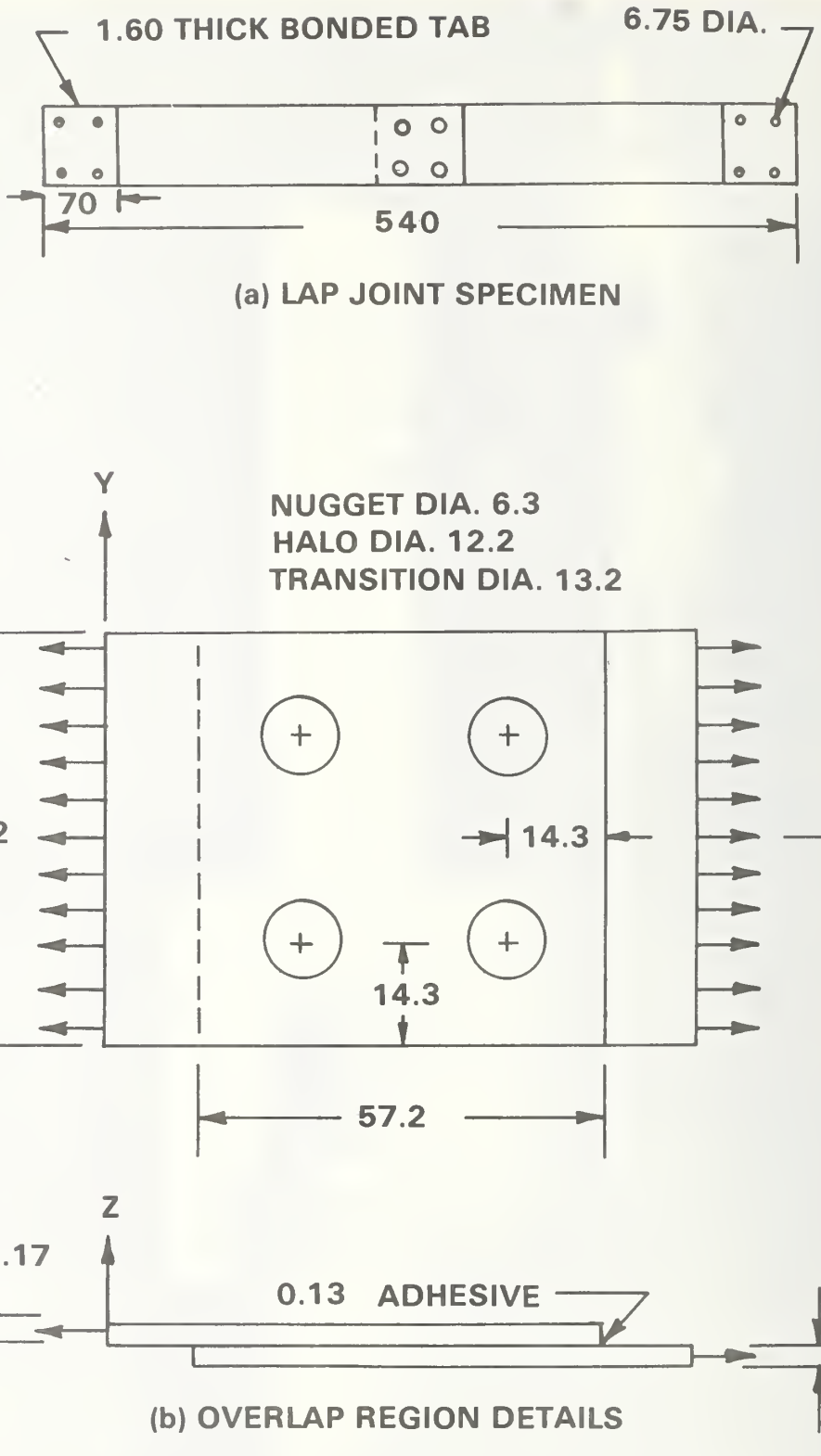

Figure 25. CENTRAL REFERENCE DESIGN OF SINGLE-LAP WELDBONDED JOINT. DIMENSIONS ARE IN MILLIMETERS (1 in = 25.4 mm).

1. Central reference joint - 57.2 mm (2.25 in) wide by 3.7 mm (0.125 in) thick 7075-T6 bare aluminum sheet weldbonded in a 57.2 mm (2.25 in) long overlap with 0.076 mm (0.003 in) thick modified epoxy paste adhesive and four 6.3 mm (0.25 in) diameter spotwelds. The spotwelds were symmetrically located so that each was centered in one quadrant of the square overlap area.

2. Short joint - The same as design 1 except the overlap was approximately half as long, that is, 28.4 mm (1.12 in), with two spotwelds.

3. Long joint - The same as design 1 except the overlap was twice as long, that is, 114.3 mm (4.50 in), with eight spotwelds.

4. Welds-near-end joint - The same as design 1 except the four spotwelds were centered only 9.1 mm (0.36 in) from the ends of the overlap. The spotwelds were symmetrically located, the same as design 1, in the transverse direction.

5. Wide joint - The same as design 1 except the overlap was twice as wide, that is, 114.3 mm (4.50 in), with eight spotwelds.

6. Thin joint - Similar to design 1 except for the aluminum sheet which was 1.6 mm (0.063 in) thick. Also, the spotweld diameter was only 4.7 mm (0.19 in), which is more appropriate for this sheet thickness.

7. Spotwelded joint - Similar to design 1, but without adhesive bond.

8. Bonded joint - Similar to design 1, but without spotwelds. Also, because of a difference in the specimen fabrication process, the adhesive thickness ranged from 0.18 mm (0.007 in) to 0.71 mm (0.028 in).

Young's modulus and Poisson's ratio for the metal sheet were determined from resistance strain gage measurements with back-to-back gages located midway between the joint and an end tab; the average values obtained from three specimens are those used in the numerical examples (Sec. 3.3). The shear stress-strain relationship for the adhesive, as determined by three "napkin ring" torsion tests, is given by equation (2) and the empirical constants G_o, A, B, C, and τ_p in Section 3.1.

The lap joint specimens of a particular design were fabricated* by first joining two large sheets of the aluminum alloy in a seam joint, and then sawing the joined sheets, at right angles to the seam joint, to form the individual specimens. The seam widths were equal to the overlap lengths of the specimens. The aluminum end-tab material was also bonded to the large sheets before sawing the individual specimens. The overlap surfaces were degreased and then chemically etched before joining. The bonded joints were fabricated by applying the paste adhesive to the large sheets, clamping the sheets together during a 40-minute curing cycle in a large 121 °C (250 °F) oven, and then sawing the individual specimens. The weldbond joints were fabricated by applying the paste adhesive to the large sheets, spotwelding through the uncured adhesive, sawing the individual specimens, and then curing in a smaller 121 °C (250 °F) oven for 40 minutes. The weldbonding process gave significantly greater uniformity of bondline thickness than did the bonding process.

4.2 Quasi-Static Tests

One specimen of each of the eight designs was tested to failure in tension. Load was applied very slowly over a period of 5 to 20 minutes. These results are plotted as single-cycle points in Figures 26 through 33.

One specimen of each of seven designs and two specimens of the bonded joint were instrumented with from 11 to 27 resistance strain gages and subjected to from 58 to 140 cycles of quasi-static tensile load. Multiple cycles of load were applied at progressively higher peak load levels until failure. The different peak load levels are indicated by the cross symbols connected by dashed lines in Figures 26 through 33. Loads were cycled between a peak value and 10 percent of that value. Surface strains were monitored throughout each loading program. These strain measurements indicated a relatively linear loading range, a relatively stable nonlinear range, and an unstable nonlinear range for most of the specimens. Within a stable nonlinear loading range, successive cycles to the same load level, although clearly involving nonlinear deformation, resulted in convergence to a sequence of roughly similar load-strain hysteresis loops. Within an unstable nonlinear range, successive loading cycles resulted in progressive strain growth with no indication of stable hysteresis. An indication of these loading ranges, as subjectively interpreted from the strain data, is given on Figures 26 through 33.

4.3 Fatigue Tests

Several specimens of each design were fatigue tested at different load levels within the linear range and the stable nonlinear range. Essentially all of the fatigue results (Figures 26 through 33) fall into a clear pattern that is also in a reasonable relationship to the quasi-static data.

---

*All of the lap joint specimens were fabricated by Feltman Research Laboratory, Picatinny Arsenal, Dover, NJ.

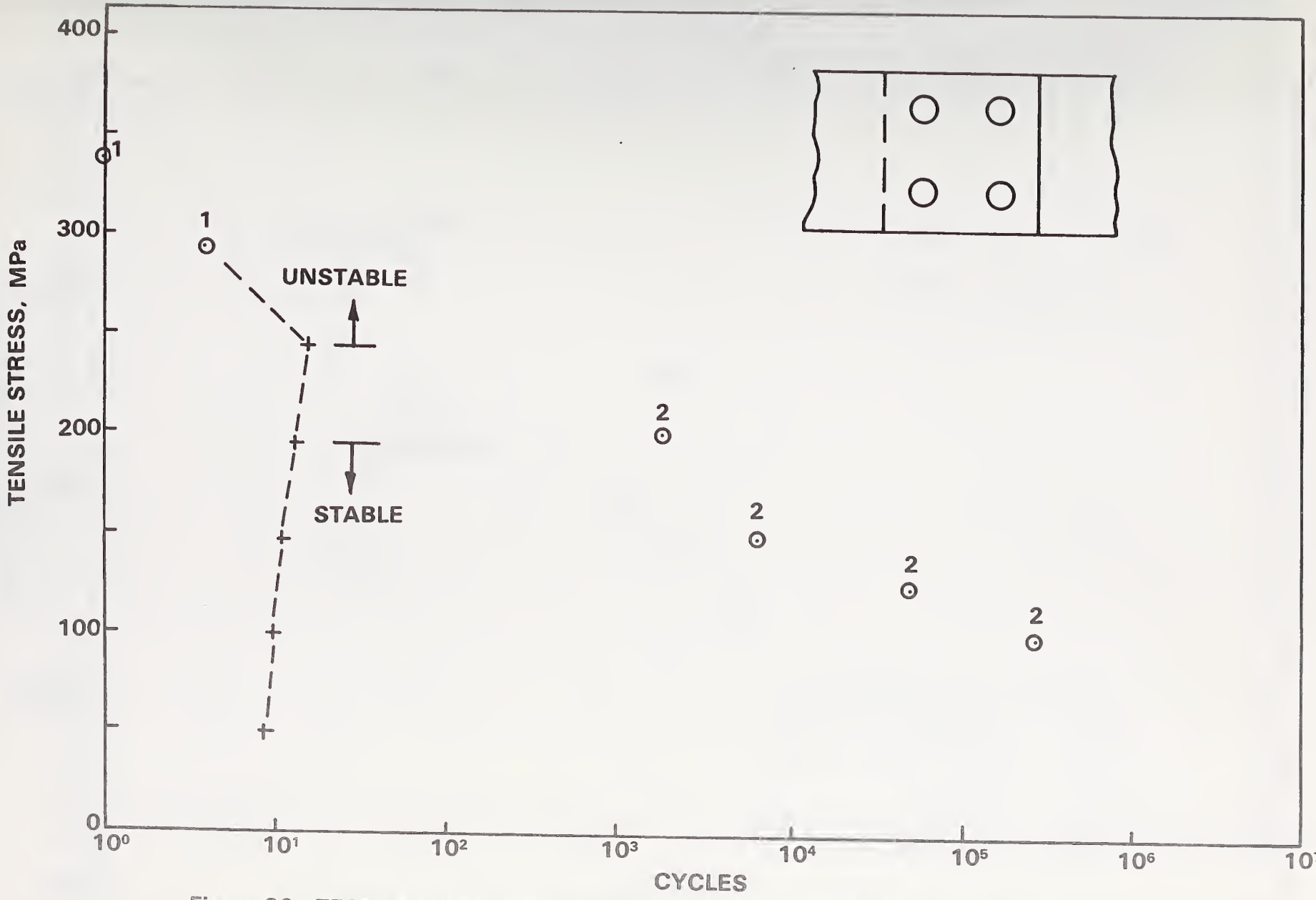

Figure 26. TEST RESULTS FOR CENTRAL REFERENCE JOINT (DESIGN 1).

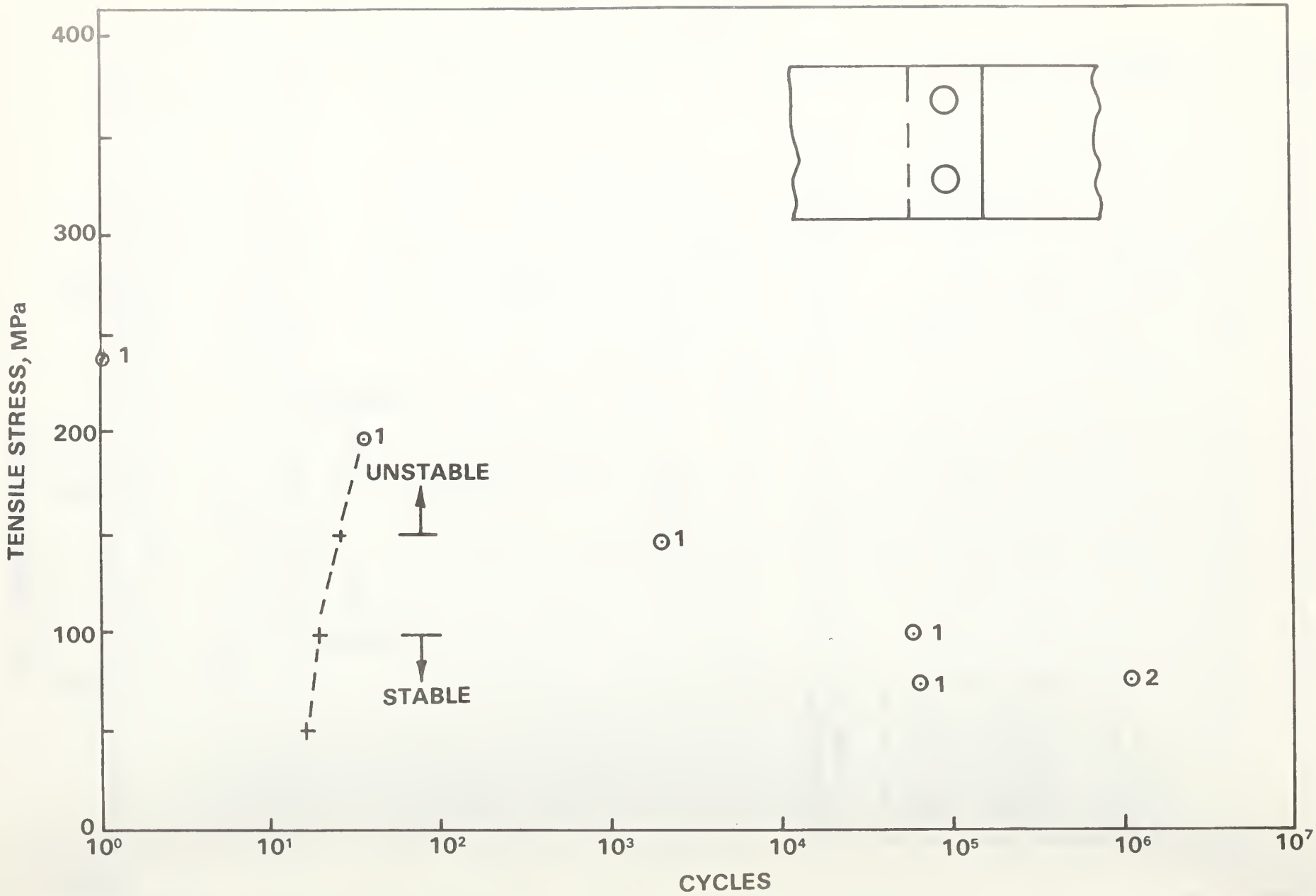

Figure 27. TEST RESULTS FOR SHORT JOINT (DESIGN 2).

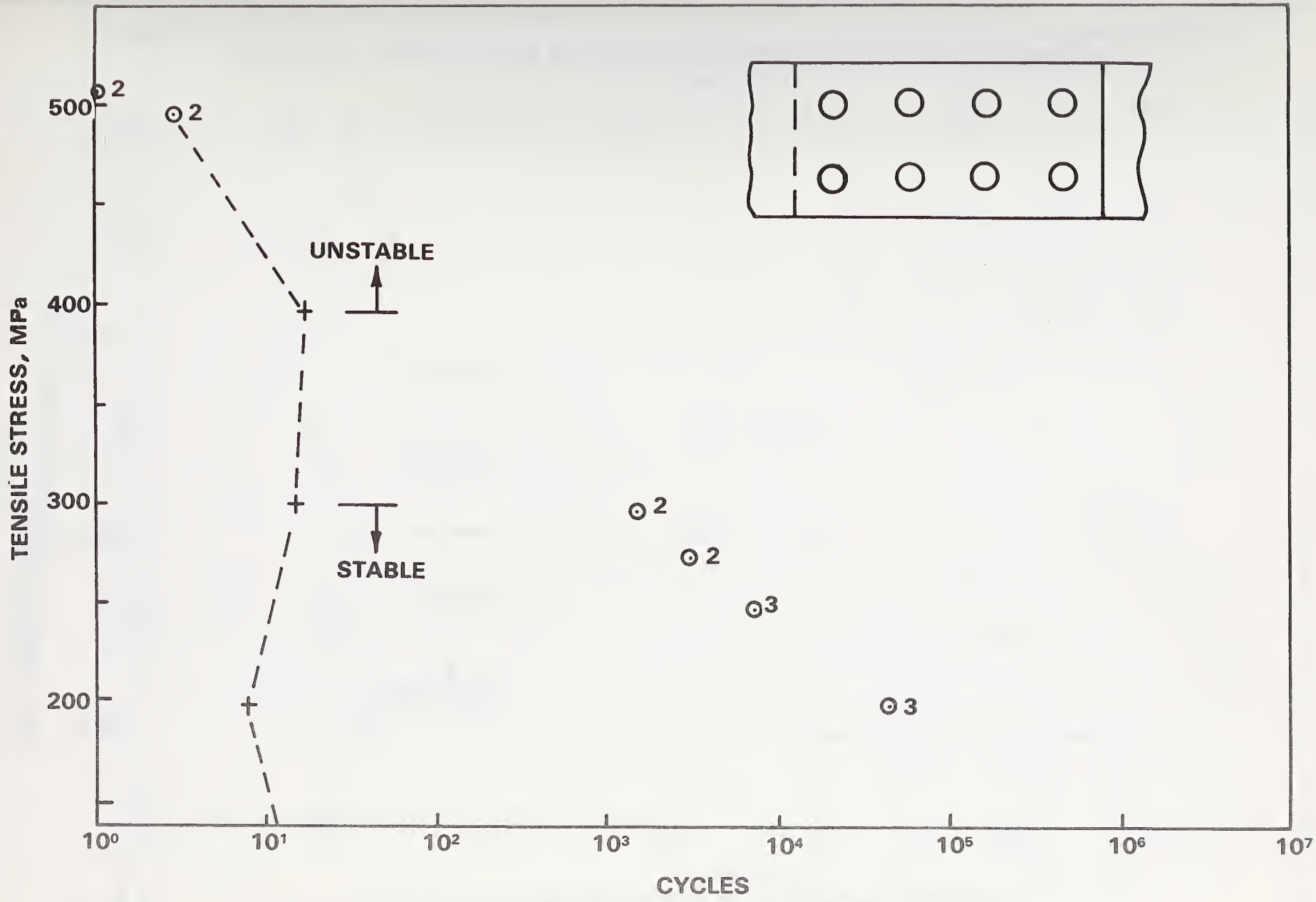

Figure 28. TEST RESULTS FOR LONG JOINT (DESIGN 3).

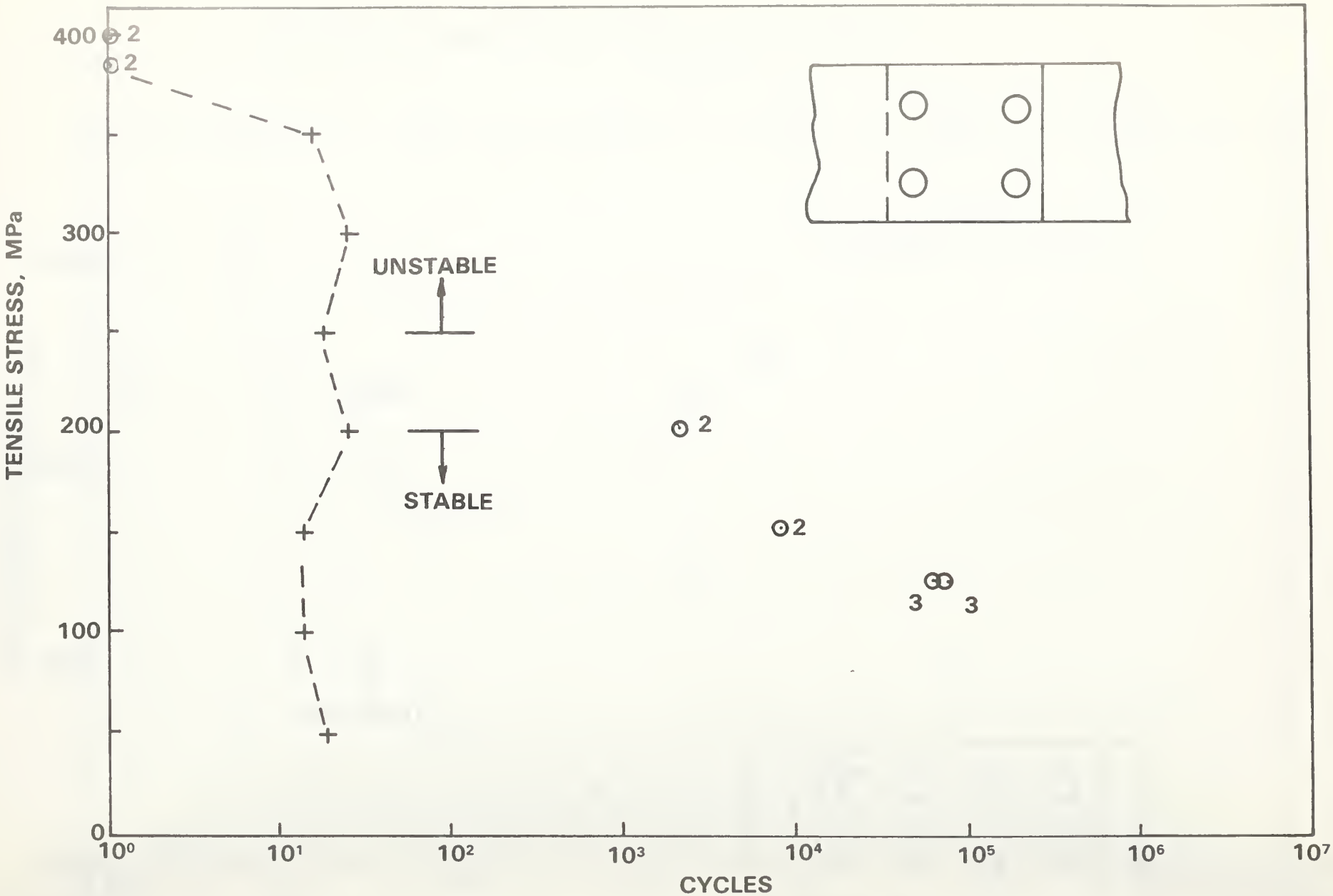

Figure 29. TEST RESULTS FOR JOINT WITH WELDS NEAR END (DESIGN 4).

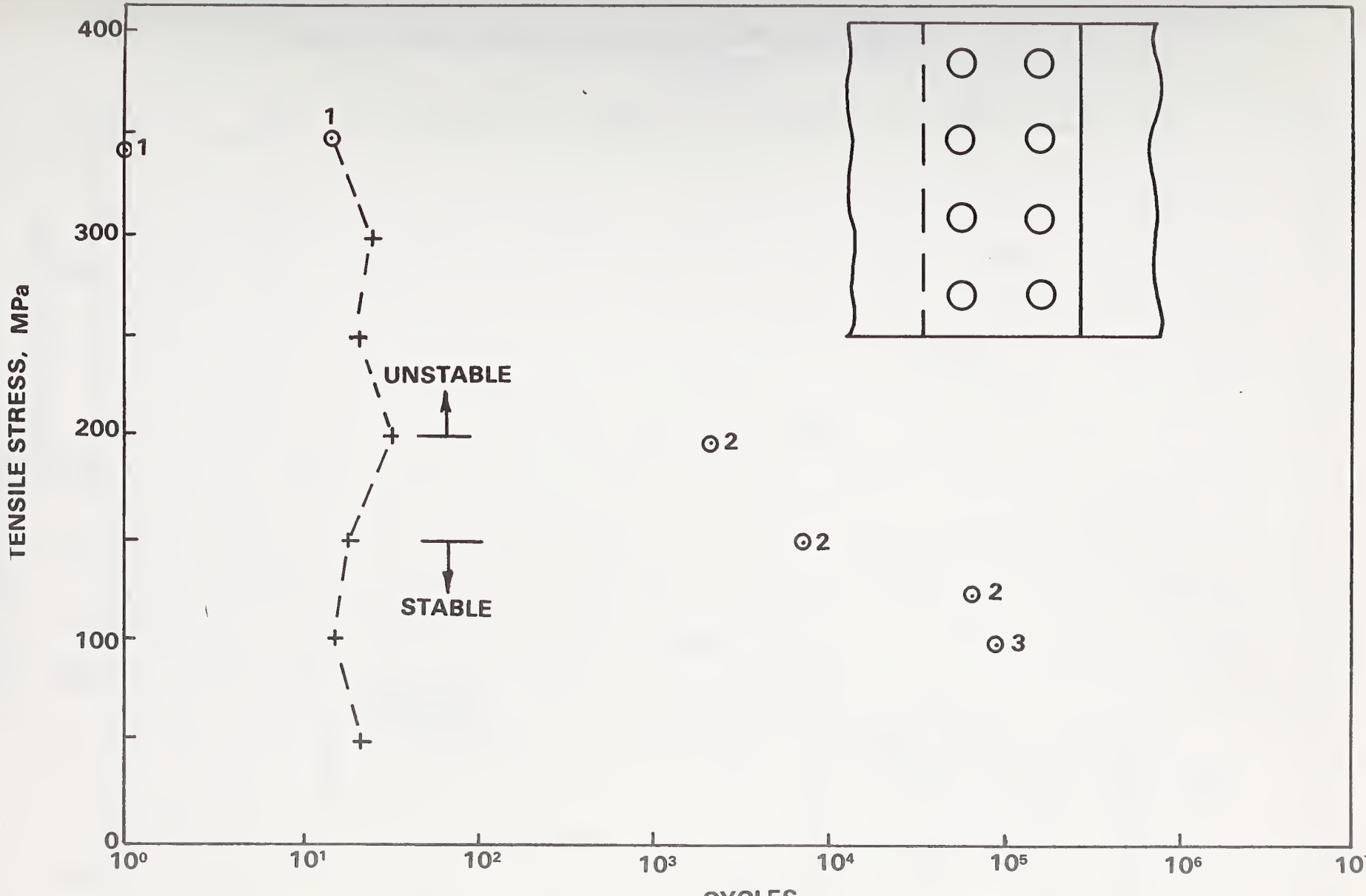

Figure 30. TEST RESULTS FOR WIDE JOINT (DESIGN 5).

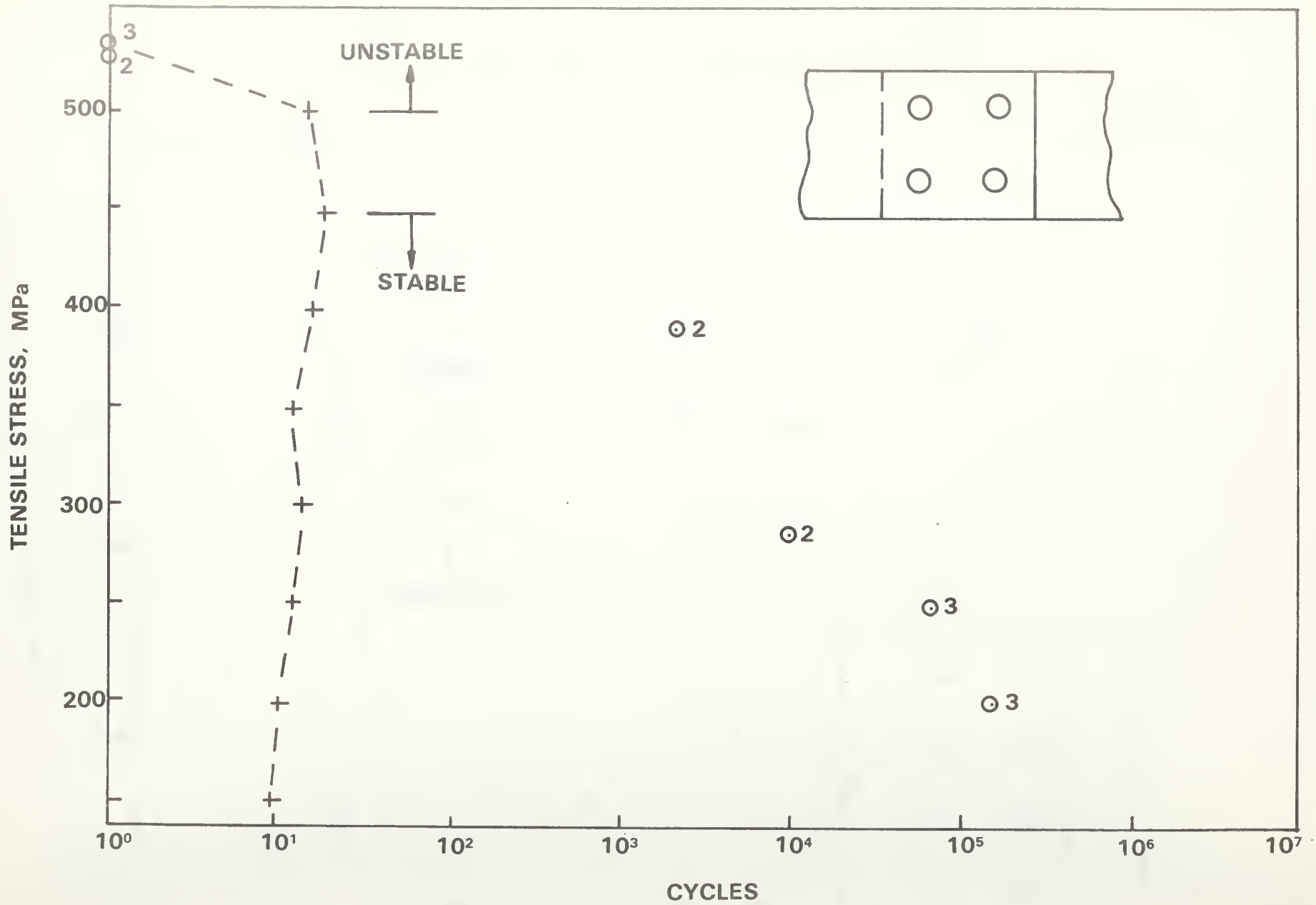

Figure 31. TEST RESULTS FOR THIN JOINT (DESIGN 6).

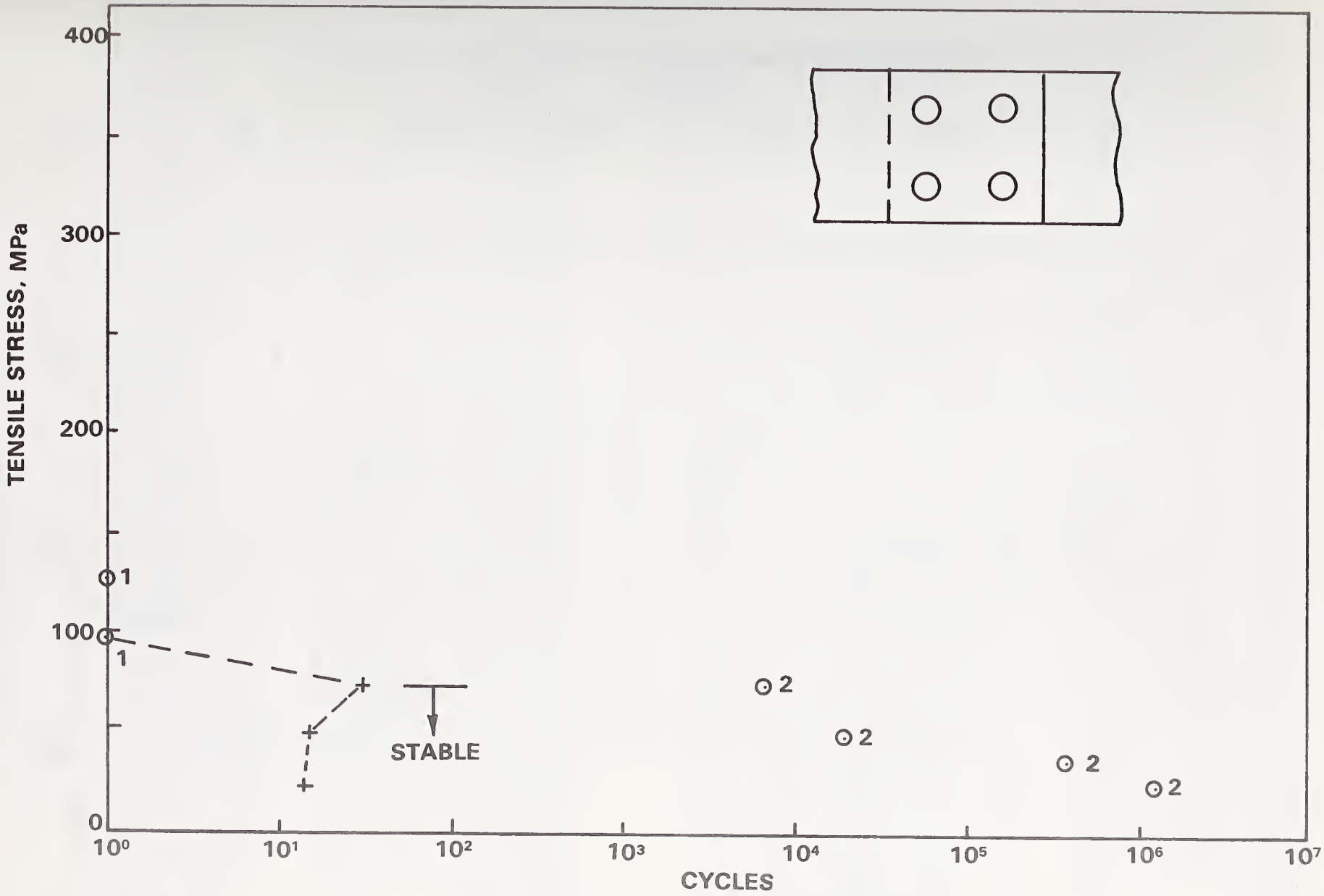

Figure 32. TEST RESULTS FOR SPOTWELDED JOINT (DESIGN 7).

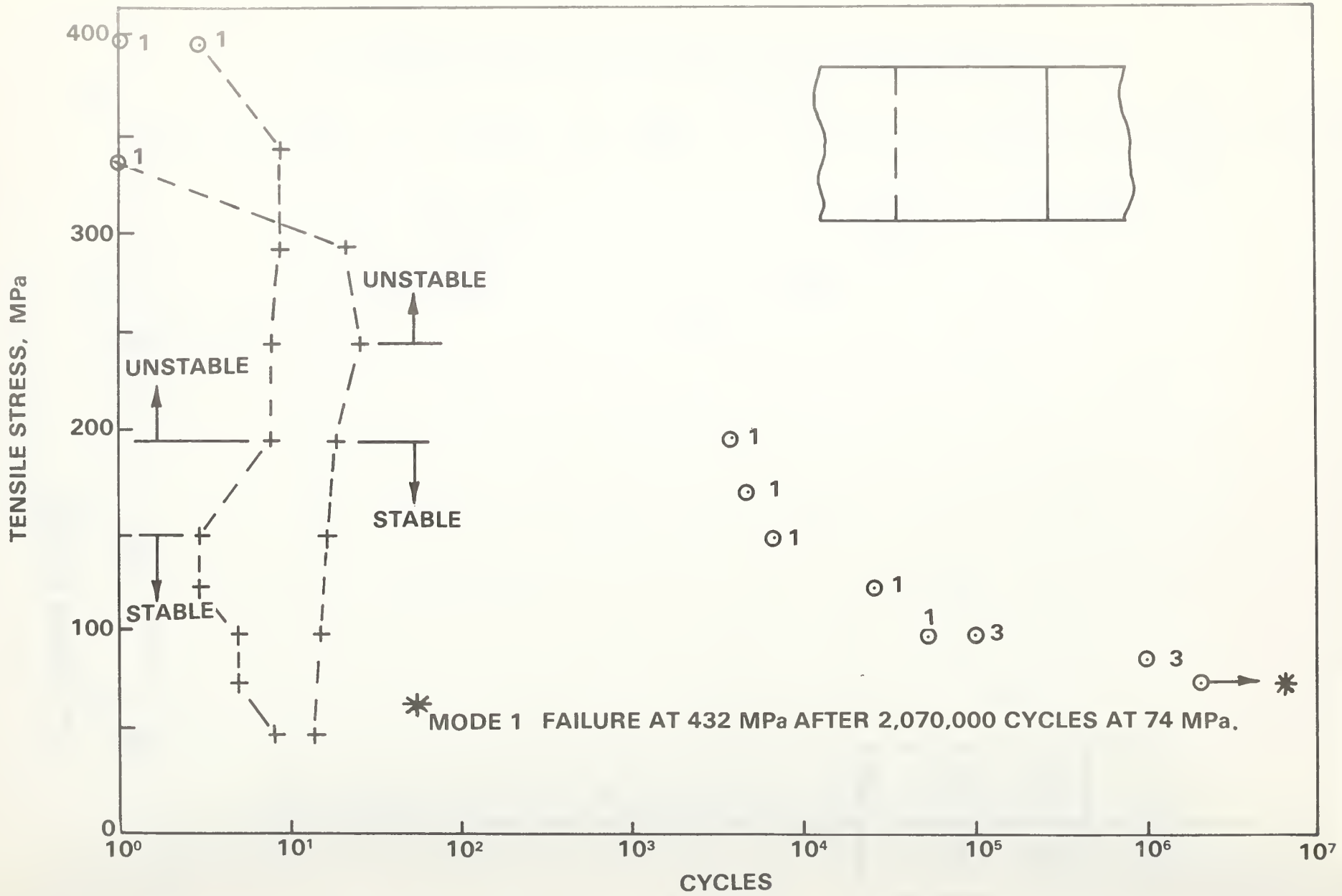

Figure 33. TEST RESULTS FOR BONDED JOINT (DESIGN 8).

Figure 34 is a summary plot of the fatigue results. The thin sheet joint (design 6) had the greatest fatigue strength. Ranking second in fatigue strength was the long joint (design 3). These two joints were probably over-designed in terms of weight and material utilization. The spotwelded joint (design 7) was the weakest in fatigue, followed by the short joint (design 2). There was no significant difference in the fatigue strengths of the other four joint designs; their fatigue strengths all plot within the cross-hatched region in Figure 34.

4.4 Failure Modes

All specimen failures can be broadly classified into one of three distinct fracture modes: (1) lap-shear fracture through the entire bonded and/or spotwelded overlap area; (2) transverse fracture through one metal sheet, at the outer edge of a row of spotwelds, after adhesive debond to that point; and (3) transverse fracture through one metal sheet at or near the end of the overlap. Figure 35 shows examples of each of these failure modes. Figures 26 through 33 indicate which of these three failure modes was present for each test by a numeral 1, 2, or 3 at the data point. There is an apparent correlation between failure mode and load level for all eight specimen designs. With few exceptions, lap-shear failures (mode 1) occurred in relatively high-load, low-cycle tests; transverse fracture near the overlap end (mode 3) occurred in relatively low-load, high-cycle tests. Transverse fracture at a row of spotwelds (mode 2) usually occurred in tests run at intermediate load levels.

5. ANALYTICAL-EXPERIMENTAL STRAIN COMPARISONS

To evaluate the finite element analyses, strains measured on the surfaces of the test specimens were compared with strains computed by the planform and cross-section computer programs. Figures 36 through 43 give strain gage locations and comparable experimental and analytical results for each of the eight specimen designs for a load level in the linear elastic range; Figure 44 gives similar results for a load level in the stable nonlinear range. The linear-range test data were recorded the first time a specimen was loaded to a nominal level of 8900 N (2000 lbf) and then normalized to the level of an applied tensile stress of 69 MPa (10,000 lbf/in^2). Stable-nonlinear-range test data were recorded at nominal load levels of 17,800 N (4000 lbf) and 26,700 N (6000 lbf) and then linearly interpolated to 25,130 N (5650 lbf), corresponding to an applied tensile stress of 138 MPa (20,000 lbf/in^2).

Each of the instrumented test specimens was analyzed in the linear elastic range by the planform computer program and all except the spotwelded joint were analyzed by the cross-section program. For each of the seven joints analyzed by both computer programs, bending corrections, based on the cross-section analysis, were computed and added to the planform analysis strains. A reasonable bending correction was suggested by the linear nature

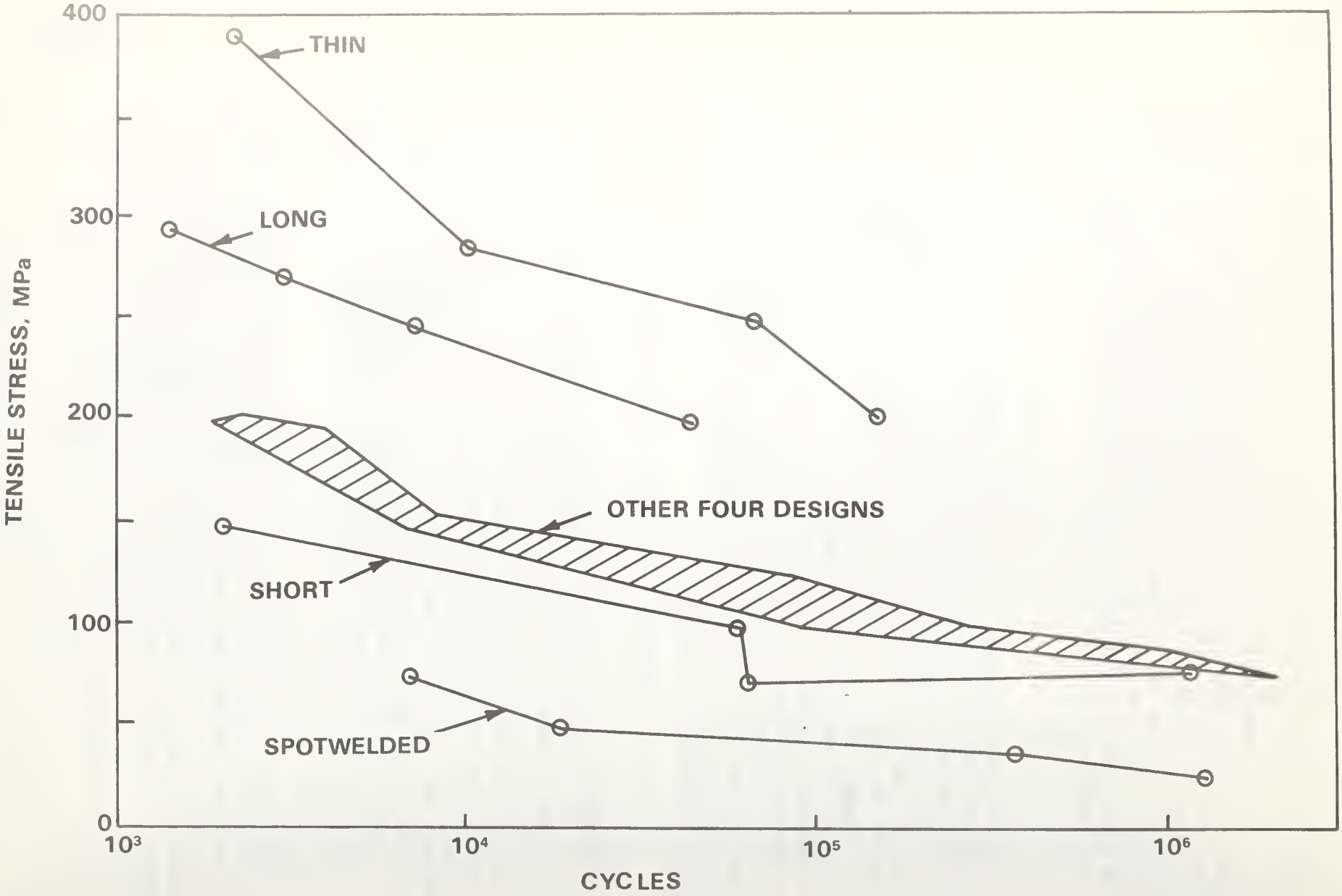

Figure 34. SUMMARY PLOT OF FATIGUE TEST RESULTS.

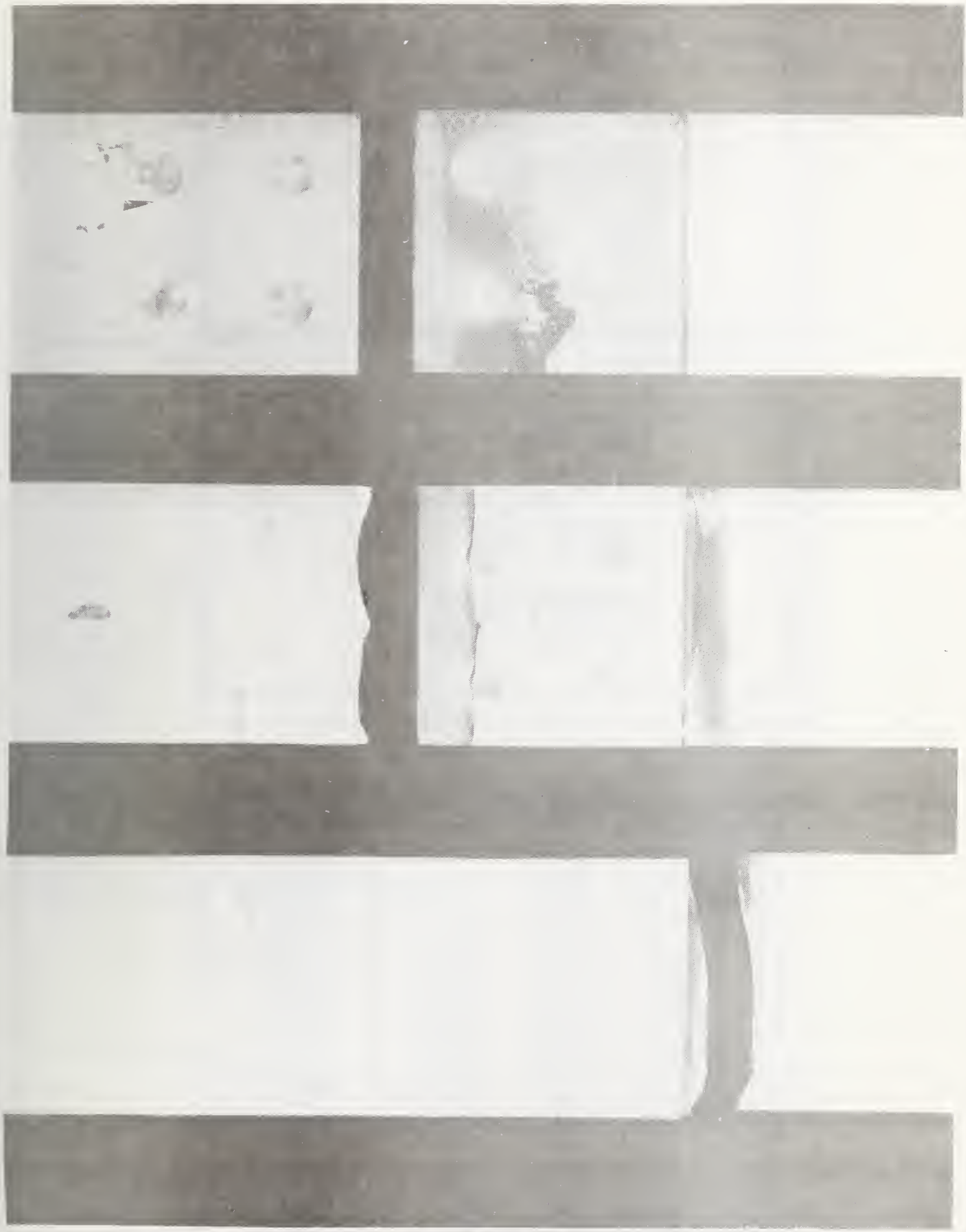

Figure 35. EXAMPLES OF THE THREE FAILURE MODES. FROM TOP TO BOTTOM: MODES, 1, 2 and 3.

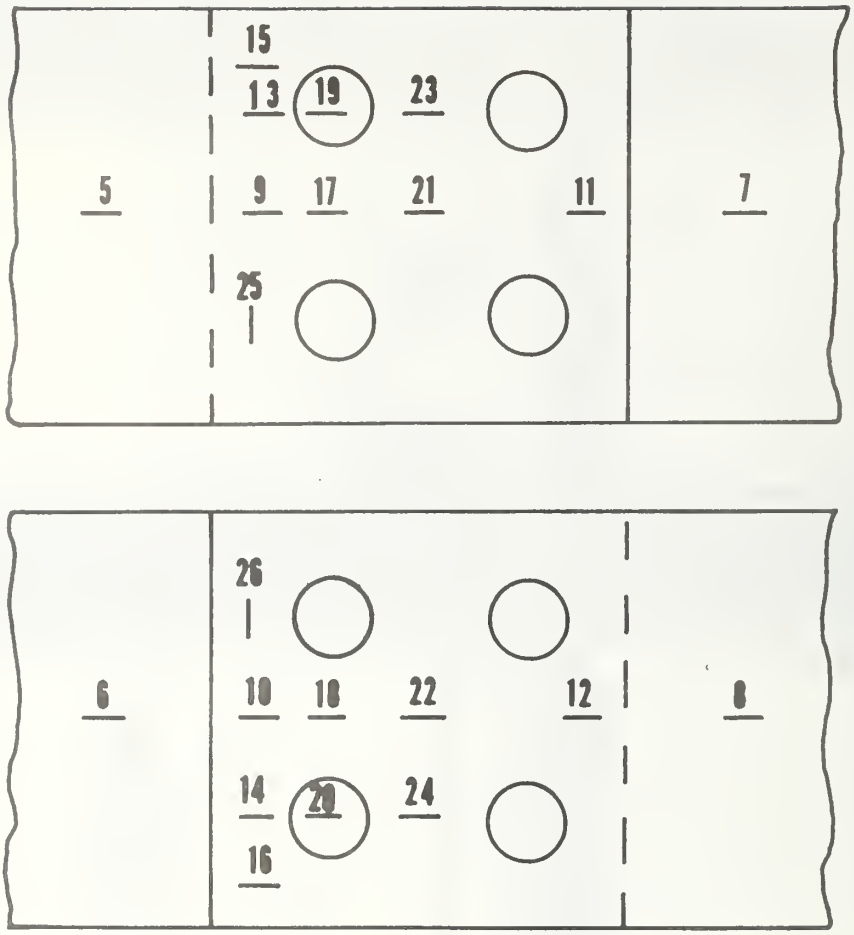

GAGE NO.	MEASURED	ANALYTICAL		
		PLANFORM	CROSS-SECTION	PLANFORM (PLUS BENDING)
5	1	996	---	---
6	2035	996	---	---
7	1982	996	---	---
8	36	996	---	---
9	654	604	628	716
10	301	401	284	311
11	280	383	237	191
12	685	628	720	820
13	660	616	628	727
14	287	384	284	294
15	722	621	619	722
16	202	384	284	294
17	600	509	624	637
18	370	486	379	356
19	620	512	624	639
20	371	486	379	357
21	432	489	523	510
22	462	490	484	468
23	458	500	523	520
24	498	498	484	477
25	-165	-197	---	---
26	-195	-196	---	---

Figure 36. LINEAR MICROSTRAIN COMPARISONS FOR THE CENTRAL REFERENCE JOINT.

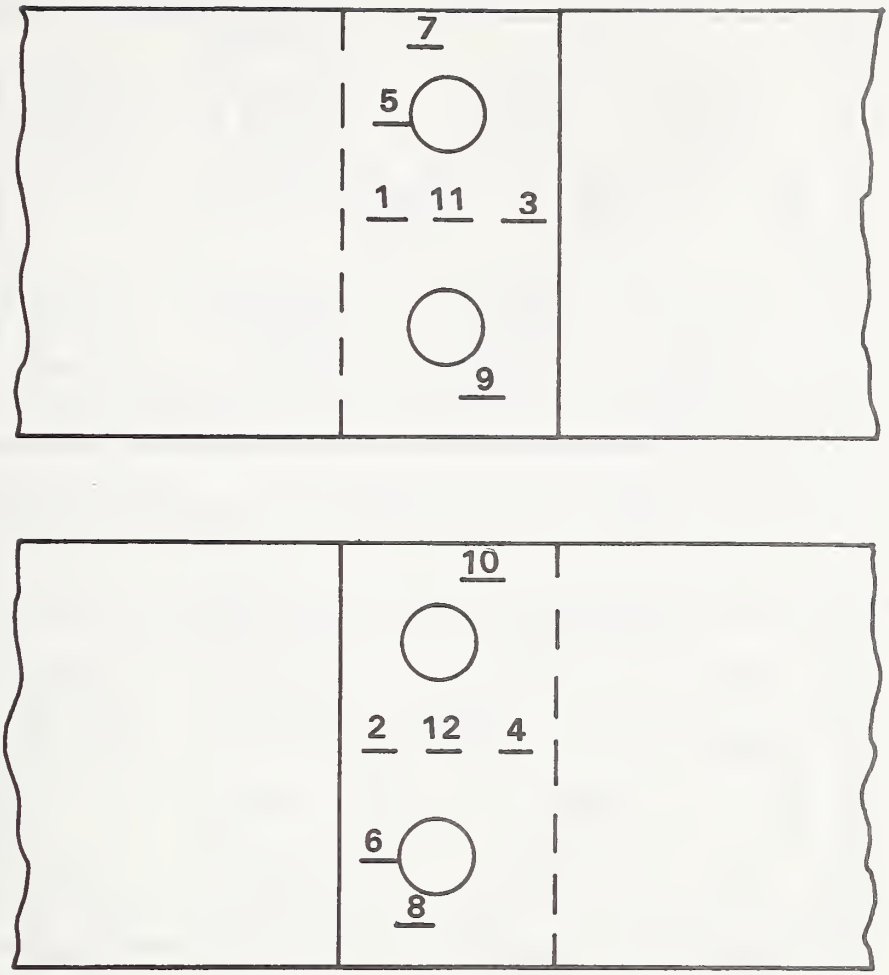

GAGE NO.	MEASURED	ANALYTICAL		
		PLANFORM	CROSS-SECTION	PLANFORM (PLUS BENDING)
1	505	591	630	712
2	439	412	331	299
3	377	402	350	289
4	567	611	603	721
5	500	610	620	719
6	421	405	331	292
7	532	550	591	634
8	451	484	423	402
9	409	494	436	426
10	618	550	582	625
11	536	499	510	506
12	508	499	498	490

Figure 37. LINEAR MICROSTRAIN COMPARISONS FOR THE SHORT JOINT.

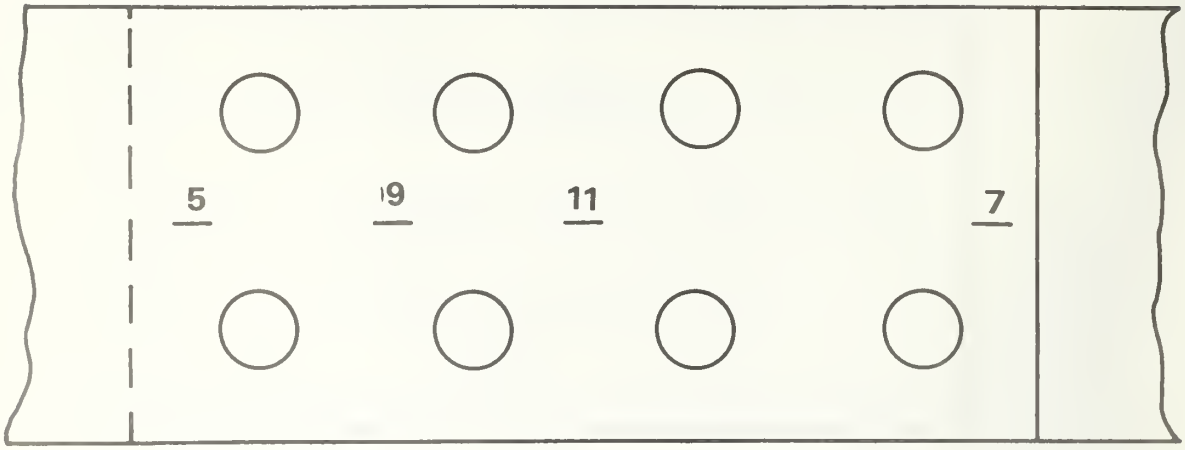

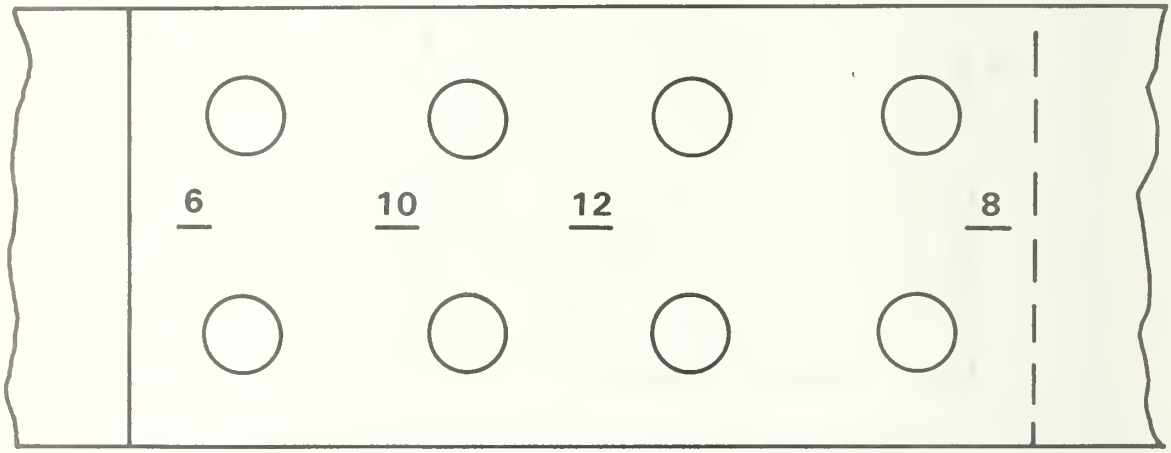

GAGE NO.	MEASURED	ANALYTICAL		
		PLANFORM	CROSS-SECTION	PLANFORM (PLUS BENDING)
5	781	584	706	751
6	210	455	320	290
7	177	417	281	224
8	807	620	736	813
9	638	504	501	504
10	349	504	507	505
11	473	504	502	504
12	498	504	501	504

Figure 38. LINEAR MICROSTRAIN COMPARISONS FOR THE LONG JOINT.

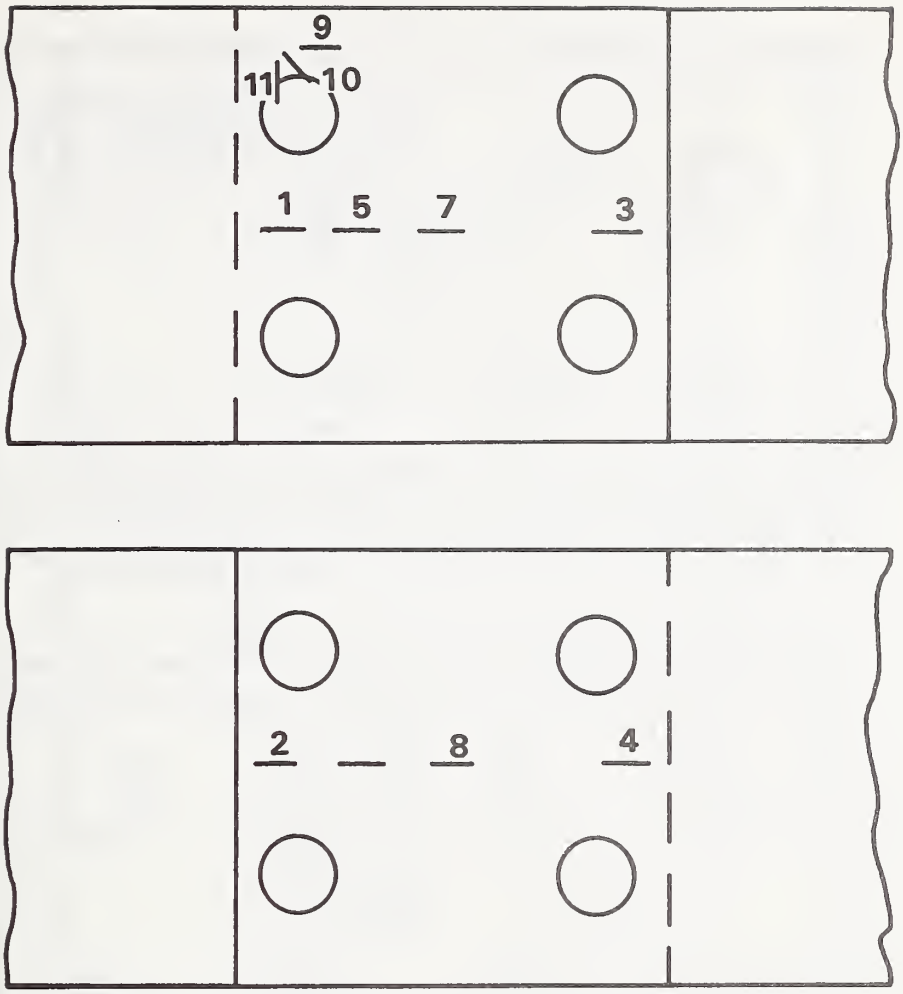

GAGE NO.	MEASURED	ANALYTICAL		
		PLANFORM	CROSS-SECTION	PLANFORM (PLUS BENDING)
1	775	629	690	804
2	189	405	248	226
3	422	369	360	320
4	571	649	526	690
5	701	508	590	577
6	257	492	412	420
7	604	494	468	455
8	353	495	541	534
9	797	548	685	766
10	294	216	---	313
11	-211	-191	---	---

Figure 39. LINEAR MICROSTRAIN COMPARISONS FOR THE JOINT WITH SPOTWELDS NEAR OVERLAP ENDS.

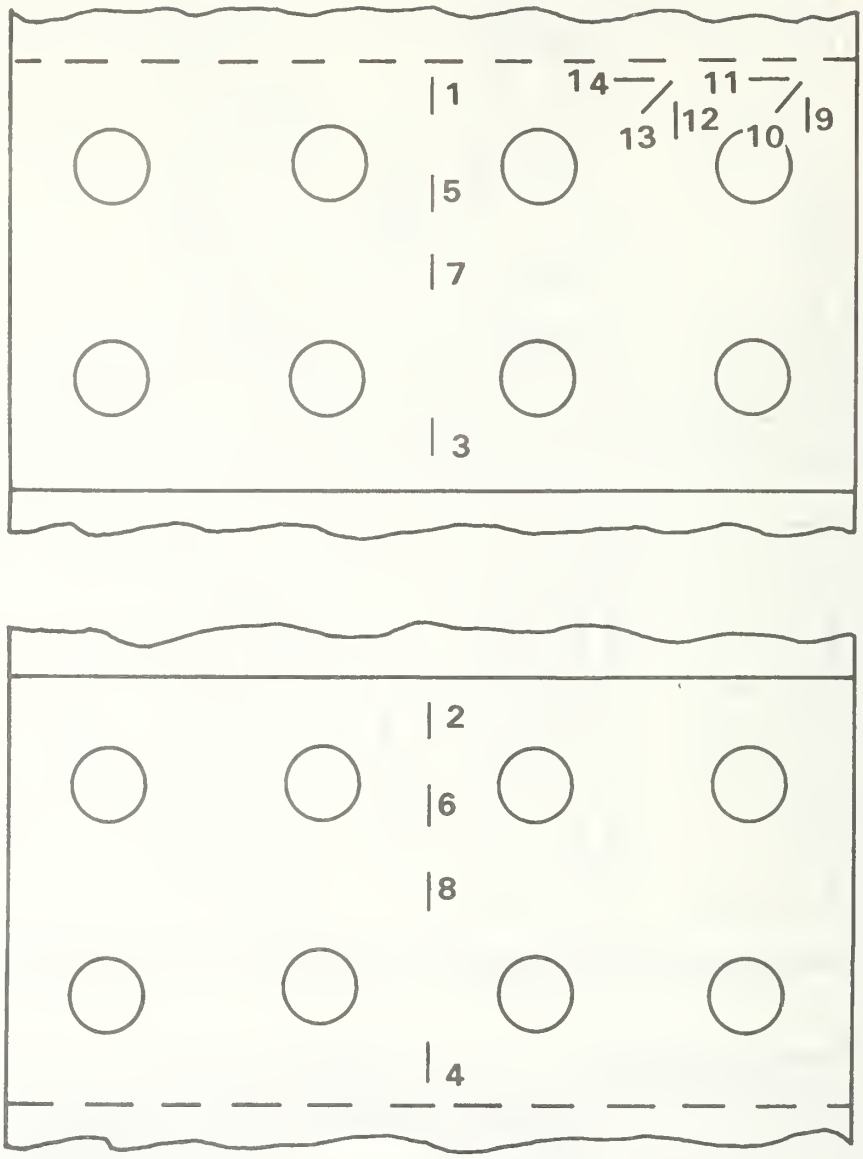

GAGE NO.	MEASURED	ANALYTICAL		
		PLANFORM	CROSS-SECTION	PLANFORM (PLUS BENDING)
1	620	613	546	680
2	408	412	364	326
3	288	364	279	259
4	679	654	624	782
5	525	515	594	605
6	475	502	411	412
7	447	506	514	516
8	561	506	492	480
9	374	590	625	696
10	424	249	---	273
11	-127	-216	---	---
12	656	579	632	689
13	254	236	---	270
14	-169	-202	---	---

Figure 40. LINEAR MICROSTRAIN COMPARISONS FOR THE WIDE JOINT.

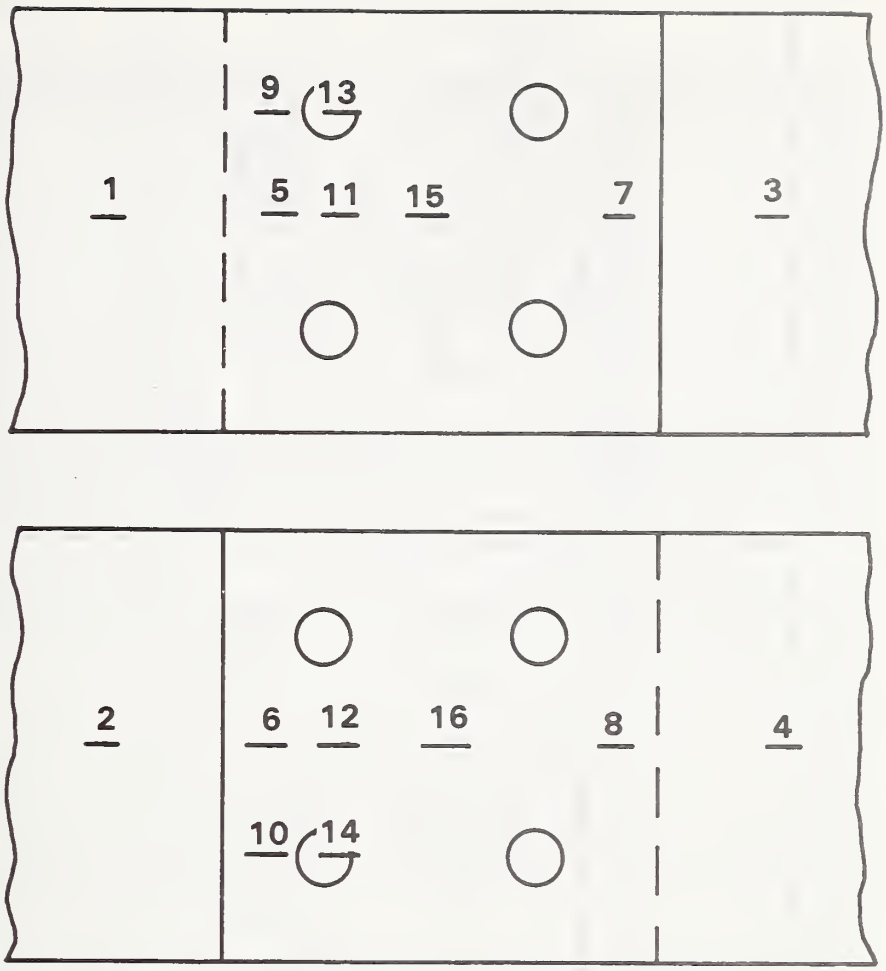

GAGE NO.	MEASURED	ANALYTICAL		
		PLANFORM	CROSS-SECTION	PLANFORM (PLUS BENDING)
1	666	996	---	---
2	1308	996	---	---
3	1310	996	---	---
4	670	996	---	---
5	797	535	672	684
6	185	477	344	332
7	169	460	334	300
8	811	554	685	712
9	784	542	674	690
10	163	470	345	322
11	670	498	517	517
12	295	496	495	488
13	665	501	517	520
14	281	498	495	491
15	477	488	498	485
16	477	488	504	491

Figure 41. LINEAR MICROSTRAIN COMPARISONS FOR THIN JOINT.

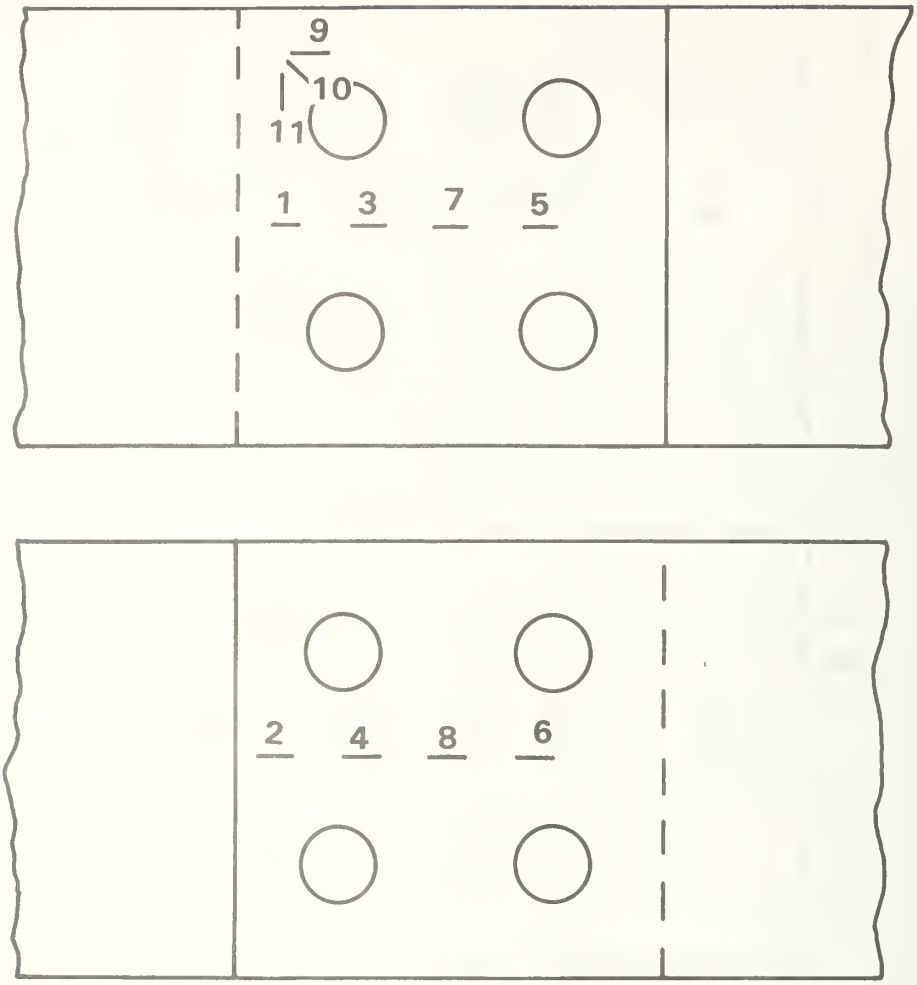

GAGE NO.	MEASURED	ANALYTICAL (PLANFORM)
1	-482	880
2	123	108
3	0	737
4	283	293
5	428	311
6	617	703
7	674	505
8	333	518
9	-391	862
10	100	201
11	-316	-398

Figure 42. LINEAR MICROSTRAIN COMPARISONS FOR THE SPOTWELD JOINT.

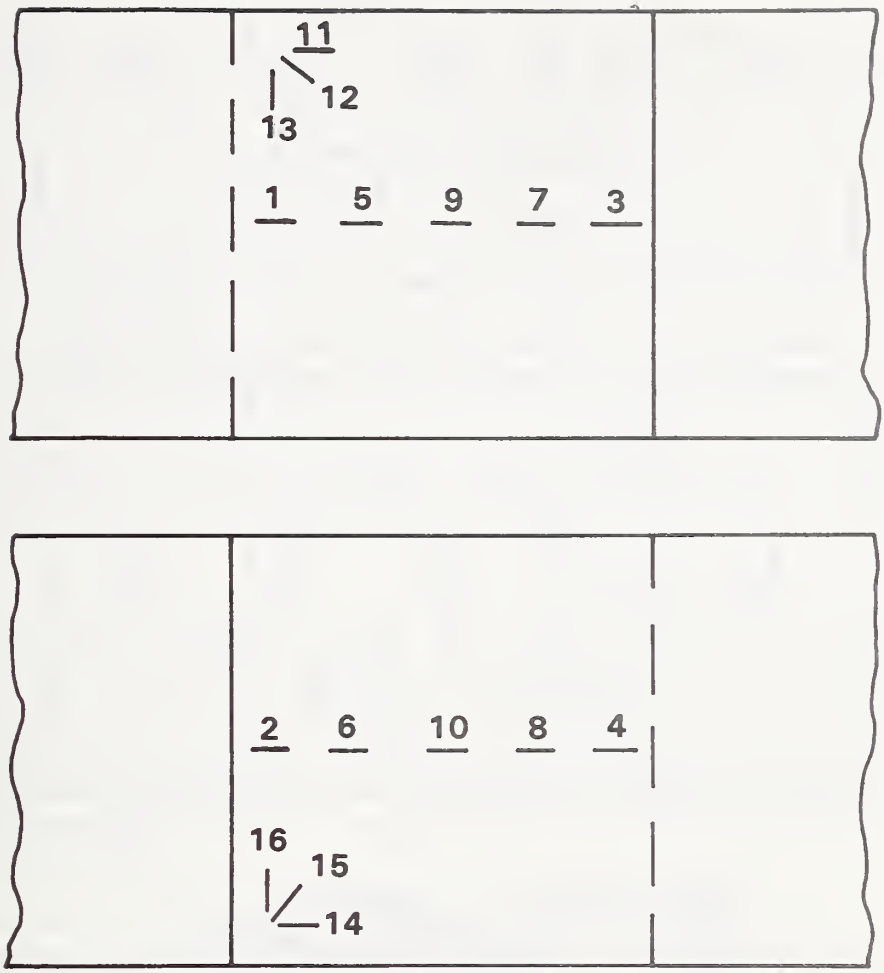

GAGE NO.	MEASURED	ANALYTICAL		
		PLANFORM	CROSS-SECTION	PLANFORM (PLUS BENDING)
1	617	680	565	677
2	344	351	284	347
3	331	304	268	351
4	648	710	524	663
5	584	527	621	644
6	377	477	383	362
7	382	468	375	345
8	581	527	626	651
9	479	496	480	490
10	473	498	508	506
11	686	579	694	736
12	280	235	---	302
13	-161	-205	---	---
14	284	425	334	270
15	36	113	---	54
16	-168	-180	---	---

Figure 43. LINEAR MICROSTRAIN COMPARISONS FOR THE BONDED JOINT.

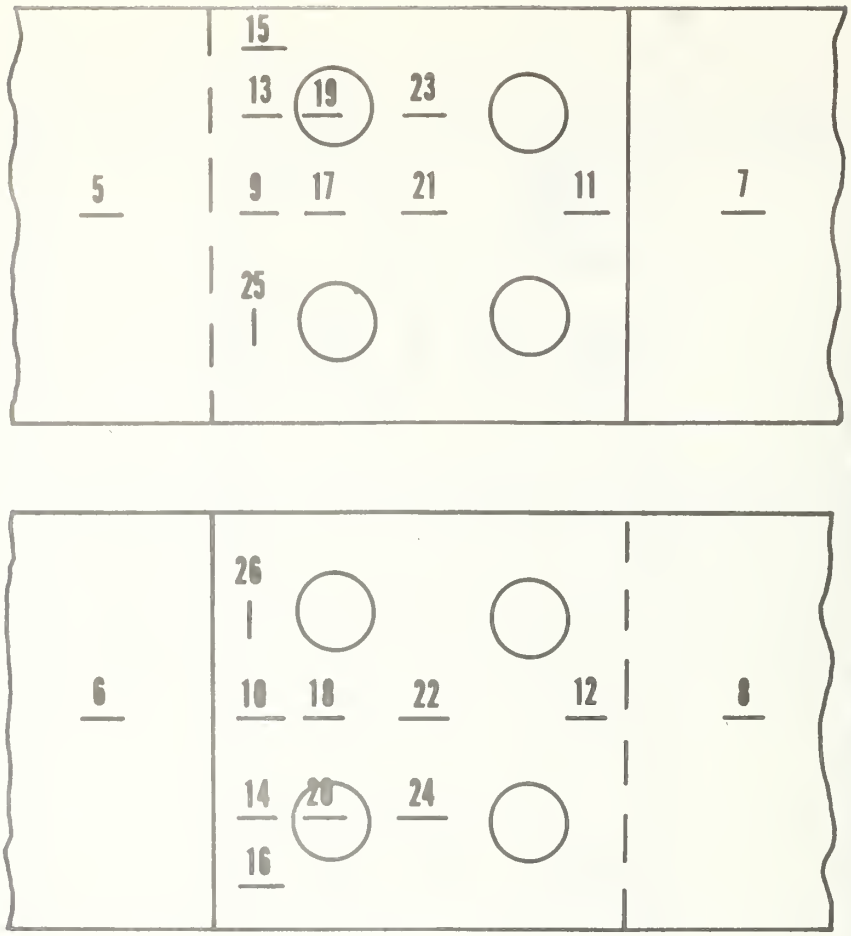

GAGE NO.	MEASURED	ANALYTICAL	
		PLANFORM	PLANFORM (PLUS BENDING)
5	853	1992	----
6	3188	1992	----
7	3147	1992	----
8	918	1992	----
9	1489	1245	1555
10	434	799	548
11	413	741	206
12	1524	1288	1823
13	1473	1262	1572
14	394	757	502
15	1545	1276	1557
16	283	859	608
17	1324	1030	1384
18	626	977	412
19	1330	1037	1391
20	628	969	404
21	886	986	1074
22	916	987	892
23	915	1003	1091
24	970	1003	908
25	-410	-399	----
26	-321	-394	----

Figure 44. NONLINEAR- RANGE MICROSTRAIN COMPARISONS FOR CENTRAL REFERENCE JOINT.

of the bending strain evident in Figure 8 and the bending strains indicated by back-to-back gages located just outside the overlap region on two specimens (Figures 36 and 41). Figure 45 illustrates the application of this correction for the central reference specimen (design 1). The test data shown are the strains indicated by gages 10, 12, 18 and 22 (Figure 36). The two interior gages (18 and 22) were assumed to define a linear variation in bending strain, with respect to position, for most of the overlap length. The variation in bending strain was assumed to be proportional to the effective eccentricity of the tensile stress distribution in the metal sheet at the end of the overlap. The cross-section solution was obtained using the mesh shown in Figure 46 with the boundary loads acting through the eccentric interior mesh points as indicated. The amount of eccentricity was determined by extrapolating a straight line through the test data (gages 18 and 22) to the end of the overlap and computing the eccentricity that would account for the linear strain variation. The rationale for this solution is not rigorous, but it is believed to give more realistic boundary conditions than the mid-sheet boundary loading applied to the meshes shown in Figures 4(a) and 20.

For two of the seven joints analyzed for the linear-elastic range by both computer programs (designs 2 and 5) the best agreement with test data was obtained by the planform analysis. For the other five of these seven joints, there was better agreement with test data by the cross-section analysis than by the planform analysis. For three of the joints (designs 3, 4 and 6) the best agreement was obtained by applying the bending correction to the planform analysis. The above rankings are based on the mean of the percentage differences between test data and analysis for all gages located in the overlap region.

For the case of the central reference specimen loaded in the stable-nonlinear range, Figure 44, a nonlinear planform analysis was performed. The bending corrections applied to the nonlinear planform results, however, were obtained by linearly scaling the results of a linear cross-section analysis. Nevertheless, these scaled linear corrections do significantly improve the agreement between analysis and test data.

6. CONCLUSION

Both of the linear analyses, planform and longitudinal cross-section, are expected to be useful in the study of bonded and weldbonded lap joints. The planform analysis alone may be useful for some purposes in the study of either double-lap joints or single-lap joints that are constrained to prevent excessive bending. Where out-of-plane bending or peel stresses are important, however, the planform analysis should be supplemented by the cross-section analysis. When using the linear analyses, one should remain aware that these analyses do not account for nonlinear modes of response that may be significant, even at moderate load levels.

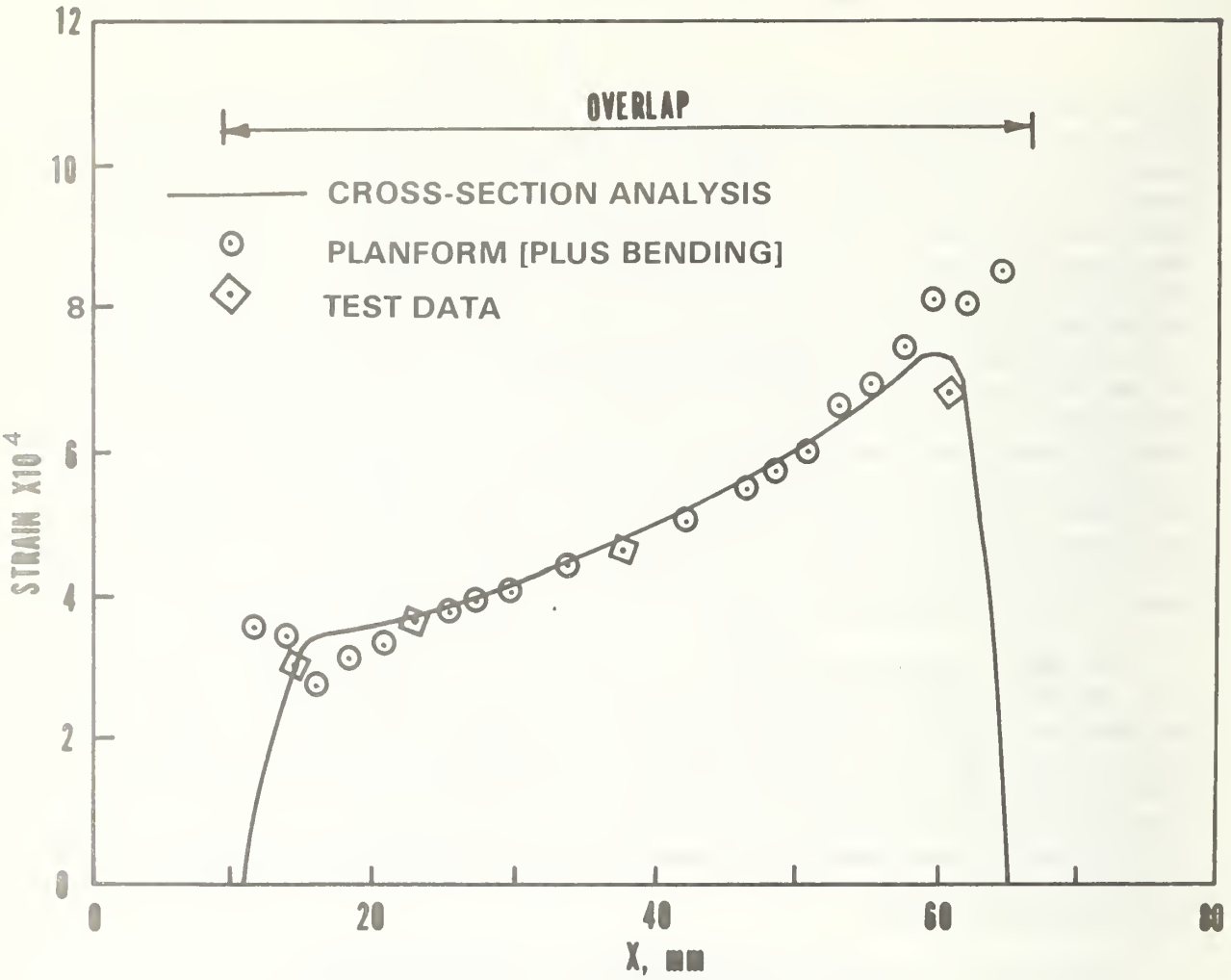

Figure 45. LONGITUDINAL STRAIN ON SURFACE OF CENTRAL REFERENCE JOINT.

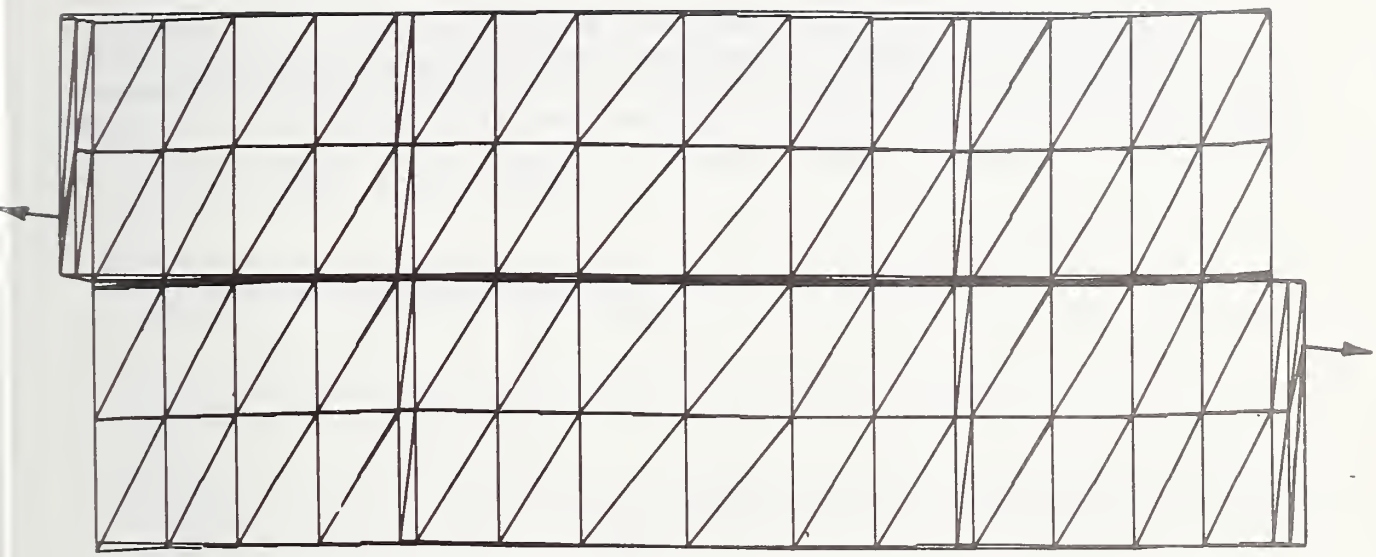

Figure 46. FINITE ELEMENT MESH USED FOR ANALYSIS OF CENTRAL REFERENCE JOINT, WITH COLLINEAR ECCENTRIC BOUNDARY LOADS INDICATED.

The nonlinear analysis algorithms show promise of adequately simulating several modes of nonlinear response. They do have practical limitations, however. The solutions are relatively expensive in computer time and storage because each nonlinear solution consists of a sequence of linear solutions and because a part of the results of previous linear solutions must be stored for use in obtaining later solutions. The nonlinear solutions ordinarily require multiple computer runs interspersed with subjective evaluation of intermediate results and adjustment of convergence parameters by the user of the computer program.

The laboratory test results support a reasonable degree of confidence in the validity of the computer programs. Apart from this, the test results for eight different lap joint configurations constitute a significant experimental parameter study, within the limited range represented by the specimens and tests.

7. REFERENCES

1. Mitchell, R. A., Woolley, R. M., and Baker, S. M., Finite Element Analysis of Spotwelded, Bonded, and Weldbonded Lap Joints, NBSIR 75-957 (Dec. 1975).

2. Mitchell, R. A., Woolley, R. M., and Chwirut, D. J., Composite-Overlay Reinforcement of Cutouts and Cracks in Metal Sheet, NBSIR 73-201 (Feb. 1973).

3. Mitchell, R. A., Woolley, R. M., and Chwirut, D. J., Analysis of Composite-Reinforced Cutouts and Cracks, J. AIAA, Vol. 13, No. 6, 744-749 (June 1975).

4. Zienkiewicz, O. C., The Finite Element Method in Engineering Science, McGraw-Hill, London (1971).

5. Hughes, E. J., and Rutherford, J. L., Study of Micromechanical Properties of Adhesive Bonded Joints, Technical Report 3744, Picatinny Arsenal, Dover, N.J. (Aug. 1968).

6. Metallic Materials and Elements for Aerospace Vehicle Structures, MIL-HDBK-5A (Aug. 1972).

7. Chwirut, D. J. (coordinator), Research and Testing Facilities of the Engineering Mechanics Section, National Bureau of Standards, Washington, D.C., NBS Spec Publ 370 (1973).

DISTRIBUTION LIST

	No. of Copies
Commander	
Picatinny Arsenal	
ATTN: Scientific & Technical Information Br.	5
SARPA-FR-M-A	15
SARPA-ND	5
SARPA-AD	5
SARPA-QA	2
SARPA-IO	2
SARPA-QA-A	1
SARPA-QA-N	1
Dover, New Jersey 07801	
Commander	
US Army Materiel Development & Readiness Command	
ATTN: DRCDE-R, Mr. J. Rivkin	1
DRCPP-PI	1
DRC-QA	1
5001 Eisenhower Avenue	
Alexandria, Virginia 22304	
Commander	
US Army Missile Command	
ATTN: DRSMI-RLM, Mr. E. A. Verchot	1
Chief, Document Section	1
Redstone Arsenal, Alabama 35801	
Commander	
US Army Armament Command	
ATTN: DRSAR-MP-PC	1
DRSAR-RDP	1
DRSAR-RDM, Mr. G. Chesnov	1
DRSAR-RDT, Dr. Daryl Penrod	1
DRSAR-RDT, Mr. J. Salamon	1
DRSAR-ASF, Mr. H. Wohlferth	1
Rock Island, Illinois 61201	
Commander	
US Army Electronics Command	
ATTN: DRSEL-TL-ME, Mr. Dan Lichenstein	1
DRSEL-TL-ME, Mr. A. J. Raffalovich	1
DRSEL-TL-ME, Mr. G. Platau	1
DRSEL-PP-EM2, Sarah Rosen	1
Forth Monmouth, New Jersey 07703	

	No. of Copies
Commander US Army Aviation Systems Command ATTN: DRSAV-FET, Mr. J. Bramlet	1
DRSAV-E-ER, Mr. W. McClane	1
DRSAV-FEU, Mr. E. Dawson	1
DRSAV-F-FE, Mr. C. Sims	1
DRSAV-E-RE, Mr. G. Gorline	1
P. O. Box 209, Main Office St. Louis, Missouri 63166	
Director US Army Tank-Automotive Command ATTN: DRSTRA-KMD, Mr. Francis S. Lemmer	1
Warren, Michigan 48090	
Commander US Army Materials & Mechanics Research Center ATTN: DRXMR-FR, Dr. G. Thomas	1
DRXMR-PL	1
Technical Information Section	1
Watertown, Massachusetts 02172	
Director US Army Production Equipment Agency Rock Island Arsenal ATTN: DRXPE-MT, Mr. H. Holmes	2
Rock Island Arsenal, Illinois 61201	
Commander Corpus Christi Army Depot ATTN: DRSAV-FES (STOP 55)	2
DRSAV-FESA, Mr. T. Tullos	2
DRSAV-FESP, Mr. Bulloch	1
Corpus Christi, Texas 78419	
Commander Aberdeen Proving Ground ATTN: Rosalie O. Forst, STEAP-TL, Bldg 305	1
Aberdeen Proving Ground, Maryland 21005	
Commander US Army Weapons Command Watervliet Arsenal ATTN: Dr. G. D. Andrea, SARWV-RDR-PS	1
Watervliet, New York 12189	

	No. of Copies
Director US Army Engineer Waterways Experiment Station, P. O. Box 631 Corps of Engineers ATTN: Mr. Hugh L. Green - WE SSS1 Vicksburg, Mississippi 39180	1
Commander US Army Medical Bio-Engineering Research and Development Laboratories Fort Deterick ATTN: Dr. C. Wade Frederick, Maryland 21701	1
Plastics Technical Evaluation Center ATTN: Mr. H. Pebly Mr. A. Landrock Picatinny Arsenal Dover, New Jersey 07801	1 1
Commander Harry Diamond Laboratories ATTN: Mr. N. Kaplan Mr. J. M. Boyd Library Washington, DC 20438	1 1 1
Commander US Army Edgewood Arsenal ATTN: SAREA-DE-EP SAREA-CL-CPM, Mr. Dave Schneck SAREA-PA-PR, Mr. M. N. Timbs SAREA-DME, Mr. M. A. Raun Edgewood Arsenal, Maryland 21010	1 1 1 1
Commander Tobyhanna Army Depot ATTN: Mr. A. Alfano Tobyhanna, Pennsylvania 18466	1
Director US Army Ballistics Research Laboratory ATTN: Mr. Emerson V. Clark, Jr. DRXBR-IB, Dr. Bruce Burns Aberdeen Proving Ground, Maryland 21005	1 1

	No. of Copies
Commander US Army Materiel Development & Readiness Command ATTN: DRCPM-UA, Mr. C. Musgrave DRCPM-LH, Mr. C. Cioffi DRCPM-HLS-T, Mr. R. E. Hahn P. O. Box 209 St. Louis, Missouri 63166'	 1 1 1
Commander Natick Research & Development Command Natick, Massachusetts 01760	1
Commander US Army Engineer Research & Development Labs Fort Belvoir, Virginia 22060	1
Department of the Navy Naval Air Systems Command ATTN: Mr. John J. Gurtowski (AIR 52032C) Washington, DC 20360	 1
Naval Ordnance Station (NOSL) ATTN: Mr. W. J. Ryan Code 5041 Southside Drive Louisville, Kentucky 40214	 1
Naval Avionics Facility ATTN: Mr. B. D. Tague, Code D/802 Mr. Paul H. Guhl, D/033.3 21st and Arlington Indianapolis, Indiana 46218	 1 1
Commander US Naval Weapons Station ATTN: Research and Development Div Yorktown, Virginia 23491	 1
Commander Aeronautical Systems Division ATTN: Mr. W. Scardino, AFML/MXE Mr. T. J. Aponyi Composite and Fibrous Materials Branch Nonmetallic Materials Division Wright-Patterson Air Force Base, Ohio 45433	 1 1

	No. of Copies
Dr. Robert S. Shane, Staff Scientist National Materials Advisory Board National Academy of Sciences 2101 Constitution Avenue, N.W. Washington, DC 20418	1
Defense Documentation Center Cameron Station Alexandria, Virginia 22314	12
US Army Air Mobility R & D Laboratory, Headquarters Advanced Systems Research Office ATTN: Mr. F. Immen, MS 207.5 Ames Research Center Moffet Field, California 94035	1
Naval Ship Engineering Center ATTN: Mr. W. R. Graner, SEC 6101E Prince George's Center Hyattsville, Maryland 20782	1
Mare Island Naval Shipyard Rubber Engineering Section ATTN: Mr. Ross E. Morris, Code 134.04 Vallejo, California 94592	1
Hanscom Air Force Base ATTN: Mr. R. Karlson, ESD/DE, Stop 7 HQ, ESD Bedford, Massachusetts 01731	1
Naval Air Development Center Materials Laboratory ATTN: Mr. Coleman Nadler, Code 30221, Div, AVTD Warminster, Pennsylvania 18974	1